DESIGN OF BFA-OPTIMIZED FUZZY ELECTRONIC LOAD CONTROLLER FOR MICRO HYDRO POWER PLANTS

ROBERT AGYARE OFOSU

MASTER OF SCIENCE

(Electrical and Electronic Engineering)

JOMO KENYATTA UNIVERSITY OF AGRICULTURE AND TECHNOLOGY

2016

Design of BFA-Optimized Fuzzy Electronic Load Controller for Micro Hydro Power Plants

Robert Agyare Ofosu

A thesis submitted in fulfilment for the degree of

Master of Science in Electrical and Electronic Engineering in

the Jomo Kenyatta University of Agriculture and Technology

2016

DECLARATION

This thesis is my original work and has not been presented for a degree in any other university.

Signature..... Date.....

Robert Agyare Ofosu

This thesis has been submitted for examination with our approval as university supervisors:

Signature..... Date.....

Dr. Keren Kaberere

JKUAT, Kenya

Signature..... Date.....

Prof. John Nderu

JKUAT, Kenya

Signature..... Date.....

Prof. Stanley Kamau

JKUAT, Kenya

DEDICATION

I humbly dedicate this work to my parents Mr and Mrs Agyare Appiah, my siblings and to my best friend Nancy Plange Ocran for their constant intercession, guidance, love and support during the course of my studies.

ACKNOWLEDGEMENT

I would like to express my heartfelt appreciation to the Almighty God for through His abundant grace, mercy, protection and divine wisdom, I have come this far.

Secondly, this work would not have come to a success without the proper supervision given to me by my noble supervisors Prof. John Nderu, Dr. Keren Kaberere and Prof. Stanley Kamau. It is through their critics, suggestions, recommendations and ideas that enabled me to complete this work. May the goodness and mercies of God follow them all the days of their lives.

I would also like to thank the management and staff of the University of Mines and Technology for their financial support throughout my studies in Kenya. Words cannot also express how grateful I am to my academic mentors Prof. Daniel Mireku-Gyimah, Mr. Erwin Normanyo, Prof. Peter Arroja Eshun, Mr. Philip Blewushie and Mr. Fuseini Mumuni. Thank you for your mentorship.

Special thanks to Mr. Asaph Mbugua Muhia who has always been my brother and friend throughout my stay in Kenya. I highly appreciate all the encouragement and the sacrifices he made to make this work a success. I will forever be grateful.

Finally, to all and sundry who in diverse ways have contributed to the success of this work. May God bless and make you prosperous in all your endeavours as we strive to make the world a better place to live.

TABLE OF CONTENTS

LIST OF TABLES

LIST OF FIGURES

LIST OF APPENDICES

LIST OF ABBREVIATIONS

AI	Artificial Intelligence
ACA	Ant Colony Algorithm
ANFIS	Adaptive Neuro-Fuzzy Inference System
ANN	Artificial Neural Network
AVR	Automatic Voltage Regulator
BFA	Bacterial Foraging Algorithm
BOO	Build Own Operate
CRO	Cathode Ray Oscilloscope
ELC	Electronic Load Controller
EMI	Electromagnetic Interference
GA	Genetic Algorithm
IGBT	Insulated Gate Bipolar Transistor
LBJ	Large Barkhausen Jump
MAW	Magnetostrictive Amorphous Wire
MHPP	Micro Hydro Power Plant
MOSFET	Metal Oxide Semiconductor Field Effect Transistor
PHPP	Pico Hydro Power Plant
PI	Proportional Integral
PID	Proportional Integral Derivative
PM	Permanent Magnet
PSO	Particle Swarm Optimisation
PWM	Pulse Width Modulation
SHPP	Small Hydro Power Plant

LIST OF NOMENCLETURES

Symbol	Quantity
α	Firing angle
ϕ	Flux, [Wb]
ω_n	Undamped natural frequency, [rad/s]
ζ	Damping factor
ω_r	Angular velocity of the rotor, $[rad/s]$
D	Generator damping constant,
E_b	Back emf, $[V]$
f_e	Electrical frequency, $[Hz]$
H	Generator inertia constant, [MW.s/MVA]
I_a	Armature current, $[A]$
J	Combined moment of inertia of generator and turbine, $[kgm^2]$
K_I	Integral gain
K_p	Proportional gain
N	Generator speed, $[rpm]$
P_C	Consumed load, $[W]$
P_D	Damped load, $[W]$
P_G	Generated power output, $[W]$
P_m	Mechanical input power, $[W]$
t	Time, $[s]$
R	Resistance of damper load, $[\Omega]$,
T_a	Armature torque, $[Nm]$
T_m	Mechanical torque, $[Nm]$
T_e	Electromagnetic torque, $[Nm]$

ABSTRACT

With the volatile oil prices and the need to reduce the emission of greenhouse gases, renewable energy resources are a very attractive alternative. Kenya has good potential for micro-hydroelectric power generation. However, only a small proportion of this potential has been harnessed. Further, most rural areas in Kenya have limited access to electric power. Unfortunately, most of the rural communities that are privileged to be connected to the grid have unreliable and expensive grid power. To meet their energy needs, some of the communities have installed and operate pico or Micro Hydro Power Plants (MHPPs) based on the build-own-operate (BOO) model. In most cases, the communities contribute both money and labour to build the plant; the design has to be simple and the cost kept low. After completion, the plants are operated by the community members who have limited technical knowledge and skills. Generally, the tariffs charged for energy supplied by the MHPP are low and sometimes, can not cover the cost of major maintenance work.

In any power generation plant, a speed governor is required for regulating the frequency of supply. However, this is the single most expensive component in a MHPP and most of the community owned MHPP can hardly afford it and thus, have no means of continuously regulating frequency. Hence, frequency is controlled manually by controlling the flow of water to the turbine when there is a change in frequency using manually operated water flow control valve. An Electronic Load Controller (ELC) is an electronic device used to control the output power and hence the frequency of a MHPP system, by maintaining a near constant load on the generator. The ELC diverts the power that is not consumed by the consumer load to a damper load which are normally resistors, heating elements or batteries. In this work, consideration was given to the design and implementation of an ELC to control the frequency of a syn-

chronous generator output by diverting excess power to a damper load, hence replacing the governor.

Magnetostrictive Amorphous Wire (MAW) was used as frequency sensor. The signal from the MAW is a low signal in the order of millivolts. An amplifier and a signal conditioning circuit were designed to convert the analog signal from the MAW to a digital signal that is fed to the Arduino microcontroller. In addition, a Fuzzy-PI ELC was designed and simulated for a MHPP and optimal PI gains were determined by using Bacterial Foraging Algorithm (BFA) to optimise fuzzy logic membership functions. These optimal PI gains were used as reference gains to the Arduino microcontroller so as to generate a Pulse Width Modulation (PWM) signal to control the firing angle of the switching circuit of the ELC. Finally, the designed ELC was tested in a laboratory experimental setup.

The results obtained clearly show the effectiveness of the ELC to dump excess power to the damper load when the consumer load changes, and maintain the supply frequency between 49.5 to 50.5 Hz. Also, from the results, it was observed that the MAW sensor was able to measure the frequency effectively with high accuracy when compared to the frequency measurement from the tachometer. This is a key finding since the application of MAW sensor for frequency measurement in ELCs has not been reported in literature.

The designed controller is cheaper and yet able to control the frequency very effectively when compared to other ELCs and speed governors that are currently on the market. When the designed ELC is implemented in a typical MHPP, the effects of frequency variation on electrical equipment will be averted. This will promote economic growth especially in the remote communities of Kenya. As a result, the life of the people living in the rural communities will be improved.

CHAPTER ONE

1.0 INTRODUCTION

1.1 Background

In the present world, electricity is one of the important ingredients for industrial and socio-economic development of a country [1]. There is evidence in most parts of the world that areas without electricity are far less developed than those with electricity [2]. In households, electricity has an impact on living standards, health and education among others. In terms of access to electricity, rural communities are the most affected due to several reasons, which include non-prioritisation where there is insufficient supply and being economically unviable when electric supply is to be implemented in the traditional way of extending the existing grid [3].

In recent years there has been a continuous improvement of power generation from renewable energy sources such as hydro, solar, wind, biogas, geothermal and tidal waves in developing countries. This is due to the volatile oil prices, infrastructural development as a result of increase in population and economic activities and the need to reduce the emission of greenhouse gases. As shown in Figure 1.1 [adapted from [4]], Africa is the third largest continent in the world having a huge technical and economic hydropower potential with the majority of that being in the Sub-Saharan Africa. However, only as low as 4 to 7% of this potential has been harnessed [5]. Despite the availability of hydro reserves in Africa sustainable provision of electrical energy is regarded as a major challenge, especially in the rural communities in Africa.

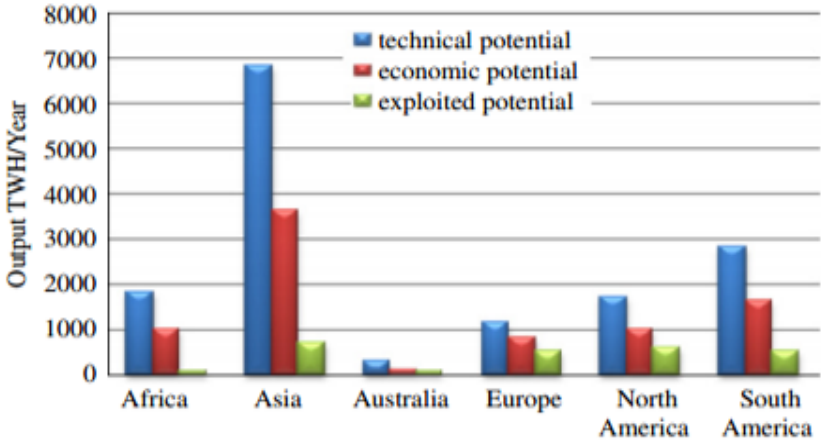

Figure 1.1: Hydro power potential by continent

Like most countries in Africa, Kenya is not an exception in facing energy crises especially in the rural communities [6]. In spite of government efforts to provide access to electricity in the rural communities, the challenge still remains for Kenya to provide sustainable and reliable energy to her people [7] [8]. Micro hydro power generation is still viewed as an important source of energy in some parts of the world such as China, Nepal, Peru, Pakistan, Vietnam, Sri Lanka, Philippines and India. It can be used to supplement the energy supply and improve the generation mix in Kenya.

According to UNIDO report [9], the estimated potential of small hydro power in Kenya is about 3,000 MW of which less than 50 MW has been developed. Studies done so far shows that more than 260 small hydropower sites are identified in Kenya with more than 600 MW of power. About 45% of these sites are located in the Lake Victoria drainage basin or the Tana River drainage basin and in the districts of Kirinyaga, Thika, Maragua, Meru South and Meru Central the so called Mount Kenya region [9]. Some of the successfully installed MHPPs are the Kathamba, Kiangima/Kiangibuinu and Thima located in Kirinyaga district, Rurathia in Muranga district, Tungu-Kabri project in Meru South district and Saosa, Dimbolil and Chemamil project located in Kericho.

Figure 1.2(a) shows the intake weir and Figure 1.2(b) is a manually operated water flow control valve at Kiangima/Kiangiboini MHPP in Kirinyaga District.

(a) Intake weir

(b) Manually operated water flow control valve

Figure 1.2: Kiangima/Kiangiboini MHPP in Kirinyaga District

Unlike the other conventional energy sources micro hydro power plants are not expensive to build, do not emit greenhouse gases and do not encounter the problem of population displacement and wildlife extinction. They are also more efficient than other sources of renewable energy like wind and solar [10]. However, the major problem with MHPPs is that often they operate as stand-alone plants isolated from the grid. Thus, they require some form of control to maintain a constant frequency. In many cases, an Electronic Load Controller (ELC) is used instead of the governor to reduce the high cost of the governor and supply good quality electric power to the rural communities. An ELC is an electronic device used to control the output power and hence the frequency of a MHPP system, by maintaining a near constant load on the generator. The ELC diverts the power that is not consumed by the consumer load to a damper load which are normally resistors, heating elements or batteries. ELC therefore maintains a constant electrical load on a generator in spite of changing consumer loads consequently keeping the frequency constant [11] [12] [13].

Various ELCs together with their frequency sensing elements have been developed [14] [15] [16]. Tachogenerators and shaft encoders are normally used as frequency sensors which are unreliable and are very expensive [17]. However, recent trends in technology have shown that Magnetostrictive Amorphous Wire (MAW) sensor can be accurately and efficiently used to measure the frequency and has numerous advantages when compared to the conventional frequency measuring devices [15] [16].

Conventional control techniques such as Proportional, Integral and Derivative (PID) controllers have also been used but these controllers attain poor control performances, such as high overshoots and long settling times. Therefore, using artificial intelligent techniques such as fuzzy logic and optimising the membership functions using stochastic optimisation algorithms can greatly improve the control performance of an ELC.

This work therefore seeks to design and implement an ELC by employing optimised fuzzy-PI controller using Bacterial Foraging Algorithm (BFA) and adopting MAW for frequency measurement.

1.2 Problem Statement

Kenya and indeed many other countries in the world have good potential of micro-hydroelectric power. However, in many such countries only a small proportion of this potential has been harnessed. As a result most rural areas in such countries have limited access to electric power. Unfortunately, those rural communities privileged to be connected to the grid also have unreliable and expensive grid power. To obtain a reliable source of energy, some of the communities in such countries have installed MHPPs but have limited technical knowledge, skills and financial resources to operate them effectively.

In a power generation plant, a speed governor is required for regulating the frequency of supply as the load changes. However, this is the single most expensive component in a MHPP. Consequently, most of the community owned MHPP can hardly afford it and thus, have no means of continuously monitoring and regulating frequency as the generator load changes. This causes a very wide variation in frequency due to imbalance between energy demand and supply hence resulting in poor power quality.

To reduce the high cost of the governor, an ELC is used in place of the governor to control the frequency of the MHPP. ELCs exist in the market but they are not user friendly due to the fact that they are designed with sophisticated components and control system. They are also not locally manufactured but rather imported making their overall cost very high. There is a need to develop a simple, reliable and cost effective ELC produced from simple electronic components to control the frequency of the MHPP under varying load conditions.

1.3 Justification

Access to electricity is one of the keys to development because it provides light, heat and power used in residential, commercial and industrial sectors. For the attainment of the country's goals of being industrialised by the year 2030 and as part of the government's effort to provide electricity to all by the year 2020, micro-hydro power generation can play a key role in achieving this vision. The findings of this work will be beneficial to remote communities in Kenya because they will have a continuous and uninterrupted power supply at rated frequency and also free power from the national grid for other industrial uses.

The designed ELC is cost effective due to the use of inexpensive components and also ensures good frequency control due to the use of a modern frequency sensor and latest

Artificial Intelligence (AI) based control algorithm. The problems encountered in the conventional ELC controllers is therefore minimised, thus ensuring an improvement in the power quality of MHPPs.

1.4 Research Objectives

1.4.1 Main Objective

The main aim of this work is to design and implement an ELC for controlling the frequency of a MHPP generator by diverting excess power to damper loads.

1.4.2 Specific Objectives

The specific objectives of this work are to:

(i) Develop frequency sensor to measure the frequency of the generator output using magnetostrictive amorphous wire;

(ii) Design a Fuzzy-PI ELC for a MHPP and determine the optimal PI gains using BFA to optimise fuzzy logic membership functions;

(iii) Simulate the controller using MATLAB/SIMULINK; and

(iv) Implement a prototype of the designed controller.

1.5 Scope of Work

This work is limited to the design and implementation of an ELC to control the frequency of a MHPP by diverting excess power to damper loads when the consumer load decreases. Thus maintaining a constant load on the generator hence keeping the frequency constant. Again, in this work only balanced, unity power factor loads are used as both consumer and damper load.

1.6 Work Organisation

This thesis is organised into five chapters as follows: Chapter one entails the general introduction. It consists of background, problem statement, justification, research objectives and the scope of work. Chapter two gives the literature review. Chapter three gives the research methodology where the design and and implementation of the ELC to control the frequency of the MHPP is discussed in details. Chapter four gives the results and discussion. Finally chapter five sums up the research with the conclusions and recommendations.

CHAPTER TWO

2.0 LITERATURE REVIEW

2.1 Overview of Micro Hydro Power Plant

Micro-hydro is the small scale harnessing of energy from falling water such as steeped mountain rivers generating typically less than 100 kW using the run-off-river type flow of water hence it does not require the construction of expensive dams. Micro-hydro power generation system is regarded as an attractive form of electrical power generation for remote communities where electrical grid is non-existent. It is thus regarded as the most economical and renewable source of energy supplements to off-grid areas in rural communities [18] [19]. It has the added advantage of being available all the time either day or night unlike other renewable energy sources such as wind and solar. Moreover, it does not incur any cost of building and maintaining dams as is the case in large hydro plant. Hydro power generation plants are usually classified according to the capacity as shown in Table 2.1 [20] [21].

Table 2.1: Classification of hydro-electric power plants

Type	Capacity
Large-hydro	More than 100 MW and usually feeding into a large electricity grid
Medium-hydro	15 MW to 100 MW; usually feeding a grid
Small-hydro	1 MW to 15 MW; usually feeding into a grid
Mini-hydro	100 kW to 1 MW; either stand-alone schemes or more often feeding into the grid
Micro-hydro	5 kW to 100 kW; usually provided power for a small community or rural industry in remote areas away from the grid
Pico-hydro	100 W to 5 kW

In principle, the working of the MHPP is similar to that of the large hydro plant. Hydro power is driven by extracting the potential energy from water over a height difference. The energy of the moving water is converted into mechanical energy by rotating a turbine. In this way the moving water energy is converted to electrical energy by means of a generator coupled to the turbine. The power available is proportional to the product of pressure head and volume flow rate of the water through the turbine given as

$$P = \eta \times \rho \times g \times Q \times H \tag{2.1}$$

where,

P = power produced (W),

η = plant efficiency ($\%$),

ρ = water density (Kg/m^3),

g = acceleration due to gravity (9.81 m/s^2),

Q = water flow rate (m^3/s), and

H = water head (m).

In an electric power system, consumers need uninterrupted power at rated frequency and voltage. Hence in a MHPP, the key factors for power quality are voltage and frequency control. Failure to control these parameter will have an adverse effect on electric power quality. The voltage is regulated by controlling the excitation of the generator [22] [23]. This is in most cases is achieved using an Automatic Voltage Regulator (AVR). The main function of the AVR is to control and maintain the terminal voltage of the generator by automatically adjusting the field current or excitation current within specified limits in spite of varying load conditions on the generator [22] [23].

The AVR operates such that the generator terminal voltage is compared with a setpoint voltage. If the generator terminal voltage is less than the reference voltage, the AVR

increases DC voltage across the generator field to the point at which the generator terminal voltage is equal to the setpoint voltage. This control action by the AVR always maintain the terminal voltage of the generator constant whenever the voltage changes. Most synchronous generators used in MHPPs have built in AVR to control the terminal voltage hence voltage control is not a major problem.

The power supply frequency is controlled by eliminating the mismatch between the power generated and the power consumed [24] [25]. For proper and effective control of the frequency, the mechanical power input (P_m) and electrical power output (P_e) of the generator must balance. If the mechanical power input to the turbine is more than the electrical load connected to the generator, the generator accelerates and hence the frequency increase. The converse is also true.

Therefore, due to the varying power needs of the electrical power users in actual power system, the load is changing continuously and randomly causing an imbalance between the power generated and the power consumed. This action always cause the frequency to vary hence, the need for frequency regulation.

All electrical equipment are designed to operate at a specific frequency range. Failure to operate these equipment at the specified frequency can cause serious damage or reduce the life span of the equipment [26] [27]. For example, rotating machinery such as AC electric motors operates at a constant speed or frequency for safe, effective and efficient operation and are designed to tolerate very small frequency fluctuation [28] [29]. An increase in frequency of motors above the acceptable limit can damage the motor due to overheating of the windings, increase in vibration and wear of the mechanical bearings.

Similarly, power turbines when operated at a frequency below 50 Hz, the rotor starts vibrating excessively which can also lead to the damage of the turbine. It is also very essential to operate electrical machines such as generators and transformers within a minimum ratio between voltage and frequency called volts-per-hertz ratio. This ratio defines the flux density in the generator or transformer core, which is proportional to the heat losses. High ratio of volts-per-hertz will cause the core laminations of these machines to overheat which in effect will cause the damage of these very expensive electrical machines [30].

Furthermore, when fluorescent lamps are operated below a certain threshold frequency, the discharge is extinguished and the lamp emits no light. Increase in frequency also causes the discharge to emits light continuously. Owing to this phenomenon, the lamp emits more light which in effect can lead to the damage of the fluorescent lamp. For incandescent lamps, a decrease in frequency will result in low luminous intensity of the lamp hence delivers light which is dimmer. An increase in frequency also increases the heat produced by the tungsten filament of the incandescent lamp. This causes the lamp to glow with high luminous intensity which can lead to the damage of the incandescent lamp. Also frequent frequency fluctuations can also result in shortened life of lighting loads such as incandescent lamps, fluorescent lamps, energy saving lamps.

Finally, the extensive use of electric clocks and the use of frequency for other timing purposes require maintenance of synchronous time which is dependent on frequency [31]. It is therefore crucial to keep stringent limits on the frequency variation in order to maintain the frequency stability of the power system to avert the challenges discussed above.

Methods applied to control the frequency in MHPP include automatic generation control or flow control techniques and automatic load control [25] [32]. In automatic

generation control, the generator is usually equipped with speed governor to control the speed hence the frequency of the generator by controlling the flow of water into the turbine via a valve on the turbine inlet as shown in Figure 2.1 [adapted from [31] [33]]. T_m is the mechanical torque, T_e is the electrical torque, P_m is the mechanical power, P_e is the electrical power and G is the generator.

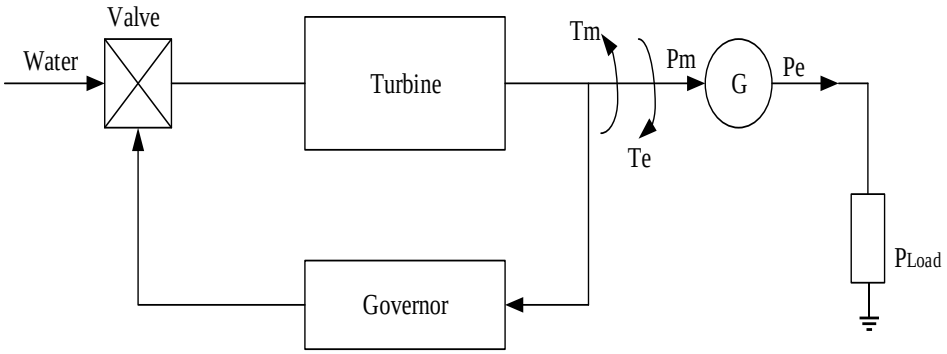

Figure 2.1: Operation of the speed governor

The principle of operation of the speed governor is that when the load on the generator changes, there occur a mismatch between T_m and T_e which results in speed and hence frequency variations. If the load on the generator increases, the speed of the generator decreases. The purpose of the speed governor is to immediately detect the load variation and command the valve of the turbine gate to open more to increase the speed of the turbine hence the mechanical power production to counteract the load increase. This action restores the generator speed or frequency at a steady state or the rated value [31] [34]. It is vice versa when the load decreases.

Although conventional speed governors are used to control the frequency of the MHPP, these governors are very expensive devices. Also mechanical control using governor is undesirable because it controls water flow directly and as a result, has a slow reaction to load variations, leading to difficulties when using sensitive loads that cannot withstand even short power fluctuations [21] [35]. They also contain many moving parts, which

will inevitably require maintenance hence making them less reliable [21] [35]. Due to these reasons conventional speed governors are not ideally suitable for MHPPs since they are uneconomical for the operation of MHPPs.

To reduce the high cost of the speed governor, one of the recent flow control techniques used in the frequency control of MHPP is the use of servomotor together with a control circuitry as a governor [36]. A servomotor is a precision electric motor whose function is to cause motion in the form of rotation or linear motion in proportion to a supplied electrical command signal. In this method of frequency control, the servomotor is used as an actuator to control the spear-valve of gate opening. This controls the opening and closing of the turbine gate hence the flow of water into the turbine when there is a variation in the generator load so as to maintain the frequency within specified limits, typically to that of the conventional speed governor.

Although, servomotors as speed governors are suited for the frequency control of MHPPs since they are less expensive than conventional governors but this actuators are subjected to wear due to friction between the gearing system, high levels of vibration, they are also subjected to large errors if a control pulse is missed. They also respond slowly and there is the tendency of the spear-valve to clog with small debris hence degrading their efficiency [37].

In automatic load control, ELC is used. The ELC keeps the speed of the synchronous generator constant under varying load conditions. In this scenario, the generator is driven by unregulated constant flow power turbine where the gate opening is kept in a specific position that guarantees a nominal mechanical power at the generator shaft and ELC dumps the excess power generated to a damper load. This permits the use of turbine with no flow regulating devices [11] [12] [13]. Compared to speed governors used in flow control technique, ELCs perform quicker, last longer, easy to install and main-

tain and cost less hence making it ideal for the frequency control of MHPP [33].

However, the controller wastes big quantities of water when little electrical power is required by the users by diverting excess power to a damper load. This is not a major concern, due to the fact that MHPPs are run-off river plants and hence, it does not matter whether the water is wasted by generating power to supply the damper load. Even, the power supplied to the damper load can be useful for other applications such as for charging batteries and providing heat for domestic use such as for cooking, boiling water and baking [32] [38].

2.2 Components of a Micro Hydro Power Plant

Basically, MHPP has three major components namely the civil, mechanical and the electrical parts.

2.2.1 The Civil Components

As shown in Figure 2.2 [adapted from [39]], the civil components include the weir intake, power canal, forebay tank, penstock, power house and the tailrace.

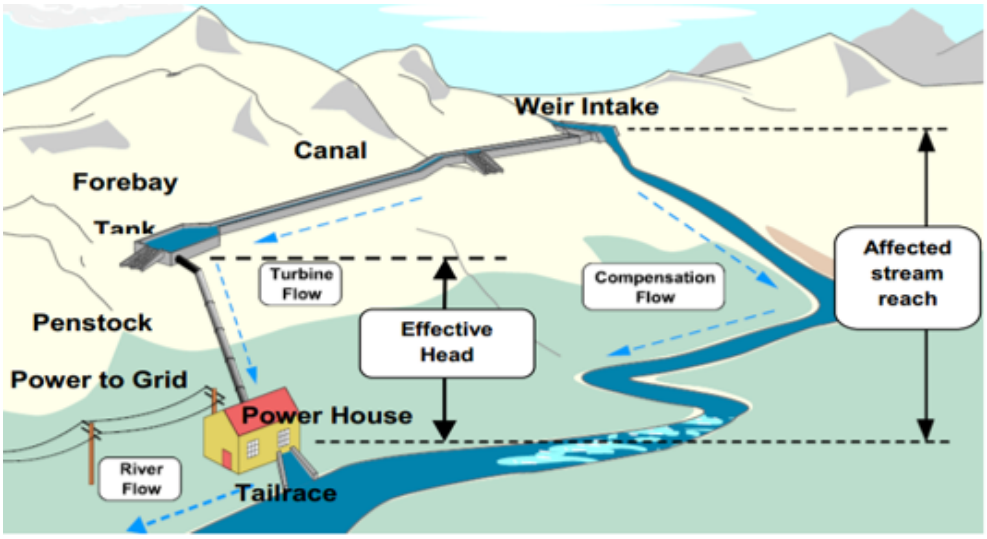

Figure 2.2: Civil work components of the MHPP

Weir intake is basically the source of water to the MHPP. It diverts stream flow from the water course and hence controls the flow of water and increases the elevation to create the head. The power canal conveys water from intake to the forebay tank usually made of earth or concrete. The forebay tank also called settling basin basically slows down sufficiently the water coming from the canal for suspended particles to settle out. It therefore prevents sediments from entering the mechanical turbine which can lead to damage or shortened life.

The penstock transfers the collected water from the forebay tank to the turbine. The purpose of the penstock is to provide the shortest path and largest elevation drop before the water enters the turbine. This head pressure provides the driving force to operate the turbine. The power house accomodates all the electric power producing equipment and control devices. The used water enters the tailrace from the turbine and returns to the stream of origin [40].

2.2.2 Mechanical Components

Basically, the mechanical components consist of the turbine and the speed governor. In modern MHPP, ELC is used instead of the governor because of the high cost, complexity and fault proneness of the governor as a result of its hydraulic moving parts. Figure 2.3 [adapted from [10]], illustrates the mechanical and electrical components with associated control system for a MHPP with ELC and dump loads.

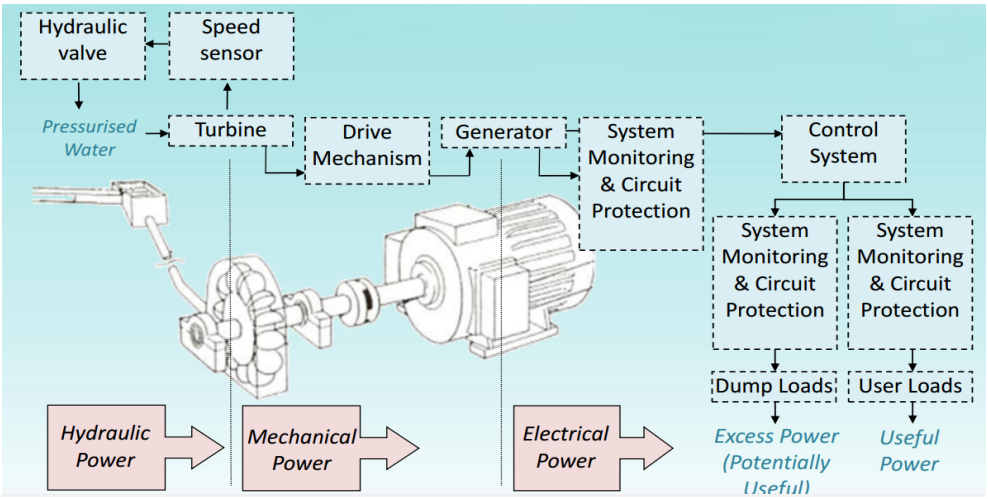

Figure 2.3: Mechanical and electrical components of MHPP with its control system

2.2.3 Electrical Components

The electrical part consist of the generator, a control mechanism to provide stable electrical power and electrical transmission lines to deliver the power to the consumer loads. In this work, consideration is given to the electrical part emphasising on the control mechanism as shown in Figure 2.3.

A generator converts mechanical energy produced by the turbine into electrical energy using the principle of electromagnetic induction. There are two basic types of generators suitable for MHPP. These include synchronous and induction generators. Synchronous generators have more advantages over induction generators because they can run in isolated grid areas, are readily available in the market, require no excitation capacitors to provide reactive power, are highly efficient, have in-built automatic voltage regulator for voltage regulation and using synchronous generator with ELC can achieve good frequency regulation. However, they are more expensive than the induction generators [41].

Induction generators require external excitation to create the magnetic field required to induce current in the windings in order for them to start. This is achieved by using suitably sized capacitors. In spite of this, induction generators are generally the cheapest option for MHPPs as induction motors which are widely and cheaply available in the market can simply be operated in reverse as induction generators which also work effectively in isolated grid areas. However, for higher application, the excitation capacitors become expensive, therefore making synchronous generators a more attractive option [42].

2.3 Synchronous Generator Modelling

Synchronous generator also called an alternator is an electrical device used to convert mechanical energy of the prime mover into electrical energy and constitute the principal source of electric energy generation in power systems. The synchronous generator is also by definition synchronous, meaning that the electrical frequency produced is locked in or synchronised with mechanical rate of rotation with the generator [31] [22].

In principle synchronous generator consist of windings in the rotor (field windings) and the stator (armature windings). The rotor is rotated by a prime mover while a DC supply called the field current, I_f or excitation current is applied to the field windings. This results in a rotating magnetic field that induces a voltage on the stator windings according to Faraday's law of electromagnetic induction. The frequency of the generated voltage is dependent on the speed of rotation of the rotor and the number of poles of the machine as given by (2.2) [31] [22].

$$f_e = \frac{nP}{120} \tag{2.2}$$

where,

f_e = electrical frequency (Hz),

n= speed (rpm),

P= number of poles.

The excitation of synchronous generators is not grid dependent since they are able to create the required magnetic field using permanent magnet or electro-magnet. This make them ideal for standalone power generation systems.

The mathematical description of the synchronous generator can be modelled using the swing equation popularly known as the equation of motion. The swing equation states that the net torque, which causes acceleration or deceleration of the rotor of the synchronous generator, is the difference between the electromagnetic torque and mechanical torque applied to the generator [31]. Therefore, when there is an imbalance between the torques acting on the rotor, the net torque causing acceleration or deceleration is given by (2.3) [31].

$$T_a = T_m - T_e \tag{2.3}$$

where,

T_a =accelerating torque (Nm),

T_m =mechanical torque (Nm), and

T_e = electromagnetic torque (Nm).

The combined inertia of the generator and prime mover is accelerated by the imbalance in the applied torques. Hence, the equation of motion is given by (2.4):

$$J\frac{d\omega_m}{dt} = T_a = T_m - T_e \tag{2.4}$$

where,

$J =$ combined moment of inertia of generator and turbine (kgm^2),

$\omega_m =$ angular velocity of the rotor (rad/s), and

$t =$ time (s) .

Normalising (2.4) in terms of per unit inertia constant H, defined as the kinetic energy in watt-seconds at rated speed divided by the VA base. Therefore using ω_{0m} to denote rated angular velocity in mechanical radians per second, the inertia constant is

$$H = \frac{1}{2}\frac{J\omega_{0m}^2}{VA_{base}} \tag{2.5}$$

The moment of inertia J in terms of H from (2.5) is

$$J = \frac{2H}{\omega_{0m}^2}VA_{base} \tag{2.6}$$

Substituting (2.6) into (2.4) gives

$$\frac{2H}{\omega_{0m}^2}VA_{base}\frac{d\omega_m}{dt} = T_m - T_e \tag{2.7}$$

Rearranging (2.7) gives

$$2H\frac{d}{dt}\left(\frac{\omega_m}{\omega_{0m}}\right) = \frac{T_m - T_e}{VA_{base}/\omega_{0m}} \tag{2.8}$$

$$2H\frac{d}{dt}\left(\frac{\omega_m}{\omega_{0m}}\right) = \frac{T_m\omega_{0m} - T_e\omega_{0m}}{VA_{base}} \tag{2.9}$$

$$2H\frac{d}{dt}\left(\frac{\omega_m}{\omega_{0m}}\right) = \frac{P_m - P_e}{VA_{base}} \tag{2.10}$$

where,

$P_m =$ mechanical input power to the synchronous generator (W), and

$P_e =$ electrical power generated by the generator (W).

In terms of per unit (2.10) can be rewritten as

$$2H\frac{d\overline{\omega_m}}{dt} = \overline{P_m} - \overline{P_e} \tag{2.11}$$

From (2.9),

$$\overline{\omega_r} = \frac{\omega_m}{\omega_{0m}} = \frac{\omega_r/P_f}{\omega_0/P_f} = \frac{\omega_r}{\omega_0} = \overline{\omega_m} \tag{2.12}$$

where,

$\omega_r =$ angular velocity of the rotor (rad/s),

$\omega_{0m} =$ rated angular velocity of the rotor (rad/s),

$P_f =$ number of field poles.

If δ is the angular position of the rotor in electrical radians with respect to a synchronously rotating reference and δ_0 is its value at $t = 0$ then,

$$\delta = \omega_r t - \omega_0 t + \delta_0 \tag{2.13}$$

Taking the time derivative, we get

$$\frac{d\delta}{dt} = \omega_r - \omega_0 = \Delta\omega_r \tag{2.14}$$

and

$$\frac{d^2\delta}{dt^2} = \frac{d\omega_r}{dt} = \frac{d\Delta\omega_r}{dt} = \omega_0\frac{d\overline{\omega}_r}{dt} = \omega_0\frac{d\Delta\overline{\omega}_r}{dt} \tag{2.15}$$

From which

$$\frac{d\overline{\omega}_r}{dt} = \frac{d\Delta\overline{\omega_r}}{dt} = \frac{d\Delta\overline{\omega_m}}{dt} \tag{2.16}$$

Substituting (2.16) into (2.11), we obtain:

$$2H\frac{d}{dt}\Delta\overline{\omega_r} = \Delta\overline{P_m} - \Delta\overline{P_e} \tag{2.17}$$

Getting the Laplace transformation of (2.17)

$$2Hs\Delta\overline{\omega_r} = \Delta\overline{P_m}(s) - \Delta\overline{P_e}(s) \tag{2.18}$$

$$\Delta\overline{\omega_r} = \frac{\Delta\overline{P_m}(s) - \Delta\overline{P_e}(s)}{2Hs} \tag{2.19}$$

Equation (2.19) represents the equation of the synchronous generator coupled with a prime mover. Now including the effect of load damping on the system in (2.19) as shown in Figure 2.4, the closed-loop transfer function relating the output and the input of the synchronous generator used in this work was modelled as follows:

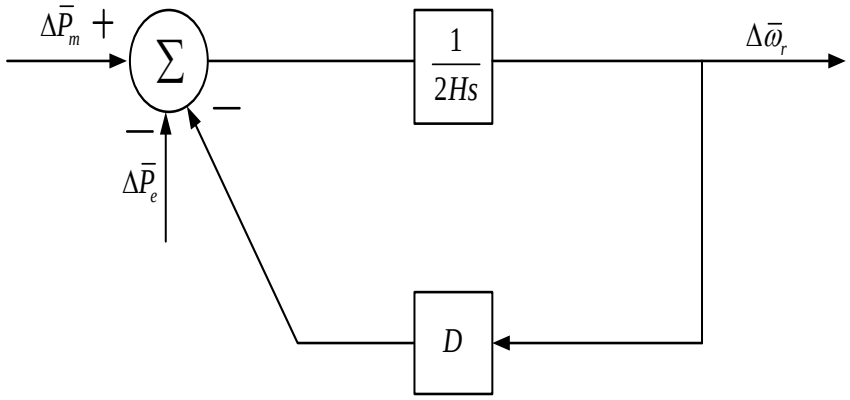

Figure 2.4: Synchronous generator model

From control theory, the closed-loop transfer function of a system is

$$G(s) = \frac{Y(s)}{U(s)} = \frac{C(s)}{1 + C(s)H(s)} \tag{2.20}$$

Therefore, the transfer function of the synchronous generator was modelled as:

$$G(s) = \frac{Y(s)}{U(s)} = \frac{\Delta\overline{\omega}_r}{\Delta\overline{P_m} - \Delta\overline{P_e}} = \frac{1}{2Hs + D} \tag{2.21}$$

where,

$H =$ inertial constant (MW.s/MVA), and

$D =$ damping constant.

2.4 Voltage Control Methods for Synchronous Generator

In synchronous generators, voltage is controlled by the control of reactive power balance of the system [31]. There are two main methods used in the voltage control of synchronous generators. This include automatic voltage control and manual voltage control.

2.4.1 Automatic Voltage Control

In automatic voltage control, the synchronous generator is normally equipped with AVR to control the voltage. The AVR basically functions to control the excitation system of the generator to provide necessary direct current to the field winding of the synchronous generator so as to maintain the required terminal voltage. The excitation system is therefore the main component in the AVR loop which delivers DC current to the synchronous generator field [31] [43]. The following are the different types of excitation systems. This include DC excitation system, AC excitation systems, brushless AC excitation systems and static excitation systems. DC excitation system used in this work is discussed.

DC Excitation Systems

In DC excitation system, the field of the main synchronous generator is fed from a DC generator, called exciter driven from the same shaft as the synchronous generator itself or from an external DC source. Since the field of the synchronous generator is in the rotor, the required field current is supplied to it through slip rings and brushes. A simple DC excitation system with AVR is shown in Figure 2.5 [adapted from [43]]. The AVR operates such that when the terminal voltage of the main generator decreases, there results a decrease in $|V|$. This immediately results in an increased error voltage

which in turn, causes increased values of excitation current I_e of the exciter, and field current I_f of the main generator. As a result the generator flux increases, thus raising the magnitude of the internal generator emf and hence the terminal voltage [43].

The major challenge of DC excitation system is that it has a slow response and sometimes a huge DC generator is required to supply the required field current to the synchronous generator. For these reason, DC excitation system are gradually disappearing [43].

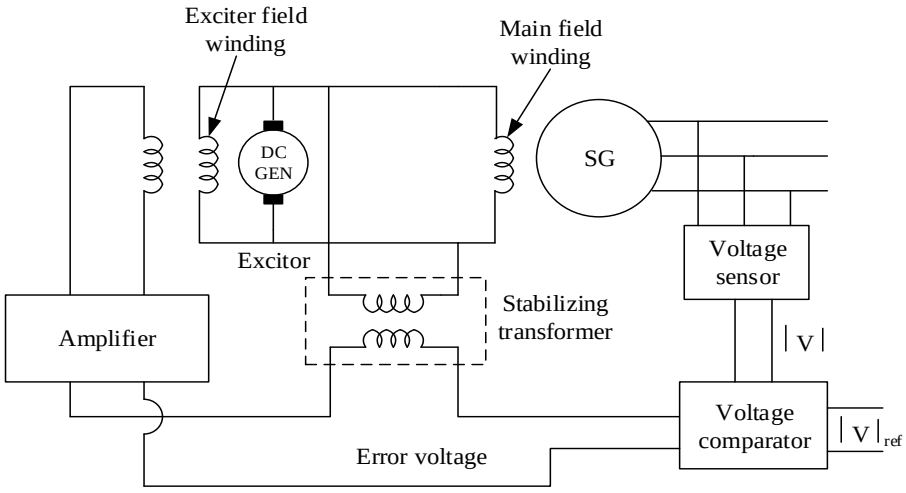

Figure 2.5: DC excitation system with field current provided by DC generator

2.4.2 Manual Voltage Control Method

In the event where the synchronous generator have no inbuilt AVR, the voltage of the synchronous generator can be controlled manually by an operator. In manual control mode, the operator monitors the level of the generator output voltage with a voltmeter and then adjust the field current of the generator to maintain desired voltage. This method of voltage control is not commonly used since the accuracy and smooth voltage control by the operator may not be achieved [44].

2.5 Frequency Control of Micro Hydro Power Plants

A control system is needed in MHPP to maintain the desired frequency of electrical equipment and shaft speed of the power generating equipment within the desired limits. Since most MHPPs are constructed without speed governors to reduce the cost, ELC together with a sensing transducer and a damper load are normally used to act in place of the governor to control the frequency of the generator output. The principle behind the design of the ELC is that the generator power output remains constant despite varying consumer load. Since most MHPPs are run-off river plants without water storage facilities, it does not matter that there is energy wasted through the damper load; the water would still have flowed downstream anyway without generating useful energy. The design of the ELC is guided by the following mathematical equation

$$PG = P_C + P_D \tag{2.22}$$

where,

$PG =$ generated power output (W),

$P_C =$ consumed load (W), and

$P_D =$ damped load (W).

2.5.1 Electronic Load Controller

An ELC is an electronic device used to control the output power and hence the frequency of a MHPP system by maintaining a near constant load on the generator. As shown in the load response diagram (a) and the single line diagram (b) of ELC in Figure 2.6 [adapted from [45]], the generating unit continuously operates at constant power output which is at any instant absorbed by the consumers. The mismatch between generated power and load causes deviation in system frequency from the nominal value. Therefore, when disconnecting an electrical load another one of similar magnitude

must be switched on immediately in order to keep generated and consumed power in equilibrium. These adjustments of loads is done automatically by ELC.

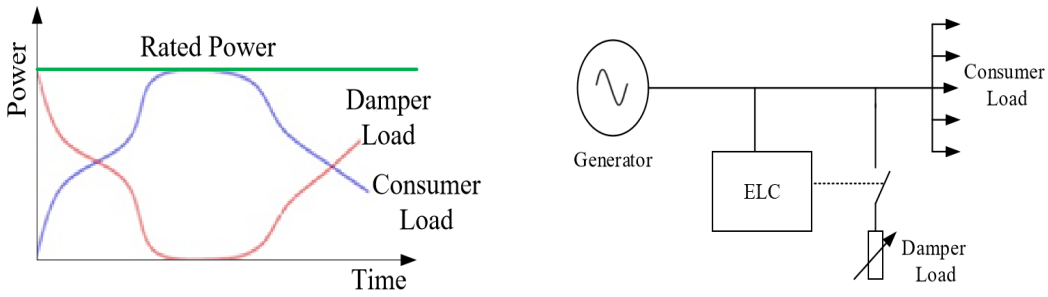

(a) Load response diagram (b) Single line diagram

Figure 2.6: Load response diagram and single line diagram of ELC

Therefore, ELC govern the generator speed thus frequency by automatically sensing and adjusting the sharing of the total load between the consumer and damper loads, since frequency is directly proportional to the speed of the generator. This control action by the ELC causes the generator load to remain constant [13]. The ELC switches any power not consumed by the consumer circuit into a damper load which are normally resistors, heating elements or batteries. The ELC therefore maintains a constant electrical load on a generator in spite of changing consumer loads.

The importance of the ELC cannot be overemphasised in that it protects the generator and electrical appliances connected to the generator from damage. It does so by maintaining a constant speed and thus frequency at the generator shaft. It has no moving parts. It is cost effective, reliable and it is virtually maintenance-free [11].

2.5.2 Damper Loads

In a micro-hydro system, damper loads are used to absorb the excess power not required by the consumer loads through the activation by an ELC. Damper loads are electrical resistive loads sized to equal or be slightly greater than the total power out-

put of the generator they are connected to. It is therefore very important to know the ratings of damper load during sizing in order to ensure its proper operation [12]. Figure 2.7 shows a space heater for a 3-phase load. Other examples of damper load include water heaters which can be used by people living together for common bathrooms, cookers and batteries.

Figure 2.7: Space heater for a 3-phase load

2.5.3 Damper Load Control Methods

The power electronic devices used to actuate the power flow to the damper loads can be relays, thyristors, MOSFETs, IGBTs and TRIACs. The switching of these electronic devices can be controlled using a microcontroller. In principle, relays are not normally used because they offer basic flow on/off resulting in unstable control and tend to wear out quickly. Thyristors, MOSFETs, IGBTs and TRIACs are mostly used for sophisticated control applications because they have a better power handling to price ratio. But for effective and smooth switching of the AC power to the damper load a TRIAC is more reliable and efficient since it is bidirectional. TRIACs are also cheaper than the other switching devices. However they have limited current ratings of up to

40 A, when compared to thyristors, MOSFETs and IGBTs [46] [47].

For applications involving high power ratings MOSFETs, IGBTs and thyristors are normally preferable since they can withstand high current without the need for heatsinks. These devices have a maximum current rating of up to 600 A. However these switching devices are very expensive as compared to TRIACs [46] [47]. There are two main techniques employed for controlling the amount of power diverted to the damper load. They include phase angle control and binary load configuration [33].

Phase Angle Control

In phase angle regulation, the damper load comprises of a permanently connected single resistive load of magnitude equal to or slightly greater than the total power output of the generator. As a result of the detection of a change in the consumer load, the firing angle of power electronic switching device, such as a TRIAC, is adjusted, to divert power to the damper load corresponding to the change in consumer load so as to keep the frequency constant. A TRIAC is basically, a three terminal semiconductor device for controlling current in either direction of the AC sine wave. It is basically two thyristors joined back to back with common gate. This method of damper load control is efficient since it provides a smooth switching of the TRIAC to control the power to the damper load [33] [48].

To epitomize it all, phase angle control uses a switching device to chop the AC mains supply such that only part of each half cycle of the AC mains supply is applied to the load. For the remaining part the switch is open and no power is applied to the load. The amount of power to the load is therefore determined by the phase angle of the AC supply at which the switching occurs. The switching is synchronised to each half cycle to reduce the visual impact of momentarily switching off the damper loads. Figure 2.8

[adapted from [49]] shows the firing angle of phase angle control.

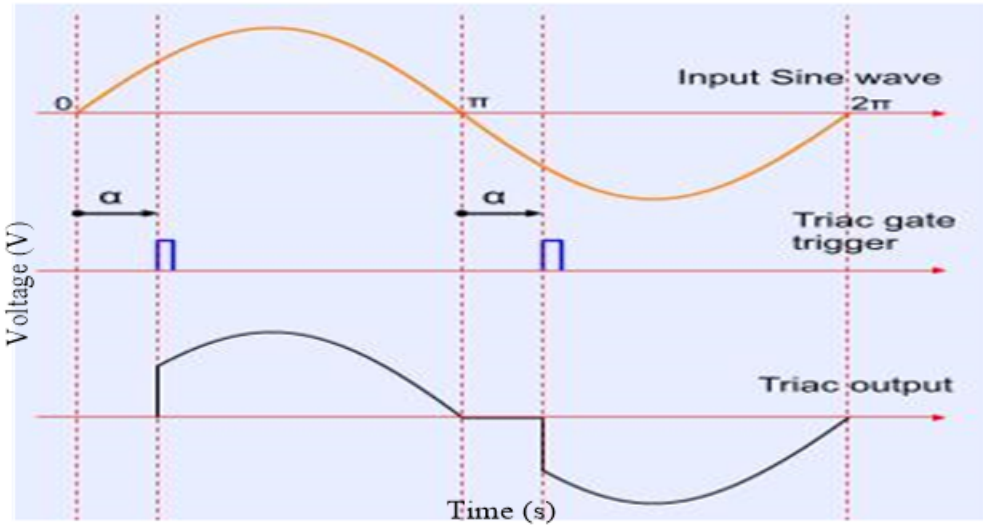

Figure 2.8: Diagram depicting phase angle control

Binary Load Configuration

In binary load regulation the damper load is made up from a switched combination of binary arrangement of separate resistive loads. In response to a change in the consumer load, a switching selection is made to connect the appropriate combination of load steps using solid state relay. Hence with a binary set of damper loads, each damper load is switched either completely on or completely off [33] [48].

Although, the control algorithm employed in this system is simple since a simple ON and OFF control by a solid state relay is used, but it is quite expensive because the cost of solid state relay are much higher than the TRIACs. Also the number of damper loads and the associated wiring cost is high and to achieve smooth regulation, the damper loads should all have exactly the right capacity. This is because with a low number of damper loads, steps between damper load combinations remain too large and the system cannot regulate smoothly [33] [48].

2.5.4 Zero Crossing Detector Circuit

The zero crossing detector circuit is an electrical circuit that gives a pulse as indication when the mains sine wave crosses the zero line. The purpose of the circuit is to synchronise the firing angle of TRIACs with the zero crossing detector pulse to ensure proper operation of the TRIACs. In other words, the purpose of the zero crossing detector circuit is to start the TRIAC conducting at the point when the sine wave crosses the zero line. The AC sine wave has a zero crossing point twice every cycle from 0°-180° and 180°-360°.

The zero crossing point is very essential in the control of TRIACs as applied in phase angle control, in the sense that if the control signal to the TRIAC is applied at any point during the AC output wave other than the zero crossing point, the TRIAC will wait to switch on until the next zero crossing point.

Again, the AC power is controlled by varying the firing angle to the TRIAC gate in both half cycles with respect to zero crossing points. Hence to generate the pulses with appropriate delay, the microcontroller has to be given the zero crossing instants. Moreover, to avert the problem of Electromagnetic Interference (EMI) and safe operation of the switching device a zero crossing detector circuit is necessary.

The supply to the TRIAC is an AC signal and it will always turn off when the applied voltage reaches zero at the end of the current half-cycle. If a turn-on pulse is applied at some controllable point after the start of each half cycle, it will directly control the percentage power of that half-cycle that gets applied to the load. This makes the TRIAC ideal for controlling power to a damper load. The equation governing the average power that flows to the damper load in relation with the firing angle in phase angle control is discussed as follows [50]: In this work a purely resistive loads were

used as damper loads hence the voltage and current are in phase. Also, in phase angle control, the firing angle (α) of the TRIAC is controlled by varying between ($0^\circ \leq \alpha \leq 180^\circ$) which controls the average power to the damper load.

Hence the rms output voltage is given by

$$V_o = V_s\sqrt{\frac{1}{\pi}(\pi - \alpha + \frac{sin2\alpha}{2})} \tag{2.23}$$

Since the voltage and the current are in phase for a purely resistive damper load, the rms current is also given by

$$I_o = I_s\sqrt{\frac{1}{\pi}(\pi - \alpha + \frac{sin2\alpha}{2})} \tag{2.24}$$

But power is a product of voltage and current, hence the average power output to the damper load is given by

$$P_o = V_o I_o \tag{2.25}$$

Substituting the values of V_o and I_o in (2.23) and (2.24) into (2.25) and simplifying gives

$$P_o = V_s I_s \frac{1}{\pi}[\pi - \alpha + \frac{sin2\alpha}{2}] \tag{2.26}$$

But,

$$I_s = \frac{V_s}{R} \tag{2.27}$$

Substituting, I_s in (2.27) into (2.26), the average power to the damper load is given as

$$P_o = \frac{V_s^2}{\pi R}[\pi - \alpha + \frac{sin2\alpha}{2}] \tag{2.28}$$

where,

$P_o =$ output power (W),

$V_s =$ peak voltage (V),

$R =$ resistance of damper load (Ω),

$I_s =$ peak current (A) and,

$\alpha =$ firing angle.

It must however be noted that, in this work a 3-phase circuit with different zero crossings for each phase is used and thus, the triacs are not fired simultaneously.

2.5.5 Frequency Sensing Transducer of the ELC

The frequency sensing element of the ELC measures the generator frequency so as to serve as the basis for the ELC to take appropriate control measures to keep the frequency constant by diverting excess power to the damper load.

Some of the conventional sensors used as frequency sensors for generators are tachogenerators and shaft encoders. Tachogenerator is a device capable of producing electrical power from mechanical energy, usually turning of a shaft. When not connected to a load resistance, the generator will generate voltage roughly proportional to shaft speed, thus used for measurement of shaft speed of generators.

Shaft encoders are electromechanical devices which convert angular position or motion of a shaft to a digital or pulse signal. The most popular type of shaft encoders is the optical shaft encoder. In operation, an optical shaft encoder uses optical sensing technology which relies on the rotation of a disk that has patterns of opaque and transparent sectors coded into the disk. The disk is rotated in a beam of light such as an LED and the markings on the disk act as shutters blocking and unblocking the light.

An internal photodetector senses the alternating light beam and the encoder's electronics convert the pattern into a digital signal or pulse output that is then passed on to an external control system through the encoder's output [51].

Among the various sensors discussed, shaft encoders are most commonly used in MHPPs [52]. This is due to the fact that shaft encoders are characterised by high resolution and high operating speeds [51]. However, the limitations of these sensors are that they are mechanical devices hence several environmental factors such as temperature fluctuations, vibrations and contaminants such as dirt and dust affect their performance. Also, the disk in the encoder can break and the LED inside the shaft encoder has limited lifespan hence can lead to eventual failure of the shaft encoder [52]. The shaft encoder is also mounted on the shaft of the generator, hence any small misalignment on the shaft can also affect the performance of the sensor. Moreover, they are also very expensive [17]. Hence there is the need for a more accurate and reliable sensor. This is achieved using Magnetostrictive Amorphous Wire (MAW).

Magnetostrictive Amorphous Wire Sensor

MAW sensor is prepared by rapid quenching in rotating water. The molten alloy cools rapidly to bypass crystallisation phase resulting in a wire shaped amorphous solid [53]. The MAW sensor operates based on the principle of Large Barkhausen Jump (LBJ) and its unique magnetic properties have successfully been applied in various electronic sensors and devices [53]. Figure 2.9(a) shows the magnetic hysteresis loop and Figure 2.9(b) shows LBJ for $(Fe_{50}Co_{50})_{78}Si_7B_{15})$ Wire.

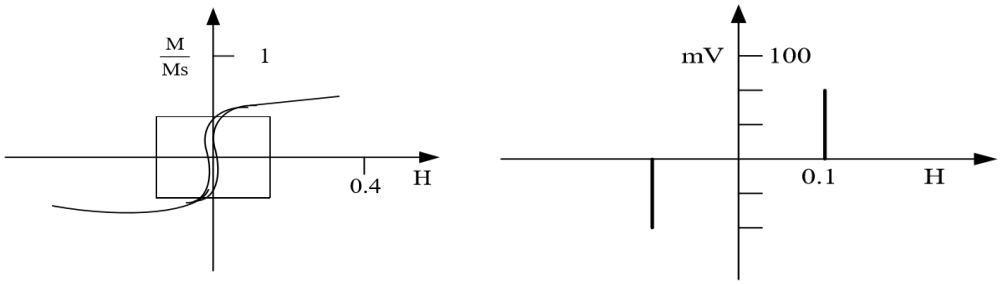

(a) Low and high field M-H loops (b) Voltage pulse induced in a pick-up coil during LBJ

Figure 2.9: MAW characteristics

MAW sensor is characterised by the following unique magnetic properties [15]: they show LBJ/discontinuity resulting from the combination of wire geometry and stress induced anisotropy. LBJ is defined as the sudden change of magnetisation at a single value of magnetic field. LBJ is important, since almost all sensors communicate to the outside world by providing a voltage and the induced voltage is proportional to the rate of change of flux with time hence necessity for large flux change with time.

Secondly, they show matteucci effect due to torsional stress induced during rapid quenching of the molten alloy. This makes it suitable for applications such as accelerometers, stress sensors, etc. A sharp voltage pulse generated between the ends of the amorphous wire is referred to as the matteucci effect. This occurs because when amorphous wire is placed in a coil, it generates magnetic field when an alternating current is applied. Further, they show magneto impedance effect quite useful for sensor applications such as for a magnetic field sensor. This property refers to the change in impedance with an external field Hex due to skin effect when a high frequency wire current is applied through it. And lastly, they show magneto elastic properties, which can be applied in distance sensors.

Other striking features of the wire are high maximum tensile stress (σ :200 - 400 kg/mm^2) and hence can be drawn to very small diameters, small in size (50 μm - 300 μm diameter), uniformity (due to the absence of grain boundaries) and smooth surfaces this results in smooth and stable flux reversal by domain wall motion due to small number of nucleation centres and domain wall pinning points, reduced eddy currents due to magneto-elastic wave causes the wire to possess high resistivity (σ :120 - 190 $\mu\Omega cm$) and resistance to corrosion. In this work the LBJ property in the MAW will be employed for generator frequency sensing.

Advantages of MAW Sensor

MAW sensor has the following advantages that make it suitable for use as a sensor: high signal to noise ratio, quick response with cut-off frequency of more than several kilohertz, high stability against temperature variations, insensitivity to mechanical vibrations, it is small in size (wire diameter is in the order of micrometre), high reliability and little aging for long time usage, digital output for good matching with microcomputer, good corrosion resistance, outstanding elasticity and excellent electromagnetic properties [16].

Disadvantages of MAW Sensor

The major disadvantage is that a critical wire length is required to give optimal results. Also, the distance of the wire with respect to the object to be sensed and the strength of the magnet used influence the performance of the sensor [16].

2.6 DC Motor as Prime Mover

A DC motor is a machine which converts DC electrical energy into mechanical energy. In this work a DC series wound motor is used as a prime mover because of its torque speed characteristics against the armature current. Also, it is very much easy to control the speed of a DC motor than AC motor [22] [54]. The DC series motor equivalent circuit is shown in Figure 2.10.

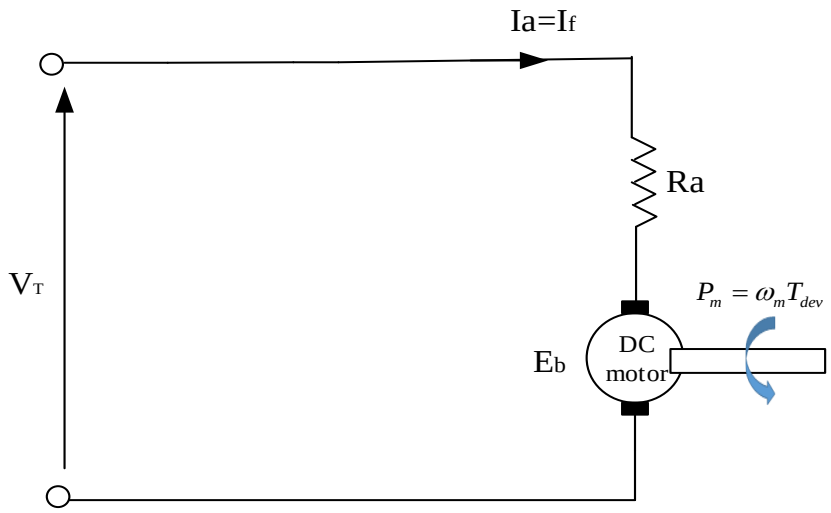

Figure 2.10: DC series motor equivalent circuit

The torque developed by the armature of the DC motor when running is given as

$$T_a = 0.159\phi Z I_a \left(\frac{P}{A}\right) Nm \tag{2.29}$$

where,

T_a= armature torque(Nm),

ϕ= flux (Wb) ,

Z= number of conductors,

I_a= armature current(A),

P= number of poles, and

A= number of parallel paths.

From torque equation in (2.29), it can be seen that

$$T_a \propto \phi I_a \tag{2.30}$$

Since a series DC motor is used, the flux(ϕ) is also directly proportional to the armature current(I_a) due to the fact that the field winding carry full armature current.

Hence,

$$T_a \propto I_a^2 \tag{2.31}$$

Again, from the voltage equation of a DC motor, the back emf(E_b) produced in the armature conductors when the armature starts rotating which opposes the applied voltage(V) is given by

$$E_b = V - I_a R_a = \phi Z N \left(\frac{P}{A}\right) \tag{2.32}$$

where P, Z and A are constants. Therefore, from (2.32) it can be said that the back emf is directly proportional to the flux and speed (N) given by (2.33).

$$E_b \propto \phi N = K \phi N \tag{2.33}$$

or

$$N \propto \frac{E_b}{\phi} = \frac{K E_b}{\phi} rpm \tag{2.34}$$

With the two governing equation in (2.31) and (2.34) it can be observed that flux is directly proportional to I_a and speed is inversely proportional to I_a. It can also be found that when speed is high, torque is low and vice versa. Therefore, when armature current I_a is very small, the speed becomes dangerously high. But at heavy loads, armature current I_a is large and hence the speed is low which results in decreased

back emf E_b. These characteristics makes series DC motor useful for variable speed application [54]. This therefore justifies why a series DC motor is used in this work as the prime mover to the synchronous generator since in a typical MHPP, speed and thus the frequency increases with decrease in load and vice versa.

2.6.1 DC Motor Speed Control Methods

The back emf generated by a DC motor is given by

$$E_b = K\phi N = V_T - I_a R_a \tag{2.35}$$

where,

$E_b =$ Back emf (V,)

$K =$ armature constant,

$\phi =$ flux/pole ($Weber$),

$N =$speed of rotation (rpm),

$V_T =$ terminal voltage (V),

$I_a =$armature current (A), and

$R_a =$ resistance of armature winding (Ω).

Rearranging (2.35) the speed of the DC motor is given as

$$N = \frac{(V_T - I_a R_a)}{K\phi} \tag{2.36}$$

Hence from (2.36), it is evident that the speed of a DC series motor can be controlled by armature voltage control and armature resistance control.

Armature Voltage Control

In this method of speed control, R_a and ϕ are kept constant. In normal operation, the drop across the armature resistance is small compared to E_b and hence:

$$E_b = V_T \tag{2.37}$$

Since,

$$E_b = K\phi N \tag{2.38}$$

The speed can be expressed as

$$N \cong \frac{V_T}{K\phi} \tag{2.39}$$

From (2.39), if the flux is kept constant, the speed changes linearly with the terminal voltage. Hence when the terminal voltage is increased, the speed of the DC motor also increases and vice versa. This method provides smooth variation of speed control.

Armature Resistance Control

In this method of DC motor speed control, the voltage across the armature is varied by inserting a variable resistance in series with the armature circuit. As the armature resistance R_a is increased, the p.d across the armature is decreased hence the speed of the motor decreases. This method is used when speed below the no-load speed is required.

2.7 Artificial Intelligence

There are so many definitions of Artificial Intelligence (AI). Basically, AI is the study and creation of computer systems that can perceive, reason and act like a human. The primary aim of AI is to produce intelligent machines which perform humanlike operations and decisions in order to speed up production, to eliminate humans in tasks done in dangerous environments or just to give humans support in their decisions and actions. Over the years AI has played tremendous roles in the control of power systems and thus improve their performance and reliability. This is because AI techniques have the ability to handle non-linear, dynamic, non-convex, discontinuous and non-differentiable functions. In this work two AI methods of fuzzy logic and BFA optimised fuzzy logic are used. BFA (Bacterial Foraging Algorithm) is a biologically inspired algorithm as explained in section 2.7.2 while fuzzy logic is explained in section 2.7.1.

2.7.1 Fuzzy Logic Controller

The fuzzy logic theory was introduced by Lotfi Zadeh in 1965 to increase the ability of controllers to cope with the problem of uncertainty, modelling human reasoning from imprecise and incomplete information by giving definitions to vague terms and allowing construction of a rule base [55]. Fuzzy logic is a set of mathematical principles for knowledge representation based on the degree of membership and degree of truth. Fuzzy logic uses the range of logical values between 0 (completely false) and 1 (completely true). The block diagram of fuzzy logic model in shown in Figure 2.11 [adapted from [56]].

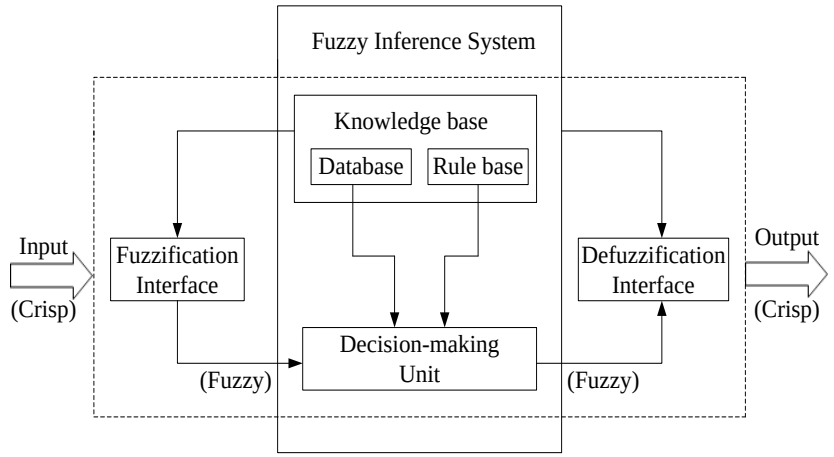

Figure 2.11: Block diagram of fuzzy logic model

The input of the fuzzy logic model is crisp value. This is then converted into fuzzy linguistic variables through the process of fuzzification using membership functions which can be triangular, trapezoidal, bell, Gaussian, etc. Basically, a fuzzification interface converts crisp values of the control inputs into fuzzy values, so that they are compatible with the fuzzy set representation in the rule base. The fuzzified output is fed into the fuzzy inference system which initiates the decision making process by using fuzzy set theory or fuzzy reasoning to map nonlinear input data set into an output scalar data using rule base. Rule base have control rules obtained from an expert knowledge or heuristics and expressed as a set of IF-THEN rules and the associated database.

The commonly used fuzzy inference system are the Mamdani and Takagi Sugeno methods, each with its own merits and demerits. In essence, the operational procedure of Mamdani inference engine is similar to that of Takagi Sugeno method. The procedures involve fuzzification of the input variables, rule evaluation, aggregation of the rule outputs, and finally defuzzification.

Rule evaluation uses fuzzy logic operators such as AND, OR and NOT to evaluate the antecedent and consequence membership functions of fuzzy IF-THEN rules. Aggregation is the unification or the summation of all the outputs of fuzzy rules by taking the membership functions of all rule consequences previously clipped or scaled and combining them into a single fuzzy set. However, the only difference between Mandani and Takagi Sugeno inference system is that for the Takagi Sugeno system, all consequence membership functions are represented by singleton spikes or the output of each fuzzy rule is constant. The outcome of the FIS is transformed to crisp values that can be sent to the plant/process as a control signal through the defuzzification process. Some of the methods used in defuzzification are centre of gravity, weighted average, mean-max, etc. [57].

Fuzzy Logic Parameter Tuning

Once the control rules are determined, the next step which is necessary is to tune or optimise the parameters of the membership functions that define the fuzzy sets. This in effect, affects the shape of the fuzzy set to give a better and improved control performance. This can be done conventionally by an expert or trial and error methods which is very difficult and subjected to errors [58]. However intelligent optimisation techniques such as Genetic Algorithm (GA), Particle Swarm Optimisation (PSO), Ant Colony Algorithm (ACA) and Bacterial Foraging Algorithm (BFA) are recently used to optimise this parameters.

Advantages of Fuzzy Logic

Fuzzy logic uses rules that express imprecision of the real world, it is easy to understand, test and maintain, easily prototyped. It can be built on top of the experience of experts, needs less rules and parallel evaluation of rules, can model nonlinear functions

of arbitrary complexity and lastly, robustness and reliability make fuzzy controllers useful in solving a wide range of control problems.

Disadvantages of Fuzzy Logic

The major problems of fuzzy logic is that they need more tests and simulation and it is difficult to exhaust all possible rules due to lack of precise mathematical models.

2.7.2 Bacterial Foraging Algorithm

Bacterial Foraging Algorithm (BFA) has been widely accepted as a global optimisation algorithm of current interest by researchers because of its efficiency in solving real-world optimisation problems arising in several application domains [59] [60] [61]. BFA is inspired by the social foraging behaviour of $Escherichia\ Coli$ bacteria present in the human intestine. The unique features of this algorithm overcome the premature convergence problem encountered in GA and PSO. Foraging theory introduced by Passino [59] is based on the assumption that animals search for and obtain nutrients in a way that maximises their energy intake E per unit time T spent given the constraints of its own physiology and environment. Hence, they try to maximise a function $\frac{E}{T}$.

The optimisation technique consists of determining the minimum of a function $J(\theta)$, where θ is the position of a bacterium in P-dimensional space i.e. $\theta \epsilon \Re^p$. J can be denoted as the nutrient surface. If $J(\theta)$ is negative, it indicates that the bacterium is in nutrient-rich environment, 0 indicates a neutral environment and a positive value indicates a noxious environment at location θ. The objective will be to try and implement a biased random walk for each bacterium where it will try to climb up the nutrient concentration, avoid noxious substances and will attempt to leave a neutral environment as soon as possible. These actions undertaken by the bacterium can be described as

chemotaxis, swarming, reproduction, and elimination and dispersal.

Chemotaxis

This process simulates the movement of an $E.\ coli$ cell through swimming and tumbling via flagella. Biologically an $E.\ coli$ bacterium can move in two different ways. It can swim for a period of time in the same direction or it may tumble and alternate between these two modes of operation for the entire lifetime. Suppose $\theta^i(j,k,l)$ represents $i-th$ bacterium at $j-th$ chemotactic, $k-th$ reproductive and $l-th$ elimination-dispersal step. $C(i)$ is the size of the step taken in the random direction specified by the tumble (run length unit). Then in the computational chemotaxis the movement of the bacterium may be represented by (2.40) [59]:

$$\theta^i(j+1,k,l) = \theta^i(j,k,l) + C(i)\frac{\Delta(i)}{\sqrt{\Delta^T(i)\Delta(i)}} \tag{2.40}$$

where, Δ is a vector in the random direction whose elements lie in [-1,1]

Swarming

A group of $E.\ coli$ cells arrange themselves in a traveling ring by moving up the nutrient gradient when placed within a semisolid matrix with a single nutrient chemoeffecter. The cells when stimulated by a high level of succinate, release an attractant aspertate, which helps them to aggregate into groups and thus move as concentric patterns of swarms with high bacterial density. The cell-to-cell signalling in $E.\ coli$ swarm may be represented by the objective function by (2.41) [59]:

$$\begin{aligned} J_{cc}(\theta, P(j,k,l)) = &\sum_{i=1}^{S}[-d_{attractant}exp(-w_{attractant}\sum_{m=i}^{P}(\theta_m - \theta_m^i)^2] \\ &+ \sum_{i=1}^{S}[h_{repellant}exp(-w_{repellant}\sum_{m=i}^{P}(\theta_m - \theta_m^i)^2] \end{aligned} \tag{2.41}$$

where, $J_{cc}(\theta, P(j,k,l))$ is the objective function value to be added to the actual objective function to be minimised to represent a time varying objective function, S is the total number of bacteria, p is the number of variables to be optimised, which are present in each bacterium and $\theta = [\theta_1, \theta_2, ...\theta_p]^T$ is a point in the p -dimensional search domain. $d_{attractant}$, $w_{attractant}$, $h_{repellant}$, $w_{repellant}$ are different coefficients that should be chosen properly.

Reproduction

The least healthy bacteria eventually die while each of the healthier bacteria, those yielding lower value of the objective function asexually split into two bacteria, which are then placed in the same location. This keeps the swarm size constant.

Elimination and Dispersal

Gradual or sudden changes in the local environment where a bacterium population lives may occur due to various reasons. For example, a significant local rise of temperature may kill a group of bacteria that are currently in a region with a high concentration of nutrient gradients. Events can take place in such a fashion that all the bacteria in a region are killed or a group is dispersed into a new location. To simulate this phenomenon in BFA some bacteria are liquidated at random with a very small probability while the new replacements are randomly initialized over the search space [60] [61]. The flowchart for BFA is in Figure 2.12 [adapted from [62]].

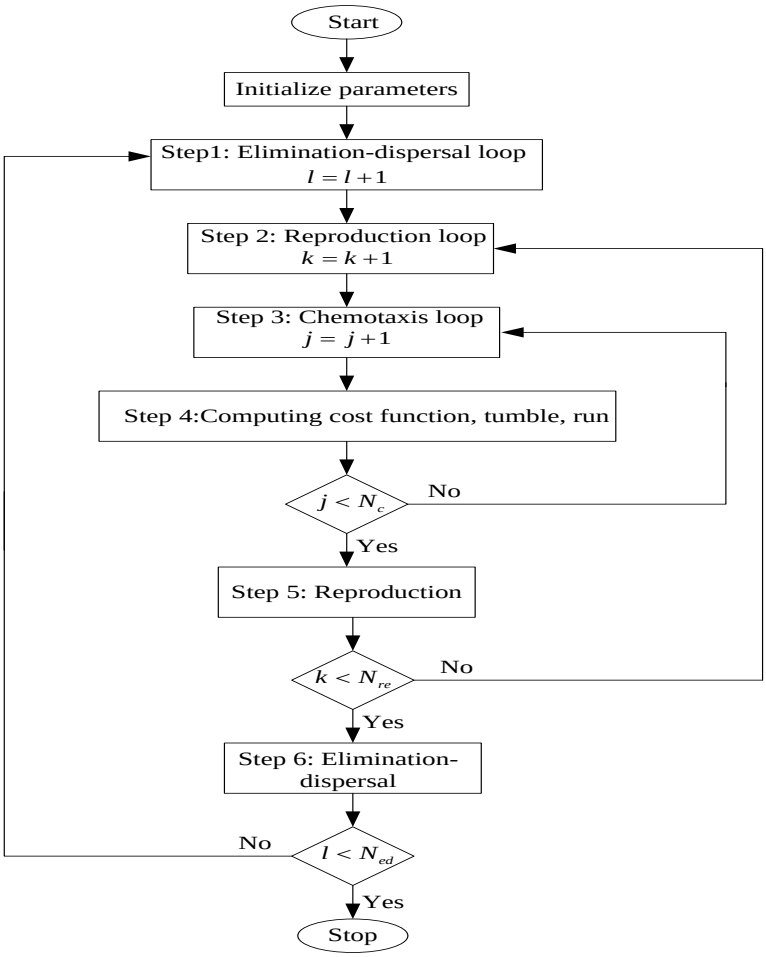

Figure 2.12: Flowchart for BFA

2.8 PID Controller

Proportional Integral Derivative (PID) controller is a control loop feedback controller used in control systems. The proportional part is responsible for desired set-point, while the integral and derivative parts account for the accumulation of past errors and the rate of change of error in the process respectively. A PID controller calculates an error value as the difference between a measured process variable and a desired setpoint and then attempts to minimise the error by adjusting the process through use of a manipulated variable. The basic block diagram of a PID controller is shown in

Figure 2.13.

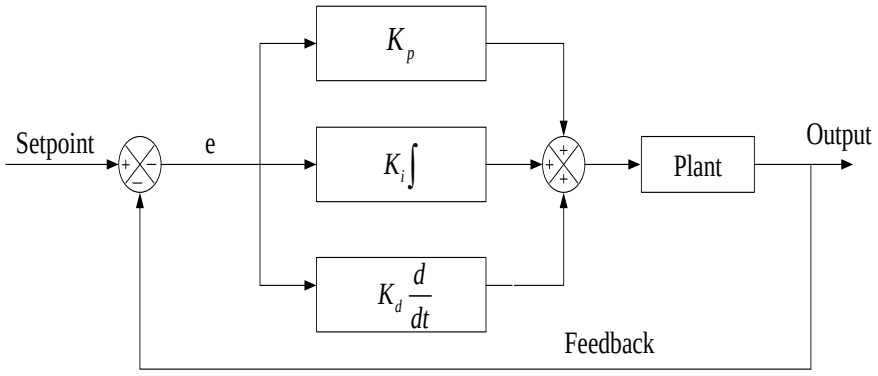

Figure 2.13: Block diagram of classical PID controller

PID controllers are commonly used in process industries. This is because of their various merits: it can be easily understood by plant operators, it has near optimal performance and wide applicability. PID controllers can be tuned using Ziegler-Nichols method. In Ziegler-Nichols tuning method, the K_i and the K_d gains are initially set to zero. The K_p gain is then increased from zero to a critical value at which sustained oscillations occur. Then, K_i is increased until any offset is corrected. Finally, K_d is increased until the loop is acceptably quick to reach its reference after a load disturbance. However, the drawbacks of using PID controllers are that they require frequent tuning and give poor performance for systems which are highly nonlinear and subjected to disturbances [63]. The general equation of a PID controller is given by

$$G(s) = K_p + \frac{K_i}{S} + K_d S \tag{2.42}$$

There are four major PID control modes used as automatic control of ELC designs in MHPP. These include P controller, PI controller, PD controller and PID controller.

The P controller is simple by design and inexpensive. The controller output is basically the output of the proportional control mode. However, the use of proportional control alone has a large drawback of introducing offset. Offset is a sustained error that cannot

be eliminated by proportional control alone.

PI controller is a controller whose output is the sum of the proportional and integral control actions. The main function of the integral control mode is to continuously increment or decrement the controller's output to reduce the error. Given enough time, integral action will drive the controller output far enough to reduce the error to zero. Hence the purpose of the PI controller is to eliminate offset but normally results in increased overshoot of the system [24].

PD controller reduces the system overshoots. The D component of the controller makes the system respond faster to system changes due to its ability to predict the future error of the system. In general, the PD controller improves the transient response of the system, but it does not improve the steady-state performance.

PID controller has all the necessary dynamics such as fast reaction on change of the controller input, elimination of offset and suitable action to eliminate oscillations. PID control therefore provide a stable control action much more than what is possible with P, PI and PD control. This control action provide a fast control action to shorten the time it takes for the system to return to its set point. However, the physical implementation of the PID controller is very expensive.

In this work a PI controller is used since it is the most widely used algorithm in the frequency control of MHPPs due to the inherent stability of proportional controller and the steady state error elimination ability of integral controller. It is also inexpensive when compared to PID controller and it returns the process to the setpoint. Moreover, the Derivative controller is not recommendable in presence of measurement noise and sudden load disturbances. This is because it amplifies the noise of the system [24].

2.9 Review on Frequency Control of MHPP

Various types of controllers have been developed to maintain the frequency of the generator within the specified limits for the MHPP [14]. Different control algorithms for frequency control such as conventional PID control and AI techniques are discussed.

PID controllers have also been used extensively for governor valve control in large hydro power plants and as controllers to regulate the speed of the generator output in MHPP hence maintaining a stable frequency. In view of this, Doolla and Bhatti [36] propose a technique for frequency control of mini-hydro plants operating in isolated mode for fully eliminating damper load using servomotor and a PI controller. Simulation results show that the controller effectively eliminated the frequency deviations under specific control of the gate valves. However, the settling time was very large around 200 seconds. Also the designed controller was a simulation model hence was not implemented.

The major challenges with the use of conventional PID controllers are that they are not suitable for complex, nonlinear, uncertain, high-order and time-delay systems. It is also slow, attains poor control performances such as high overshoots and long settling times. The control parameters are usually tuned based on the classical methods such as the well-known Ziegler-Nichols or trial-and-error approaches and therefore are incapable of obtaining good dynamic performance under various load conditions [64] [65].

In order to overcome the shortcomings of the conventional PID controllers, various modern intelligent techniques such as fuzzy logic, ANN, GA, PSO, ACA and BFA have been proposed in the literature and successfully used to tune PID parameters.

Hence, the application of intelligent techniques improves system performance by easy adjustment of controller parameters based on system dynamics.

Salhi and Doubabi [66] implement fuzzy logic controller to tune PI parameters for load frequency control of micro hydro power plant based on the Mamdani and Takagi-Sugeno fuzzy inference systems. In their design two fuzzy sets are performed. The first set has a fuzzy controller which minimises the waste of water by limiting the dissipated power on the damper load. This is achieved by controlling the gate position via a servomotor that governs the water flow. The second set was a fuzzy supervisor which controls the electrical load by dumping excess power to a damper load. The simulation results show the feasibility of the proposed fuzzy control system.

Ozbay and Gencoglu [67] present a novel technique based on adaptive fuzzy control for frequency control of a mini hydro plant. It compares both linear and nonlinear turbine models neglecting the surge tank effects and inelastic water column. An adaptive fuzzy controller is applied to Small Hydro Power Plant (SHPP) model as a governor which regulates the wicket gate position with a servo motor according to the load. The models were designed by using MATLAB/SIMULINK software. Simulation results show similar responses for load changes under both step and ramp input signals. The stabilising time however, was more because of hydraulic hammer and water inertia effects on the servo motor.

Adhikary [68] presents a new user friendly controller based on fuzzy logic for Pico Hydro Power Plant (PHPP) using a synchronous generator. The controller is able to maintain a constant frequency, the scheduled power and the voltage in spite of varying user loads. Further, the controller regulates the flow of water using a single gate made of spear-valve operated by a servomotor. Results obtained by simulation show the rapidity and the robustness of the fuzzy logic controller. Moreover, the system adjust-

ment time and overshoot decrease significantly. The author further suggests that his work can be extended to develop a method for relating fuzzy logic-linguistic variables with various efficient control algorithms.

Suhas et al [69] proposes a new control strategy based on the combination of a fuzzy controller and a fuzzy supervisor to ensure the best solution in terms of efficiency in the frequency control of MHPP. The proposed fuzzy controller is able to maintain MHPP frequency in spite of the load variations. In addition, it minimises the waste of water by limiting the dissipated power on the damper load. This is achieved by regulating the water flow rate. Simulation results show the feasibility of the proposed fuzzy control system.

Dhanalakshmi and Palaniswami [70] present an Adaptive Neuro-Fuzzy Inference System (ANFIS) architecture for load frequency control of an isolated wind-micro hydro-diesel hybrid power system, to regulate the frequency deviation and power deviations. The ANFIS Inference System trains the parameters of the fuzzy logic controller and improves the system performance. A PI controller and a fuzzy logic controller were designed separately to control the same hybrid power system for the performance comparison. Simulation results show the superior performance of the proposed Neuro-Fuzzy controller in comparison with the conventional PI controller and fuzzy logic controller in terms of the settling time, overshoot against various load changes hence damps out the frequency deviation and attains the steady state value.

Goyal et al [71] propose a flow control based model for the automatic control of Small Hydro Power Plant (SHPP). In the proposed model, a servomotor is used to control the flow of water by controlling the rotational motion of the spear valve. The suitability of servomotors for the control of SHPP is discussed and PI controllers are used to further enhance their governing capability. State space representation is used to math-

ematically model the proposed model. Parameter optimisation is also performed using ANN. Simulation results demonstrates the suitability of the proposed model for the control of SHPPs. Predictions made by the ANN controller is in good agreement with the actual values of Kp and Ki hence no need for damper load.

Recent research conducted on frequency control in power systems revealed that fuzzy logic membership functions can be tuned using stochastic optimisation algorithms such as GA, PSO, BFA, ACA, which gives an improved performance in terms rise time, settling time and percentage overshoot of the system than the other control techniques [72] [73]. In classical fuzzy methods, the boundaries of the membership functions are adjusted based on expert experiences that may be with trial and error and does not guarantee performance of the system [72] [73].

To improve the performance of the fuzzy logic controller, Boroujeni et al [74] present a load frequency control in multi area electric power system using genetic scaled fuzzy logic controller. In this new fuzzy technique, the upper and lower bounds of the fuzzy membership functions are obtained using GA. To show effectiveness of the proposed method, a classical PI type controller is designed in order to make comparison with the proposed genetic scaled fuzzy logic controller. The simulation results show an improvement of the genetic scaled fuzzy method in terms of rise time, settling time and percentage overshoot when compared with the traditional PI type method.

Jemal [75] design a self-tuning fuzzy controller for MHPPs on irrigation dams by optimising the membership functions using GA to control a PI controller. The performance of the proposed fuzzy logic controller is tested through simulation studies using MATLAB/SIMULINK. It is observed from the simulation results that the average overshoot for 30% load change is 4.6% and the settling time is 7.5 seconds with the proposed fuzzy logic controller while overshoot is 8.9% and 13.5% and settling time

of 11 seconds and 29 seconds with PI load control and PI flow control respectively. The proposed fuzzy controller is able to maintain the frequency of a MHPP within tolerable limits in spite of the damping constant variation and load variations.

Zargari et al [76] design a fuzzy sliding-mode governor to realize the frequency control of an isolated small hydropower system. PSO algorithm is adopted to regulate the membership functions of fuzzy system more accurately, and an estimator is suggested for estimating and identifying the system variables to reduce the costs of implementing the control method. Simulation results show an improved performance of the controller in terms of rise time, settling time and percentage overshoot.

Literature has shown that GA method is usually faster as it has a parallel search technique. PSO is one of the modern heuristic algorithms and has a great potential to solve complex optimization problems. The PSO algorithm is highly robust yet remarkably simple to implement. Thus, it is quite pertinent to apply the PSO, with more new modifications, to achieve better optimisation and handle the power system problems more efficiently. But these methods suffer from excessive numerical iterations, resulting in huge computations, premature convergence and there is a chance to trap in to local minima therefore degrading its efficiency [60] [77]. BFA is the alternative AI technique to compute the optimised controller parameters efficiently and effectively and can be successfully used in frequency control problems of power systems [60] [77].

However, the use of BFA to optimise fuzzy logic membership function parameters to control a PI controller and frequency measuring transducer using MAW sensor to the best of the my knowledge has not been applied in the frequency control of MHPP. This research therefore seeks to employ BFA to optimise fuzzy logic parameters in order to improve the performance of PI controller and thus ensure a stable frequency control of MHPP.

It has been shown that the BFA is more efficient than PSO and GA in terms of convergence, robustness and accuracy and has outperformed in many powerful optimisation algorithms in terms faster convergence speed to global optimal solution, better response, less computational time requirement and is not largely affected by the size and non-linearity of the problem when compared to the other evolutionary algorithms [60] [78] [79]. It is therefore expected that applying the BFA for frequency control of MHPP will result in shorter stabilising time than existing methods.

CHAPTER THREE

3.0 ELC DESIGN, IMPLEMENTATION AND TESTING

3.1 Introduction

In this chapter, frequency measurement using Magnetostrictive Amorphous Wire (MAW) sensor is presented. Design of the amplifier and signal conditioning circuits which convert the analog signal from the MAW to a digital signal that is fed to the Arduino microcontroller is discussed. Again, determination of the optimal PI gains to serve as a reference gains to the Arduino microcontroller is used to generate a Pulse Width Modulation (PWM) control signal for controlling the firing angle of the switching control circuit of the ELC is also explained. Finally, the implementation of the Electronic Load Controller (ELC) is considered. Design of the zero crossing detector circuit for each phase of the 3-phase circuit which detects zero crossing when the mains sine wave crosses the zero line, is used to synchronise the firing angle of TRIACs with the zero crossing detector pulse. This ensures proper operation of the TRIACs.

3.2 Design of Frequency Sensing System

The frequency sensor used in this work is MAW with the composition $(Fe_{50}Co_{50})_{78}Si_7B_{15}$, 125 μm diameter, placed in a pick-up coil of 3000 turns. In principle, the sensor is based on large Barkhausen Jump (LBJ) a magnetic feature of amorphous wire as described in Chapter two, sub-section 2.5.5.

In operation, Permanent Magnets (PM) with unlike poles facing each other were securely attached to the shaft of the generator in order that they are not displaced and to avoid causing any injuries. MAW of Critical Length (CL) 7 cm, was also placed in a pick-up Coil (PC) of 3000 turns and then positioned at a distance of 7 cm from the generator shaft as shown in Figure 3.1. These critical wire length of 7 cm and optimal

position of 7 cm were chosen based on the fact that LBJ occurs at a critical length and optimal distance. Research has shown that a weak signal or the signal is completely lost if different wire length and optimal distance other than 7 cm are used [80]. The permanent magnets were used to provide the magnetic field to cause LBJ hence generate signals in the pickup coil.

As the permanent magnets rotates due to rotation of the rotor, voltage spikes are induced in the coil due to the sudden reversal in magnetic flux in the amorphous wire core. The voltage spikes are induced in the pickup coil every time the north pole of the magnet comes close to the wire. The frequency of the induced voltage spikes is actually the speed and hence the frequency of the generator.

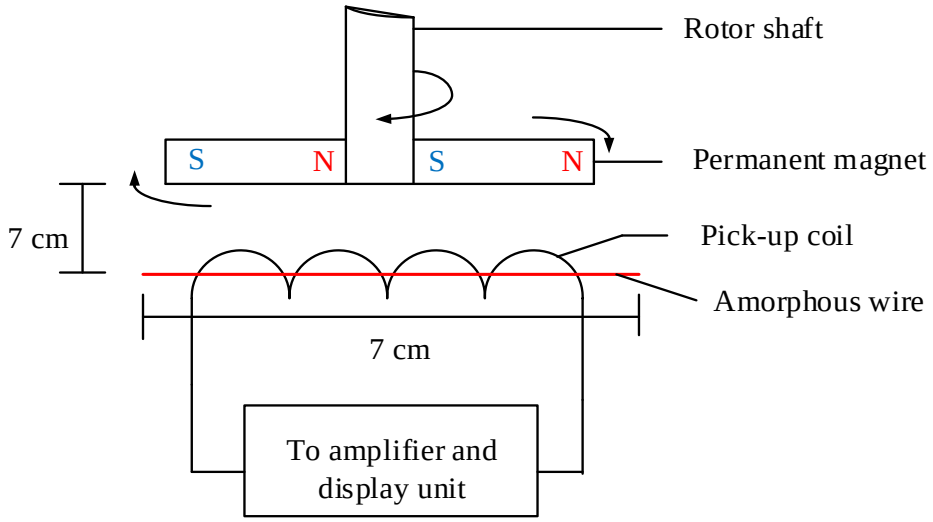

Figure 3.1: Schematic diagram of the frequency sensor

The output from the ends of the pickup coil was fed into the amplifier circuit for amplification of the low signal. From the output of the amplifier circuit the signal was fed into the signal conditioning circuit for conversion into a digital signal which is compatible with the microcontroller. Finally, the output from the digital circuit was fed to a microcontroller so as to read the frequency. The microcontroller used in this case is Arduino uno or Atmega 328P. The frequency is then displayed on a digital

oscilloscope.

3.2.1 Amplifier Circuit

The signals attained from the pick-up coil is a pulse of low value which is in the order of millivolts generally between 80 mV and 200 mV peak voltage depending on the wire length and the optimal position of the wire from the rotor shaft. For the frequency signals generated by the wire to communicate effectively with the microcontroller, it must be amplified to improve the quality of the signal waveform and then converted into HIGH (5V) and LOW (0V) signals. The amplification of the signal was achieved using a two-stage inverting amplifier as shown in Figure 3.2.

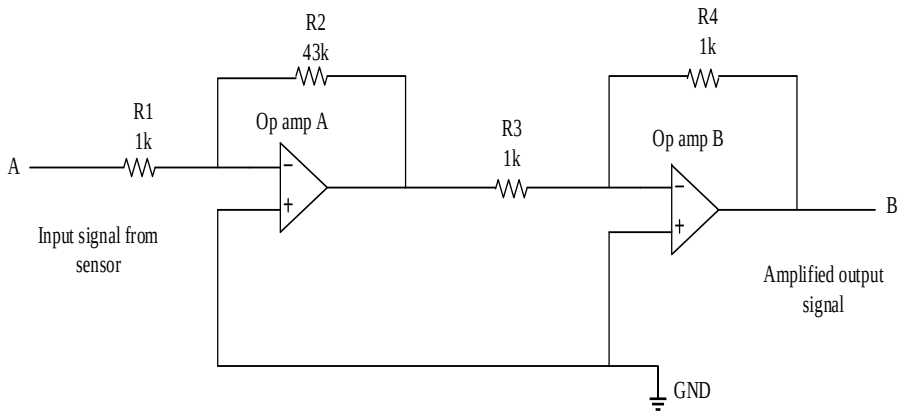

Figure 3.2: Amplifier circuit

The first stage amplifies the signal while the second stage has a gain of one which serves to invert the signal back to its initial form. In the amplifier circuit, a gain of 43 was used. This is because, since a voltage of not more than 5 V was needed for compatibility with the microcontroller, a gain of 43 was used to obtain a peak voltage of 4.4 V at the output of the amplifier circuit. The gain of the amplier circuit is calculated as shown in (3.1).

$$Gain = \frac{R_2}{R_1} = 43 \tag{3.1}$$

3.2.2 Signal conditioning circuit

The MAW generates both positive and negative voltage spikes which cannot be interfaced with the Arduino microcontroller which only operates with digital signals. Again, the signals obtained after amplification may have a peak voltage greater than 5 V which cannot be interfaced with the microcontroller. There was thus the need to regulate this signal to a voltage not more than 5 V and also to remove the negative voltage spikes so as to obtain one voltage spike per cycle for easy communication with the microcontroller. The signal conditioning circuit shown in Figure 3.3 was used for this purpose.

When a positive voltage spike appears at the base of the *npn* transistor, the base is biased which causes current to flow from positive to ground. Since almost all the drop is across resistor (R6), the input to the NOT gate is LOW hence the output is HIGH. In a different scenario, when a negative voltage spike appears at the base of the *npn* transistor, the base is not biased. Therefore, there is no drop in the resistor (R6). Hence the input to the NOT gate is HIGH thus the output is LOW. The signal conditioning circuit also serves to filter any noise component of the signal.

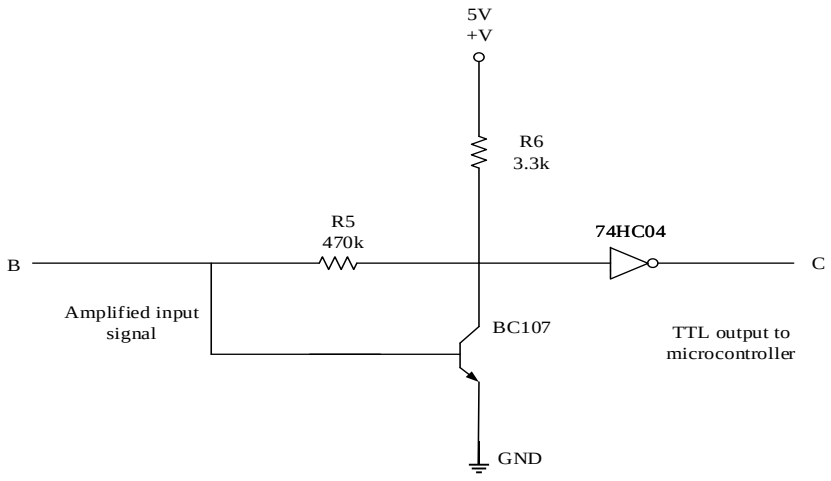

Figure 3.3: Signal Conditioning Circuit

3.3 Determination of ELC Optimal PI Gains

For the purpose of comparison, a conventional PI controller, Fuzzy-PI controller and BFA optimized Fuzzy-PI controller were simulated. This was to verify which controller gives the best control performance in terms of settling time and overshoot. The optimal PI gains obtained from the simulation of controller with the best control response were used as reference PI gains to the Arduino microcontroller. These reference PI gains generate pulse width modulation (PWM) signal to control the firing angle of the switching circuit to divert excess power to the damper load when there is a change in consumer load.

3.3.1 Simulation of the Conventional PI Controller

The initial gains of the conventional PI controller were determined as follows: Considering our plant which is a first order system and being controlled by a PI controller as shown in Figure 3.4. where, R(s) is the reference frequency signal, E(s) is the error signal, U(s) is the control signal and Y(s) is the output response.

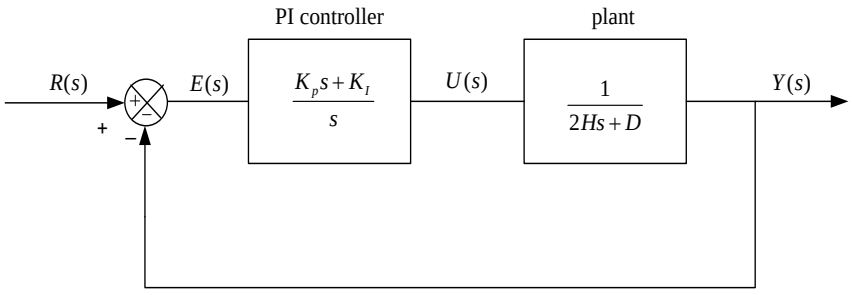

Figure 3.4: PI control first order system

The open-loop transfer function of the system is

$$\frac{Y(s)}{R(s)} = \frac{K_p s + K_I}{s(2Hs + D)} \tag{3.2}$$

Hence the close-loop transfer function of the system is

$$\frac{Y(s)}{R(s)} = \frac{K_p s + K_I}{2Hs^2 + s(D + K_p) + K_I} \tag{3.3}$$

Dividing the closed-loop transfer function by $2H$ gives

$$\frac{Y(s)}{R(s)} = \frac{(K_p s + K_I)/2H}{s^2 + \dfrac{s(D + K_p)}{2H} + \dfrac{K_I}{2H}} \tag{3.4}$$

Assuming that the desired characteristic equation of the closed-loop transfer function is

$$s^2 + 2\zeta\omega_n s + \omega_n^2 \tag{3.5}$$

Now comparing the characteristic equation of (3.4) and the characteristic equation of (3.5), it can be shown that

$$\omega_n = \sqrt{\frac{K_I}{2H}} \tag{3.6}$$

$$\zeta = \frac{1}{2}\left(\frac{D + K_p}{2H}\right)\left(\sqrt{\frac{2H}{K_I}}\right) \tag{3.7}$$

simplifying (3.7) gives

$$\zeta = \frac{1}{2}\left(\frac{D + K_p}{\sqrt{2HK_I}}\right) \tag{3.8}$$

where,

$\omega_n =$ undamped natural frequency (rad/s),

$\zeta =$ damping factor,

$H =$ generator inertia constant (MW.s/MVA),

$D =$ generator damping constant,

$K_p =$ controller proportional gain, and

$K_I =$ controller integral gain.

The H and D values used in this work are 0.038 and 1.3, respectively. These values were obtained from the data catalog of the synchronous generator used for the experiment. For $\omega_n = 20$ and $\zeta = 0.5$, K_p and K_I were calculated to be 0.22 and 30.4, respectively. The values of ω_n and ζ were arbitrary selected and are appropriate values used to initialise the system.

The simulation model of the conventional PI control for the MHPP is shown in Figure 3.5. It consist of a unit step as reference and PI block in MATLAB/SIMULINK. The output response of the plant is displayed by the scope.

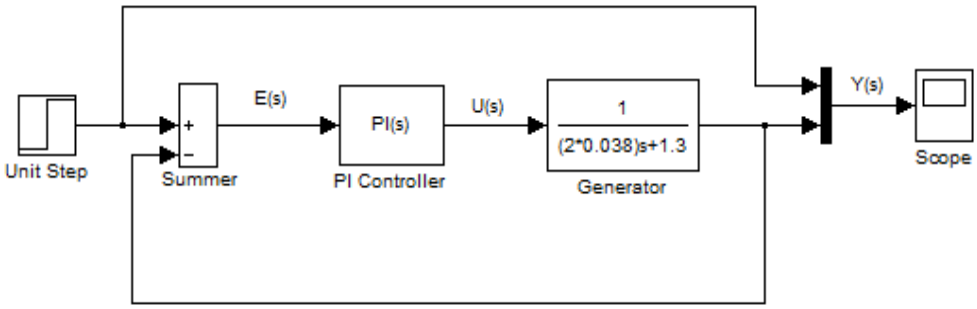

Figure 3.5: Conventional PI controller

3.3.2 Design and Simulation of Fuzzy-PI Controller

The block diagram of the designed Fuzzy-PI controller is shown in Figure 3.6. It basically measures the system output frequency or actual frequency (y) and then calculates error (e) and change in error $(\dot{e})$ based on y and the input (r) which is the reference frequency.

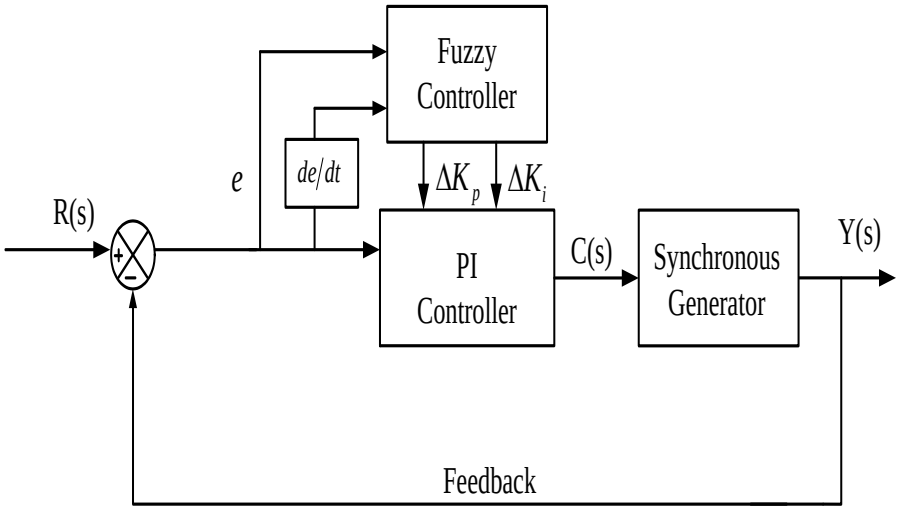

Figure 3.6: Block diagram of the fuzzy PI controller

The fuzzy controller then tunes the PI parameters using the fuzzy control rules in order that the synchronous generator achieves better dynamic PI performance in different situations. This is necessary since the fixed gains of the conventional PI controllers are not suitable for isolated MHPP due to the fact that system parameters for the MHPP are always varying.

Fuzzification

Triangular membership function with seven partitions was used for the design of the Fuzzy PI controller because of its simplicity and computational efficiency [57] [81]. In the design, two inputs to the fuzzy controller named the error (e) and rate of change in

error $(\dot{e})$ and two outputs named change in K_p (ΔK_p) and change in K_i (ΔK_i) were used.

The input and output variables were fuzzified into seven triangular membership functions as shown in figures 3.7 and 3.8, respectively where NB=Negative Big, NM=Negative Medium, NS=Negative Small, Z=Zero, PS=Positive Small, PM=Positive Medium, PB=Positive Big. The ranges of input variables e and $(\dot{e})$ are -0.5 to 0.5 and -10 to 10, respectively. The ranges of output variable ΔK_p and ΔK_i of the controller are 0 to 0.1 and 0 to 5, respectively. The range of the input error (e) is the acceptable frequency tolerance of the Kenyan grid, while the ranges of the rate of change in error $(\dot{e})$ and output variable ΔK_p and ΔK_i were obtained from the simulation model of the fuzzy-PI controller used in this work.

In terms of plant frequency control, when the error (e) is large and the rate of change in error $(\dot{e})$ is large, then ΔK_p and ΔK_i should also be large so as to bring the frequency to the setpoint. If the error (e) is small and rate of change in error $(\dot{e})$ is small, then ΔK_p and ΔK_i should also be small so as to bring the frequency to the setpoint. If the error (e) is zero and rate of change in error $(\dot{e})$ is zero, then it means that the frequency is at the setpoint frequency hence there is no change in ΔK_p and ΔK_i.

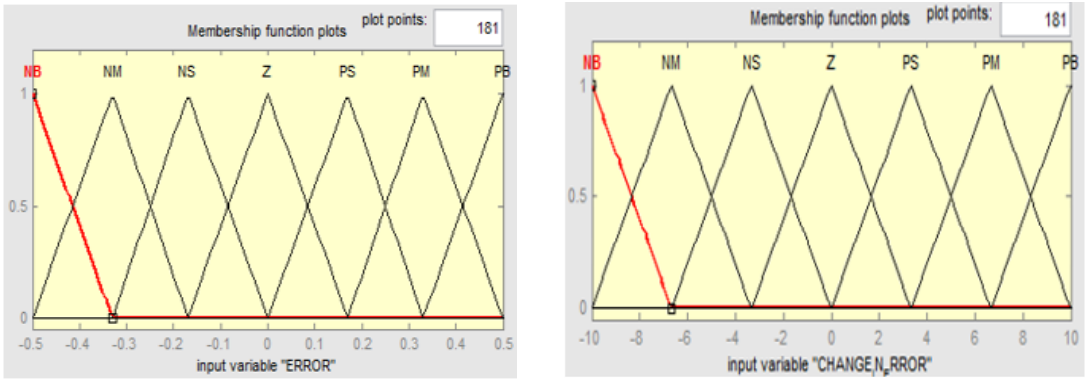

(a) Error (b) Rate of change in error

Figure 3.7: Inputs membership functions

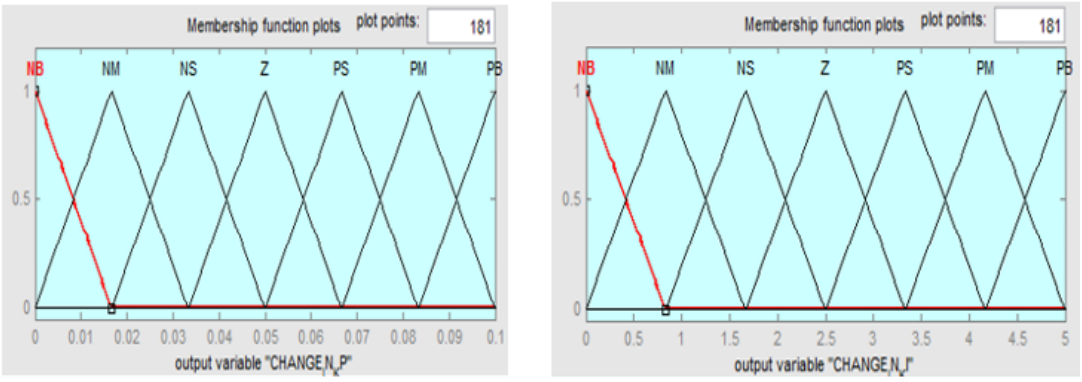

(a) Change in K_P (b) Change in K_I

Figure 3.8: Output membership functions

Fuzzy Rule Base Creation

The fuzzy inference system used was Mamdani fuzzy inference system because it is the most commonly used inference system in many applications due to its widespread acceptance [81]. The fuzzy control rules of the fuzzy-PI controller were written based on the control approach of the PI controller. PI controller was used since it is the most widely used algorithm in the frequency control of MHPPs due to the inherent stability of proportional controller and the steady state error elimination ability of integral controller. It is also inexpensive when compared to PID controller and it returns the process to the setpoint. Moreover, the Derivative controller is not recommendable in presence of measurement noise and sudden load disturbances. This is because it amplifies the noise of the system.

The operation of the PI controller is such that the K_p provides the control action effectively when the error is more and K_I provides the control action effectively when the system is operating near the set point value [82]. This means that K_p must be maximum when the error is large and should start varying to the minimum when the system is near the set point. The K_I is varied such that its value will be minimum when the system operates away from the set point and attains maximum value when it operates

near to the set point [75] [82] [83].

With the input variables having seven memberships functions, the total number of rules for the output variables are 7^2 = 49 rules. The rules are in the if-then format as illustrated below.

- If error is NB and rate of change in error is NB, then ΔK_p is PB and ΔK_I is NB
- If error is Z and rate of change in error is Z, then ΔK_p is Z and ΔK_I is Z
- If error is PM and rate of change in error is PM, then ΔK_p is NM and ΔK_I is PB

With these analogy, the control rules for changes in Kp and Ki are shown in tables 3.1 and 3.2, respectively.

Table 3.1: Fuzzy rule for ΔK_p

e / $\dot{e}$	NB	NM	NS	Z	PS	PM	PB
NB	PB	PB	PM	PM	PS	Z	Z
NM	PB	PB	PM	PS	PS	Z	NS
NS	PM	PM	PM	PS	Z	NS	NS
Z	PM	PM	PS	Z	NS	NM	NM
PS	PS	PS	Z	NS	NS	NM	NM
PM	PS	Z	NS	NM	NM	NM	NB
PB	Z	Z	NM	NM	NM	NB	NB

Table 3.2: Fuzzy rule for ΔK_I

e / $\dot{e}$	NB	NM	NS	Z	PS	PM	PB
NB	NB	NB	NM	NM	NS	Z	Z
NM	NB	NB	NM	NS	NS	Z	Z
NS	NM	NM	NS	NS	Z	PS	PS
Z	NM	NM	NS	Z	PS	PM	PM
PS	NM	NS	Z	PS	PS	PM	PB
PM	Z	Z	PS	PS	PM	PB	PB
PB	Z	Z	PS	PM	PM	PB	PB

The fuzzy rule editor for the input and output variables is also shown in Figure 3.9.

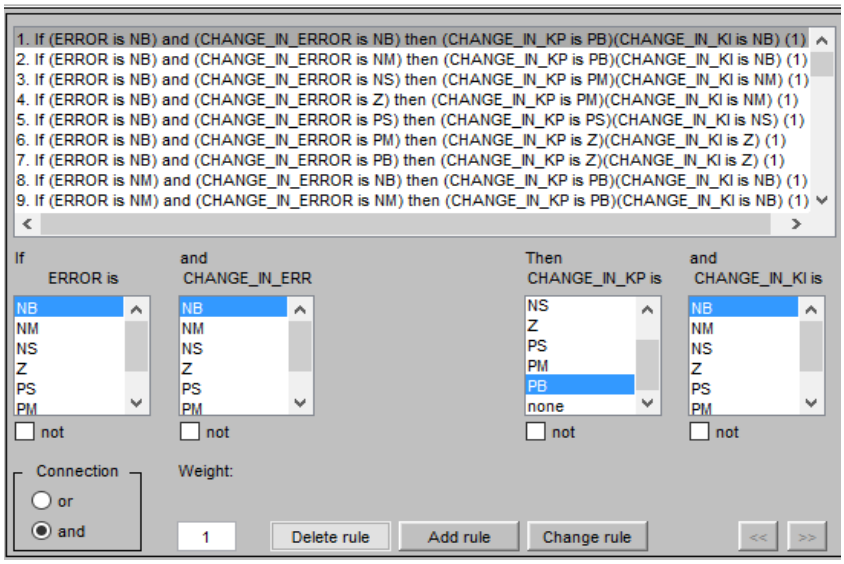

Figure 3.9: Fuzzy rule editor

Defuzzification

The center of gravity defuzzification method was applied to obtain crisp output as it is the most commonly used defuzzification method in most applications [81].

Tuning the Fuzzy-PI Controller

Generally, the purpose of tuning the gains of the PI controller is to adjust the control parameters K_p and K_i to the optimum values for the attainment of desired control response. The final K_p and K_i values for the Fuzzy-PI controller were determined using the simulation model shown in Figure 3.10.

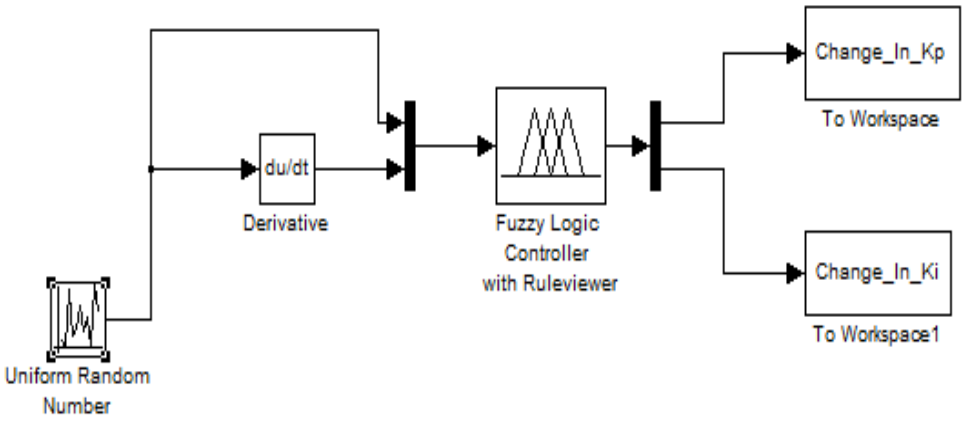

Figure 3.10: Simulation model of the fuzzy-PI controller

To mimic the dynamic behaviour of the MHPP, the system was simulated using a random number generator producing values between 49.5 and 50.5 which is the frequency tolerance for the Kenya power grid [84]. The fuzzy controller inputs are e and $\dot{e}$. The outputs are ΔK_p and ΔK_I. Finally, the new PI gains were obtained using the adaptive gain updating equation as shown in (3.9) and (3.10) respectively [83] [85] .

$$K_p = K_p initial + \Delta K_p \tag{3.9}$$

$$K_I = K_I initial + \Delta K_I \tag{3.10}$$

where, 0.22 and 30.4 are the initial values of the PI parameters. ΔK_P and ΔK_I are the change in K_P and change in K_I, respectively.

3.3.3 Design and Simulation of Optimized Fuzzy-PI Controller

The optimized Fuzzy-PI controller is an extension of the Fuzzy PI controller. Research has shown that in spite of the significant improvement in the of design of Fuzzy-PI controllers over their conventional counterparts, they still have some major disadvantage in that the location of the peaks of the membership functions are fixed and not adjustable [86]. Therefore, to improve the control performance of the Fuzzy-PI controller and to overcome the challenge mentioned above, the peak of the triangular membership functions for all the fuzzy input and output variables of the designed Fuzzy-PI controller were optimized or tuned using BFA to solve the frequency control of MHPP. Figure 3.11 shows the schematic diagram of the optimsed Fuzzy-PI controller using BFA.

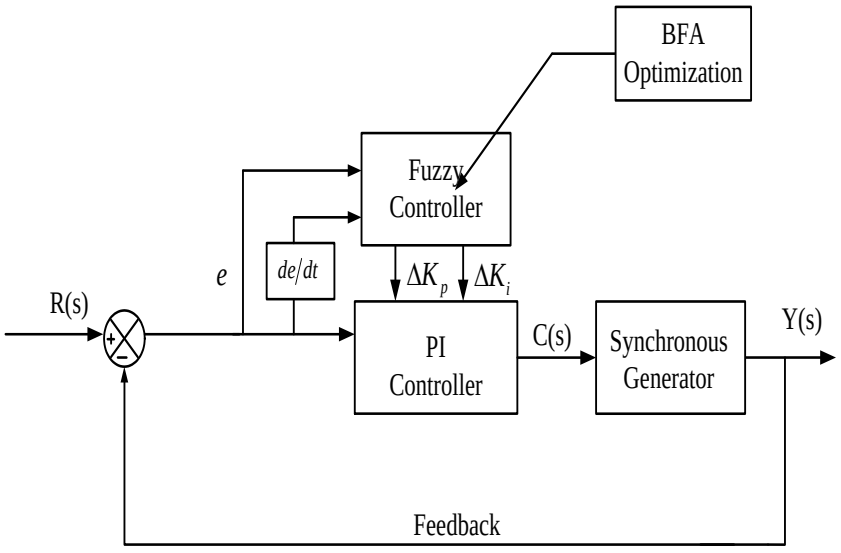

Figure 3.11: Schematic diagram of the optimized PI controller

The triangular membership function for the designed BFA optimised Fuzzy-PI controller is characterised by the the cost function or the performance index as shown in (3.11) [87]. where, a and c are the foots of the triangular membership function, b is

the peak of the triangular membership function and x is the interval in the universe of discourse.

$$f(x;a,b,c) = \begin{cases} 0 & x \leq a\ , \\ (x-a)/(b-a) & a \leq x \leq b\ , \\ (c-x)/(c-b) & b \leq x \leq c\ , \\ 0 & c \leq x\ , \\ & a < b < c\ . \end{cases} \tag{3.11}$$

In the optimization process, the cost function or the performance index was defined in such a way that the centers or the peaks b of the triangular membership functions for all the fuzzy control rules were selected as the parameter to be determined whiles the coordinates a and c were held constant.

Criteria for Selecting BFA Initial Parameter

The criteria for BFA initialisation parameter choices is necessary so as to determine the global minimum point of the nutrient media. The global minimum point is the place which has the highest nutrient level, hence regarded as a minimization problem. In this work, the bacteria were initially spread randomly over the optimization domain with the probability that a part of them will fall near the food.

BFA programming codes requires the specification of appropriate values of the following BFA initialisation parameters as the basis for the computation of the cost function: Dimension of the search space (p), Total number of bacteria in the population (S), Number of chemotactic steps (N_c), Swimming length (N_s), Number of reproduction steps (N_{re}), Number of elimination-dispersal events (N_{ed}), Elimination-dispersal

probability (P_{ed}) and the size of the step taken in the random direction specified by the tumble $C(i)$.

The effects of these initialisation parameters on the nutrient media or the cost function is based on the assumption that having a large number of these parameters increase the possibility of converging to global minimum quickly. But the consequence is that it normally result in computational complexity and computational time of the algorithm. However, having a smaller number of these initialisation parameters increase the possibility of being trapped at the local minima [59].

Selection of the Initialisation Parameters of BFA

The selection of the number of bacteria (S) was achieved by varying it in steps of 10 because it is the appropriate interval used in BFA simulation [59]. The other parameters were kept fixed as follows: Nc = 30, Nre =5, Ned =3, ped=0.25 C(i) = 0.005, Ns = 5. The BFA codes then computes the cost function or the performance index. The cost function with the lowest value was then selected as the best value to be used as an initalisation parameter. The same approach was also used to attain the other initialisation parameters which are presented in chapter four.

Tuning the BFA Optimised Fuzzy-PI Controller

The same procedure for obtaining the gains for the fuzzy-PI controller was also used for the BFA optimized Fuzzy-PI controller after the membership functions have been optimised.

3.4 Components of the ELC

3.4.1 Microcontroller

The designed ELC consists of four Arduino ATMega328P microcontrollers; one serves as the master while the other three are slaves. The master microcontroller reads the frequency of the conditioned signal from MAW sensor and also generates PWM signals using PI control codes. Each of the three slave microcontrollers reads zero crossing of each phase voltage. This was due to the fact that a 3-phase circuit was used hence one slave per phase was needed for zero crossing detection. Also, each of the three slave microcontrollers receives PWM inputs from the master microcontroller and controls the switching of the TRIACs so as to divert the excess power to the damper loads.

Moreover, the Arduino Uno board has one interrupt pin on each board. Therefore, since the zero crossing on each phase has to be detected using an interrupt pin, three of the microcontrollers were used for this purpose. The use of the four microcontrollers ensures the master microcontroller is not overloaded to enable it function very effectively.

The frequency control algorithm of the designed ELC is such that, the optimal PI gains obtained from the simulation results were used as the reference gains for the master microcontroller. The master microcontroller is the heart of the frequency control algorithm. It reads the frequency of the conditioned signal from MAW which corresponds to the frequency of the synchronous generator. Hence the MAW frequency measurement basically serves as an input to the master microcontroller. With a setpoint frequency of 50 Hz, the consumer load was varied from full load to no load. This causes the frequency of the generator to increase as the load decreases. The range of

frequency changes from 50 Hz to the maximum frequency at no load was mapped to a PWM output which range from 0 to 255. The master microcontroller using PI control codes with the initial Kp and Ki gains obtained from the optimal simulation results, generate a PWM output corresponding to a particular Frequency as the consumer load is varied from full load to no load.

The PWM output from the master microcontroller was tapped to the analog pin of all the three slave microcontrollers controlling each phase of the damper load. An analog pin generates a 10 bit value which range from 0-1023. When a zero crossing flag is set, that is when an interrupt detects zero crossing which happens on the falling edge of the rectified waveform, the slave controllers get the PWM readings from the master microcontroller. This 10 bit value was mapped to a time delay between 0 and 10 ms which represents half period of the sine wave. This time delay between the half period of the sine was used to adjust the firing angle of the TRIACs so as to divert excess power to the damper load when there is a change in consumer load.

This time delay was mapped such that when the time delay is 0 ms all the power is diverted to the damper load and when the time delay is 10 ms no power is diverted to the damper load. When the time delay has elapsed, the TRIACs are fired to divert excess power to the damper load. The firing of the TRIACs is synchronised with the rectified waveform. The control algorithm automatically controls the firing angle of the TRIACs. This maintained a balanced load on the generator hence keeping the frequency approximately constant at 50 Hz by feeding two loads in parallel such that the total power is constant. The control algorithm also maintain a balanced load on the damper load since they are all fired with the same PWM signal.

The control codes for the master and slave microcontrollers showing the operation of frequency control algorithm are as shown in Figure 3.12 and Figure 3.13 respectively.

The control codes for the ELC operates such that for as long as the frequency is within the acceptable range of 49.5 Hz to 50.5 Hz no action is taken by the controller to divert the power to the damper load.

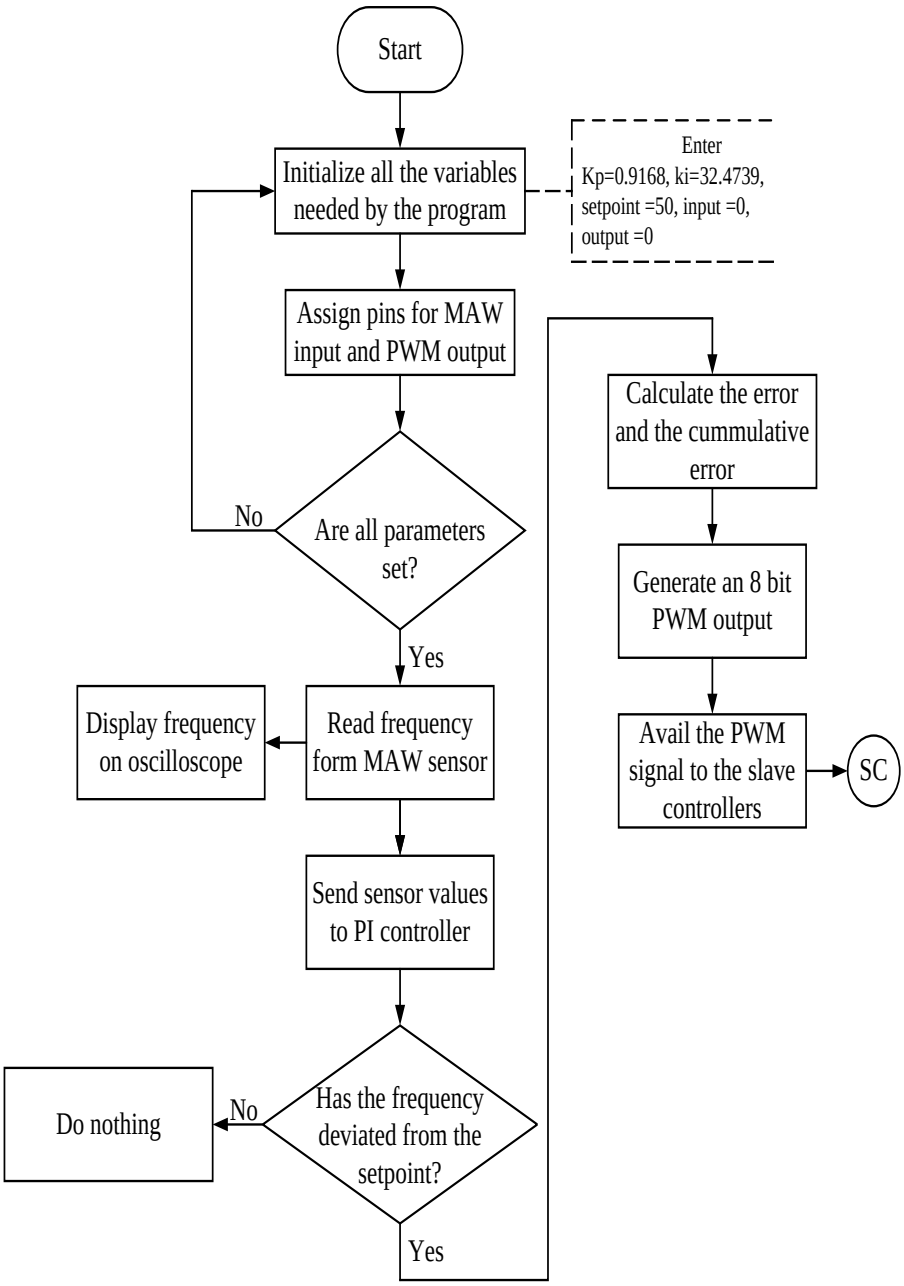

Figure 3.12: Flowchart for master microcontroller codes

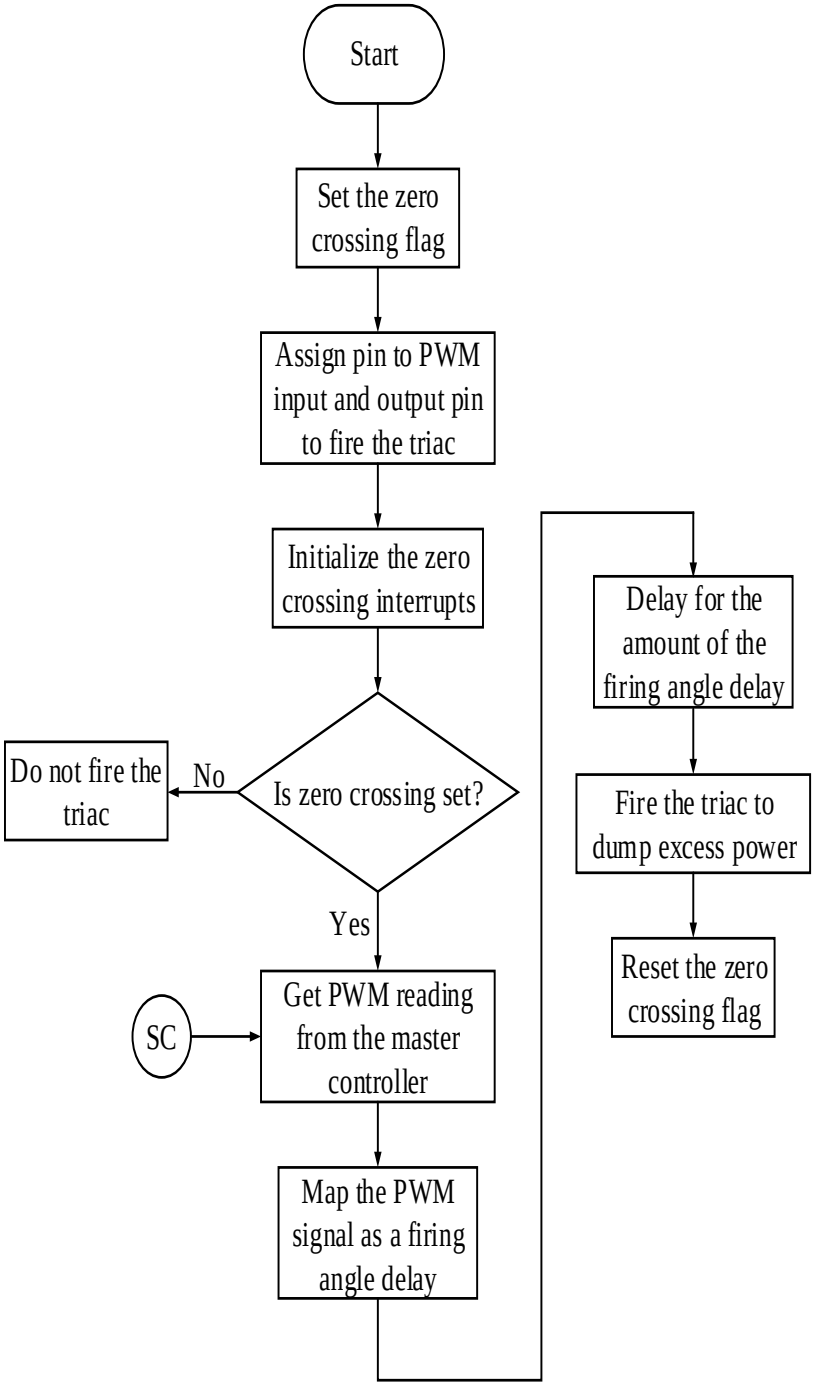

Figure 3.13: Flowchart for slave microcontroller codes

Table 3.3 shows the various pins used in both the master and slave microcontrollers.

Table 3.3: Pins used in microcntrollers

Pin No.	Function	Microcontroller	Purpose
2	Interrupt pin	Slave	To detect zero crossing so as to synchronise the firing of the TRIACs
3	PWM output	Master	Output of PWM signal for frequency control
8	MAW input	Master	Input to the master controller for frequency reading
Analog(0)	Analog pin	Slave	Reads PWM signal from the master controller
13	Digital pin	Slave	For firing the TRIACs

Arduino ATMega328P Microcontroller

Arduino ATMega328P microcontroller on Arduino Uno board is a small computer that can be programmed to control the external devices connected to it. It basically interacts with its environment through control codes called the sketches which are software component and the schematics or circuit diagrams which are the hardware components. To program the microcontroller, Arduino Integrated Development Environment (IDE) software is used.

The IDE is a software where the programing codes are written in a language that the Arduino understands, normally in C or C++ language. The codes that were developed for the ELC master and slave microcontrollers are given in Appendix A. The next step after the program has been written is to upload to the Arduino microcontroller. The

Arduino microcontroller will then perform the instruction given by the program and then communicate with the external devices connected to it so as to control a given plant.

In construction, Arduino Uno or ATmega 328p has 32 KB of flash memory for storing codes. It also has 2 KB of SRAM and 1 KB of EEPROM. It also consist of 16 MHz quartz oscillator to enable it operate at the correct frequency, a USB connection, a power jack and a reset button. Arduino Uno operate at 5V and can provide or receive a maximum current of 40 mA. Also each of the 14 digital pins on the Arduino Uno can be used as an input or output device. The Arduino Uno has 6 analog inputs each of which provide 10 bit of resolution(1024) generating a voltage ranging from 0 to 5 V. Some of the pins also have specialised function in that pin 0 (Rx) is used for transmitting serial data and pin 1 (Tx) is used for receiving serial data. Pin 2 is used for external interrupts which can be configured to activate an interrupt on a low value, a rising or falling edge or a change in value. It also has Pulse Width Modulation (PWM) pins which are also digital Pins. These pins are pin 3, 5, 6, 9 and 11. These pins basically provides an 8-bit(256) PWM output. The Arduino Uno used in this work is shown in Figure 3.14.

Arduino uno board was used in this work because it is readily available in the market and is cheaper when compared to other microcontrollers. It is the best choice for beginners since it is easy to program. It is also compatible with shield (add-on board) than other models. Also the ATMega328p microcontroller can be removed from the socket and replaced at a very low cost in the event of damage.

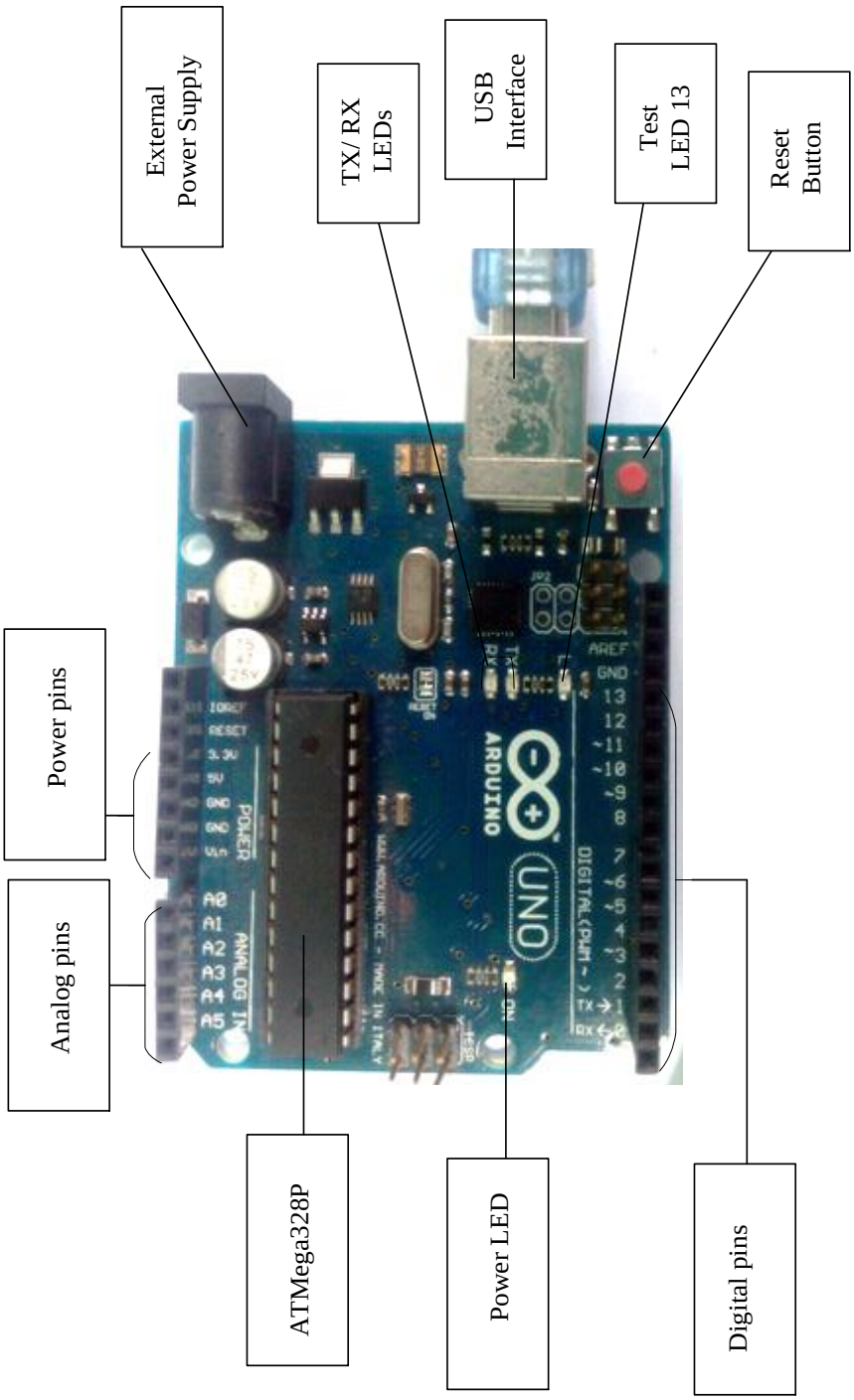

Figure 3.14: Arduino uno microcontroller

Generation of Pulse Width Modulation Signal

Pulse Width Modulation (PWM) is a technique for generating analog signals through digital means. Digital control is used in this concept to create a square wave signal switched between on and off. The on and off pattern basically simulate a signal in between full on (5V) and off (0V) by changing the duty cycle or the pulse width. Therefore, varying analog values can be obtained by changing or modulating the pulse width.

A PWM signal is an 8-bit value between 0 and 255. This means that when a PWM output has a bit value of 255, it means the PWM signal has 100 % duty cycle (always on). If the bit value is 127 the duty cycle is 50% hence the signal is on half the time. In the same scenario, if the bit value is 0 it means the duty cycle is 0 hence the signal is off. The PWM signal is generated by the master microcontroller. In this work, the duty cycle is variable and is dependent on the error which is the difference between the setpoint frequency and the instantaneous frequency. In Arduino microcontroller, the duty cycle is proportioned to a value between 0 and 255, which when written to an Arduino analog output pin, gives a voltage of between 0 and 5 V DC.

3.4.2 Zero Crossing Detector Circuit

The hardware components of the designed ELC basically detects the zero crossing of every phase voltage connected and also responsible for firing the TRIACs so as to control the amount of power to the damper load when there is a change in consumer load. The ELC was powered using a 5 V power supply tapped from the 5 Vcc and also grounded with the ground pin of the Arduino microcontroller. The schematic diagram of the designed ELC is as shown in Figure 3.15. Since the circuits for the 3 phases are the same, only one phase of the circuit is presented.

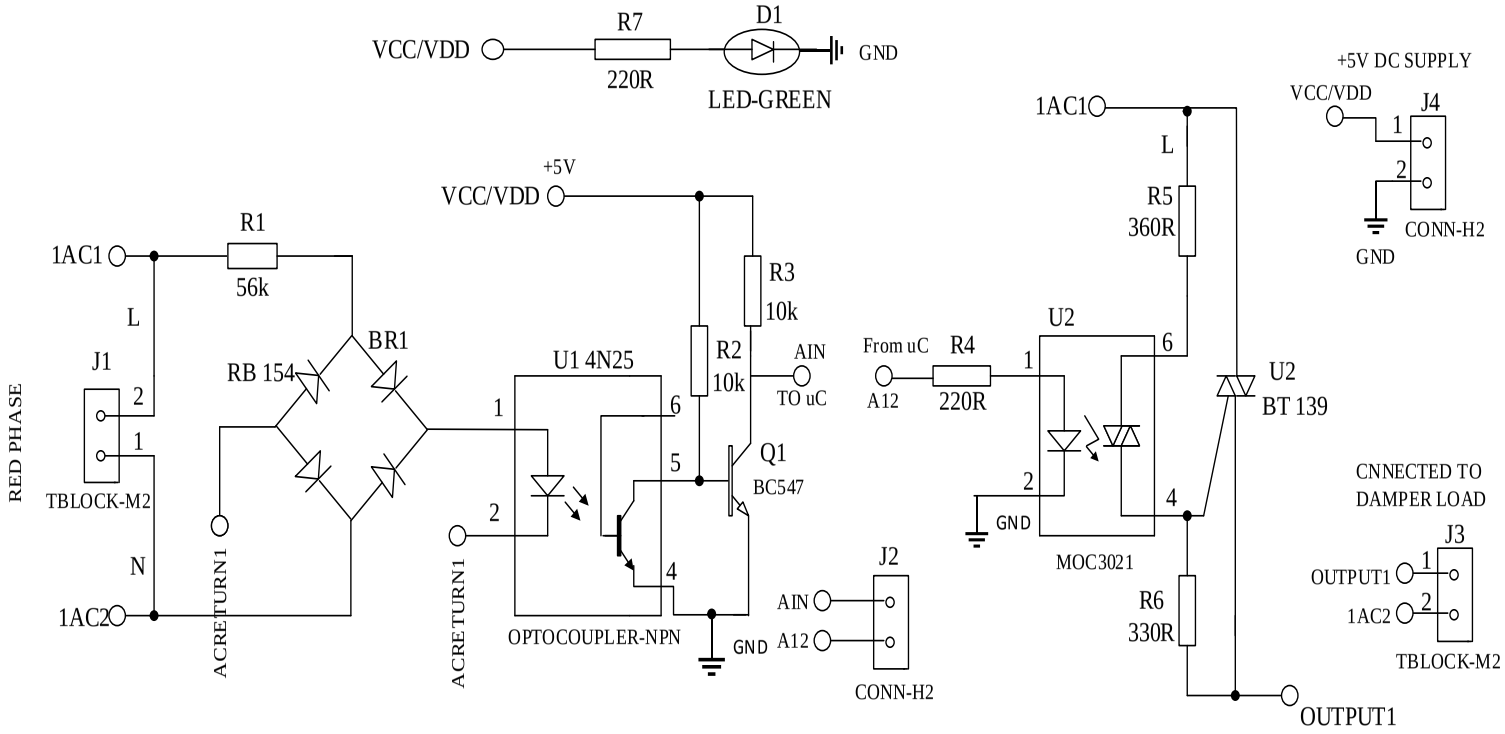

Figure 3.15: Schematics of the designed ELC

Each phase of the ELC has a zero crossing detector circuit which is fed with the AC mains from the synchronous generator output. The zero crossing detector circuit was designed using a 5W56KJ dropper resistors, RB154 full wave bridge rectifiers, 4N25 optocouplers with *npn* transistors and pull-up resistors for detecting zero crossing which is read by the slave microcontroller.

Full Wave Bridge Rectifier

The AC sine wave was rectified using RB154 full wave bridge rectifier as shown in Figure 3.15 as BR1. This rectifier is characterised by high quality and low price. A voltage of 220 V per phase was fed through a 5W56KJ dropper resistors R1 in Figure 3.15, to power the zero crossing detector circuit. The RB154 bridge rectifier has a maximum current handling capacity of 1 A. Therefore, the dropper resistor was used to ensure that the maximum current to the bridge rectifiers and the Optocouplers are kept at 4 mA. The purpose of the dropper resistors is therefore to prevent high current from damaging the zero crossing circuit components. A current of 4 mA is also enough to switch on the LED in the Optocouplers.

Since the AC sine wave was rectified using a full bridge rectifier, the two halves of the sine wave will be above the zero line. This therefore means that the zero crossing will always be detected by the microcontroller on the condition that the signal falls to zero, and not when it rises to zero. The expected output waveform after rectification is shown in Figure 3.16.

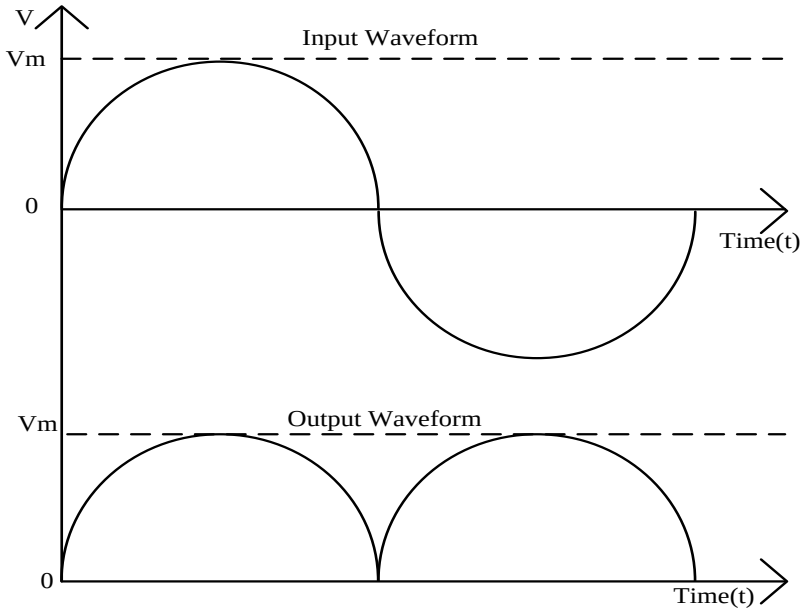

Figure 3.16: Output of the AC waveform after rectification

Optocoupler

The rectified full wave signals was fed to the 4N25 optocoupler which gives a pulse at every zero crossing. The 4N25 optocouplers consist of a gallium arsenide infrared emitting diode optically coupled to a monolithic silicon photo-transistor detector that transfers electrical signals between two isolated circuits by using light. In principle, when the rectified DC wave crosses zero line, the photo diode inside the optocoupler goes off, hence the base of the transistor inside the optocoupler is not biased. The base of the *npn* transistor is therefore biased causing current to flow from positive to ground giving a 0 V or a LOW indicating zero crossing at the output of the signal conditioning circuit shown in Figure 3.15 above. The output of the zero crossing detector circuit was fed to an interrupt pin of the slave microcontroller.

The purpose of using optocouplers is to isolate high voltage signals (220 V) from a low voltage signal (5 V) to serve as an input to the slave microcontrollers in order to prevent damaging the microcontroller. The resistor R2 in Figure 3.15, is pull up resistor with a value of 10 kΩ. The purpose of the pull-up resistor is to ensure that the voltage going to the transistor gate is greater than or equal to 0.7 V so as to control the biasing of the transistor base.

Resistor R3 in Figure 3.15, also ensures that a 0 V or 5V is sent to the slave microcontroller. The output is a pulse-width modulated signal as shown in Figure 3.17. The pulse width signal (blue line) has a peak voltage of 5V DC when a zero crossing occurs at 0 V. This pulse was used to trigger an interrupt in the Arduino microcontroller.

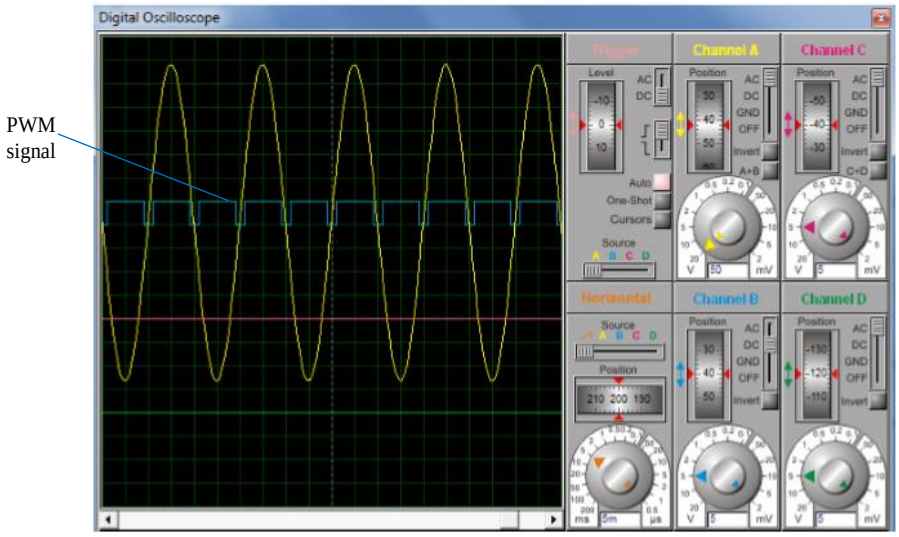

Figure 3.17: Pulse width from the zero crossing detector output

3.4.3 Switching Control Circuit

In this work, the DIAC-TRIAC combination was used as the electronic switching device. The DIAC-TRIAC switch operates based on the principle of phase angle control as explained in Chapter two, sub-section 2.5.3. Figure 3.18 depicts the sine wave showing phase angle control.

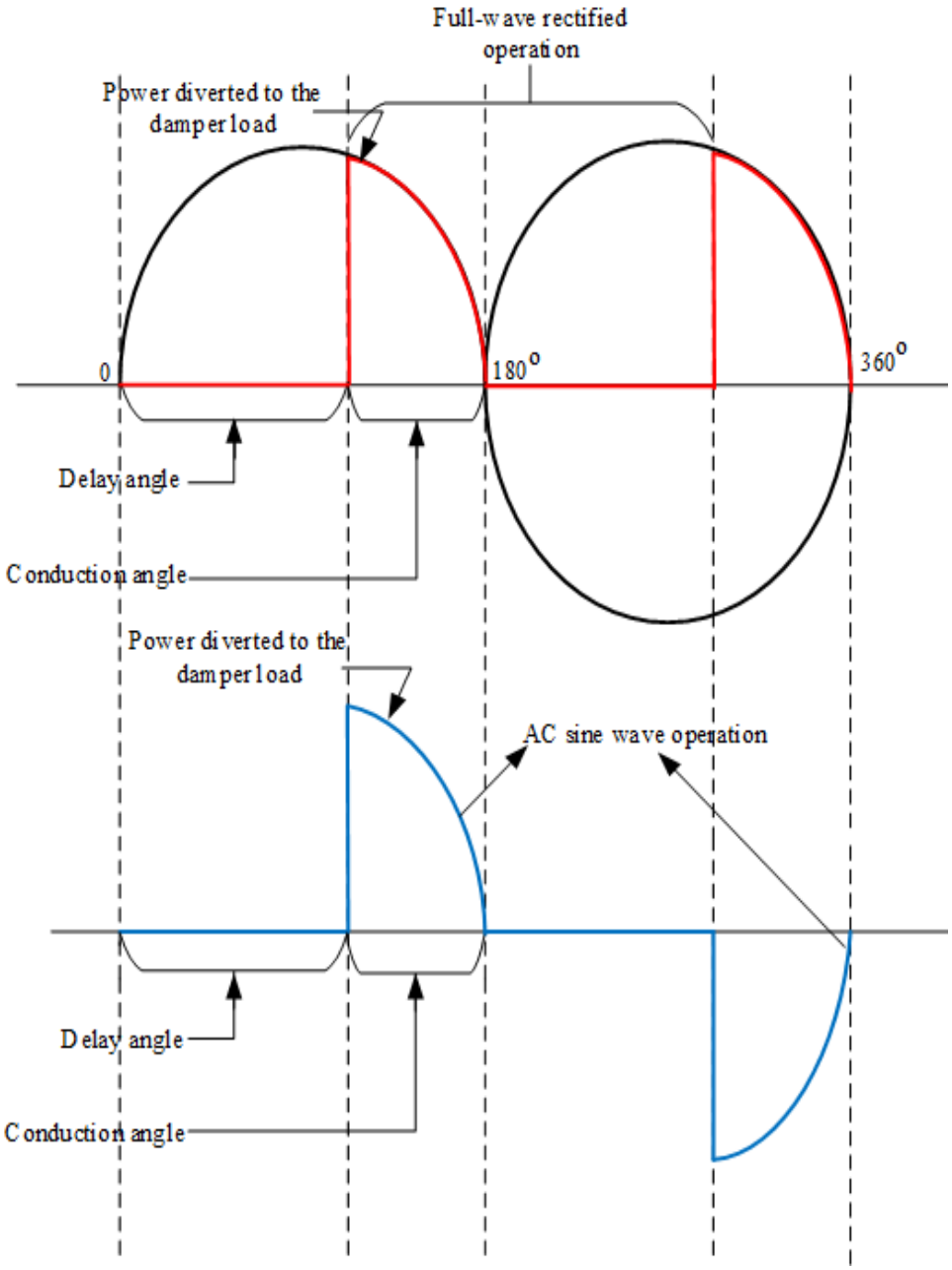

Figure 3.18: Phase angle control

DIAC

MOC3021 diac optocouplers, a bidirectional device was connected in series with the gate terminal of the TRIACs so as to control the gate terminals of the TRIACs as shown in Figure 3.15 above. The purpose of using the diac optocouplers was to provide

optical isolation between the TRIAC load circuit and the electronic circuit to prevent damaging the electronic components. It also prevents any gate current from flowing until the triggering signal is received. This thus ensures smooth operation or switching of the TRIACs.

It basically consists of an aluminum gallium arsenide infrared LED, optically coupled to a silicon detector chip. These two chips are assembled in a 6 pin Dual In-Line Package (DIP), providing insulation between the LED and the output detector. These output detector chips are designed to drive the TRIAC controlling the 220V AC power lines to the damper load.

The purpose of using resistor R4 with value 220 Ω in Figure 3.15 is a current limiting resistor used to ensure that the LED inside the MOC3021 does not burn out. It also ensures that the maximum current drawn by the Integrated circuit (IC) is 22 mA.

TRIAC

The TRIAC, a bidirectional devices used to actuate the flow of power to the damper load is the BT 139 as shown in Figure 3.15 above. Basically, the TRIAC have three terminals M1, M2 and gate. M1 is connected to the supply and M2 connected to the damper load. The gate terminal is directly connected to the gate of the diac. The reason why TRIACs are used instead of thyristors is that AC power flows in two direction and thyristors are unidirectional devices. Hence to effectively control the AC power, two thyristors will be used. Therefore since TRIACs are bidirectional devices only one is needed hence reducing the cost of our control system.

3.5 Experimental Setup

To test the ELC described in section 3.4, a motor-generator set was used as the MHPP, a three-phase rheostat was used as the varying consumer load whereas incandescent bulbs were used as dump load. Figures 3.19 and 3.20 show the schematic diagram of the plant and the experimental setup, respectively.

Three sets of meters were also installed to measure the electrical parameters such as power, current, voltage and power factor of the generator load, consumer load and the damper load. The frequency and the speed of the synchronous generator were also measured using Magnetostrictive Amorphous Wire (MAW) sensor and a digital tachometer, respectively. The signal waveform of the MAW was also displayed on the digital oscilloscope.

Details of the motor-generator set and the generator load are discussed in the following sub-sections.

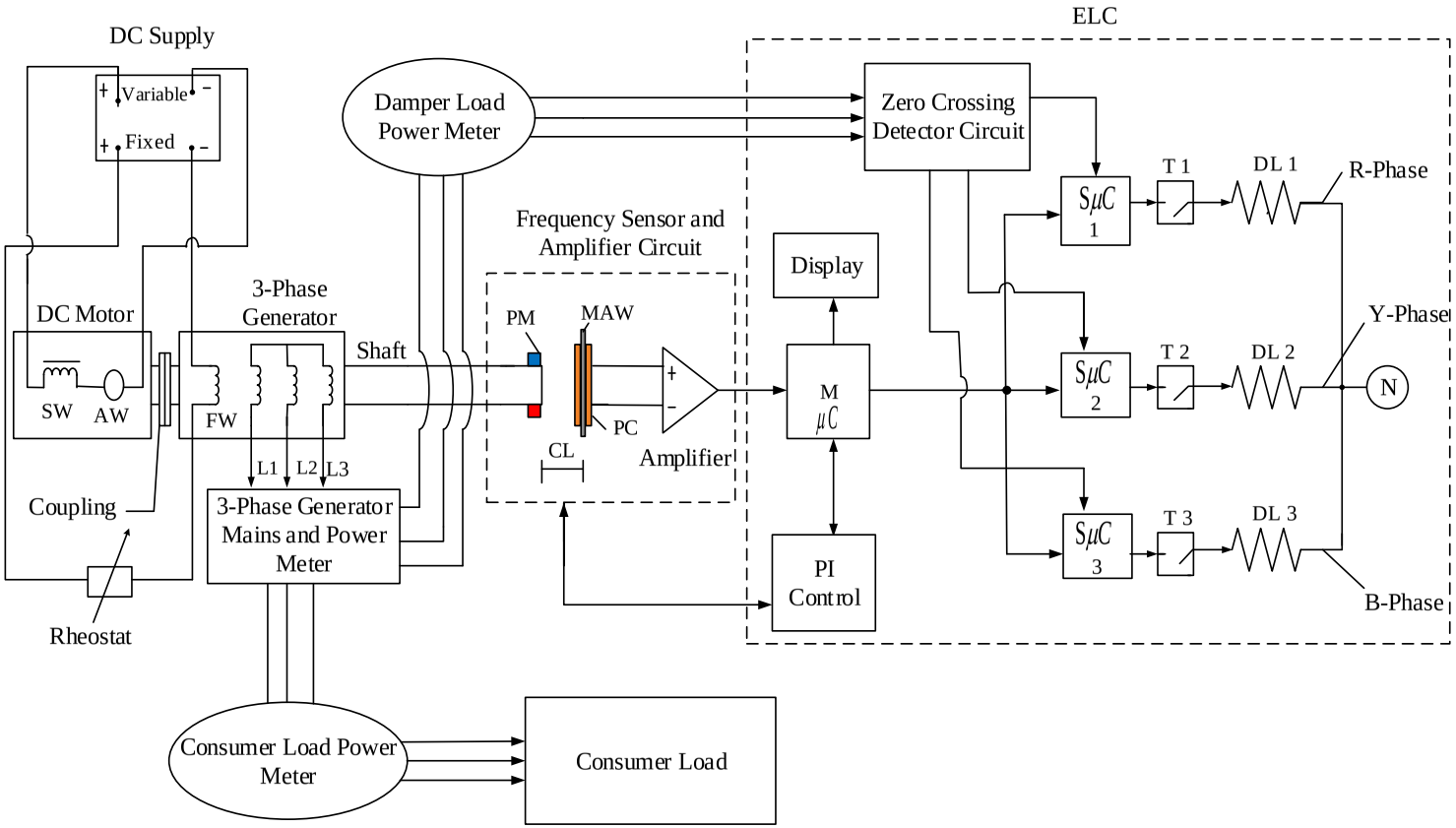

Figure 3.19: The schematic diagram of the plant

Figure 3.20: Experimental setup

3.5.1 Motor-Generator Set

For laboratory experimental purposes, the prototype MHPP was a stand-alone 3-phase synchronous generator of the following specifications: 350 VA, 415V, 50 Hz, 3000 rpm, 2-pole, 0.53 A, and a power factor of 0.8. The DC motor used as prime mover also has the following specifications: 300 W, Series excitation: D1 and D2, I= 1.9 A. Separate excitation: F1 and F2, I= 1.8 A. Vexc= 220 V, Iexc= 0.1 A.

DC series wound motor directly coupled to a 3-phase synchronous generator was used as a prime mover. A DC variable power supply (0-500 V dc, 4 A) was used to power and control the speed of the DC motor which in turn rotates the 3-phase synchronous generator. In a series DC motor, the field winding is connected in series with the armature winding.

In operation, the speed of the DC series motor was first varied so that the synchronous generator runs at 50 Hz, 3000 rpm which is the rated frequency and speed of the synchronous generator. This was achieved by increasing the voltage supply to the DC series motor using the DC variable power supply as shown in the schematic diagram in Figure 3.19. When the generator was loaded by varying the balanced rheostat, the speed and thus the frequency drops. The speed of the DC motor was increased to bring back the frequency and speed to 50 Hz and 3000 rpm respectively, by increasing the voltage supply to the DC motor using the variable DC power supply.

It is noted, the speed control method applied to control the speed of the DC series motor was the armature voltage control method discussed in Chapter two, sub-section 2.6.1. This is because increasing the supplied voltage to the motor, basically increases the armature current which causes the speed of the motor to increase. The armature voltage control method was used because it provides a smooth and linear variation of

speed control.

For voltage control of the synchronous generator, a fixed DC supply (220 V dc, 3 A) with a 5 kΩ rheostat was connected in series with the synchronous generator field windings so as to increase the excitation current to attain the required terminal phase voltage of 220 V. The circuit diagram of the excitation system is shown in Figure 3.19. When the synchronous generator was loaded with the consumer load, the terminal voltage drops, hence the excitation current to the synchronous generator field windings was increased by manually decreasing the resistance of the 5 kΩ rheostat. The manual voltage control method discussed in Chapter two, sub-section 2.4.2 was used to control the terminal voltage. The manual control of the synchronous generator terminal voltage was necessary since the generator used for the experiment does not have an in-built AVR.

3.5.2 Consumer and Damper Loads

A 3-phase balanced rheostat each with specification 5 kΩ were connected in star and then connected at the output terminals of the synchronous generator as consumer load to mimic the dynamic behaviour of the loads in the rural communities of Kenya. From the experiment, when the synchronous generator was loaded with the consumer load, the maximum 3-phase power generated as displayed on the power meter was 160.30 W. This value was not obtained with all 5 KΩ connected but rather it is the value that gives the required voltage and frequency for this set-up.

The sizing of the damper load include a 60 W incandescent bulb per phase connected in star at the output of the ELC to absorb the excess power when the consumer load decreases. This was enough to absorb all the excess power from the generator in the absence of the consumer load since the maximum power the damper load can handle

is 180 W which is slightly more than the consumer load. Both the consumer load and the damper load are connected in parallel.

It is worth noting that all the loads connected to the generator output are purely resistive. This enables the generator to operate at a unity power factor averting the challenges of reactive load and operating at a power factor other than unity.

For a generator power output of 160.3 W, an equivalent damper load of 53.44 W per phase or larger is required to work with the ELC. This implies that the resistance of the consumer load per phase (R_C) is

$$R_C = \frac{220^2}{53.44} = 906\Omega \tag{3.12}$$

Since the resistance per phase of the consumer load is 906 Ω, the resistance per phase of the damper load was calculated using the 60 W incandescent bulb as

$$R_D = \frac{220^2}{60} = 807\Omega \tag{3.13}$$

This means that an equivalent power of 53.44 W was diverted to the damper load per phase when there was no consumer load connected. The resistance of the damper load can be said to be approximately equal to the consumer load resistance.

3.6 Testing of the ELC

For the purpose of comparison, experiment was done to determine the extent to which the frequency of the synchronous generator varies without the ELC. In the experiment, the synchronous generator was first loaded with the consumer load such that the frequency of the generator is 50 Hz and a voltage of 220 V and the 3-phase power recorded on the power meter was 160.31 W. The load on the generator was then decreased by varying the consumer load from full load to no load. As the load on the generator decreases, the frequency and the voltage of the generator also increases. The

voltage was controlled to 220 V by manually decreasing the excitation current of the generator using 5 kΩ rheostat connected in series with the synchronous generator field windings. The results for generator loading without the ELC are presented in Chapter four. The above procedure was then repeated with the ELC in place. The generator, consumer load and damper load meter readings were recorded, in addition to frequency and generator speed.

CHAPTER FOUR

4.0 RESULTS AND DISCUSSION

4.1 Frequency Sensing System of the Generator

4.1.1 Pickup Coil Output Signal

Figure 4.1 shows a screen shot of the CRO display of the low signal from the pickup coil. The signal has a peak to peak voltage of 250 mV. The signal also has noise component which is filtered by the amplifier and the signal conditioning circuit. The frequency measured is 50.21 Hz.

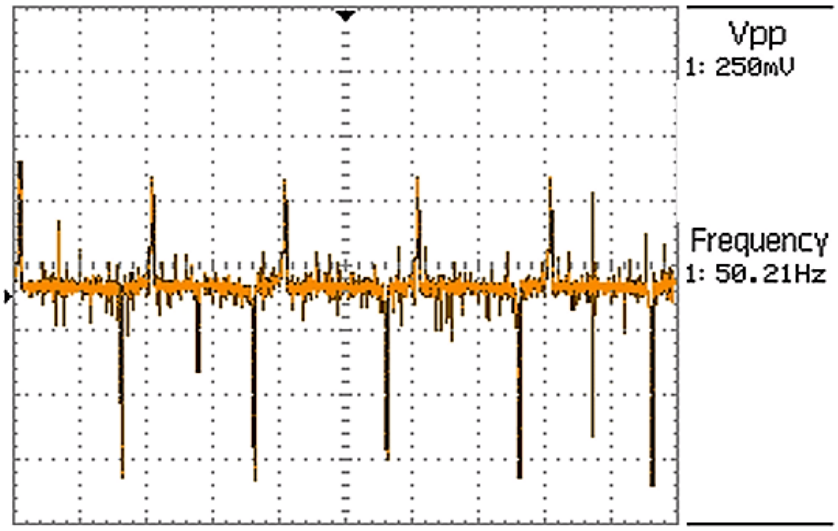

Figure 4.1: Low signals from the pickup coil

4.1.2 Amplifier Circuit Output Signal

The amplified signal waveform is shown in figures 4.2 and 4.3. It can be seen that the signal in Figure 4.2 is inverted since in the first stage of amplification, an inverting amplifier is used. Figure 4.3 shows the signals in its initial form after a unity gain is applied at the second stage of amplification. It can also be observed that the

noise component in the signal has been filtered by the amplifier circuit. The frequency recorded is 50.20 Hz for the amplified inverted signal with a peak to peak voltage of 10.70 V.

Also the frequency recorded after the amplified signal has been inverted back to its normal form is 50.21 Hz with a peak to peak voltage of 10.80 V. It is observed that the frequency measured at the outputs of the two stage amplifier network matches well with that of the original signal. The measured value of the peak to peak voltage after amplification also agrees well with the expected value of 10.75 V for a design amplifier gain of 43.

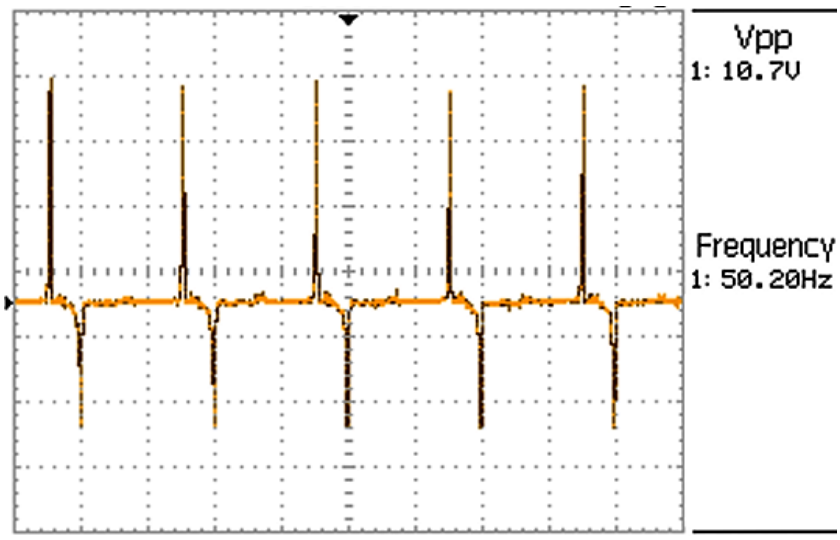

Figure 4.2: Amplified inverted signal

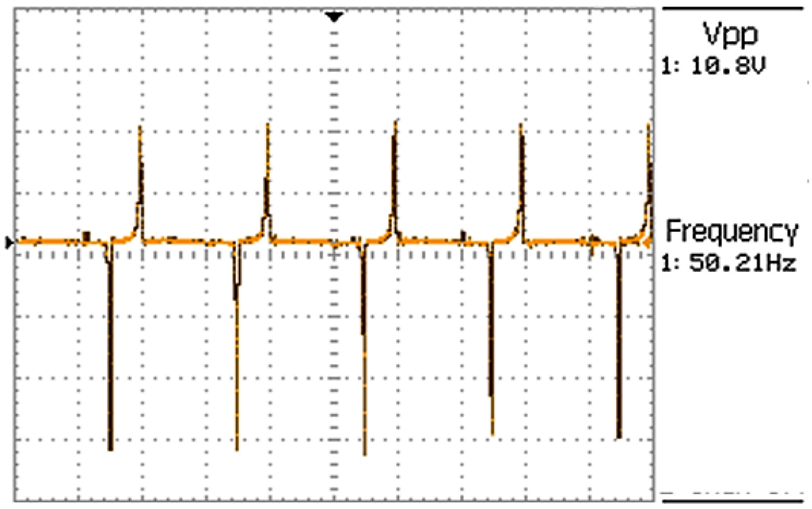

Figure 4.3: Amplified signal in normal form

4.1.3 Conditioning Circuit Output Signal

Figure 4.4 shows the signal waveform at the output of the signal conditioning circuit. It can be seen that the negative signal is chopped off remaining only with the positive waveform which is a HIGH and LOW signals for easy communication with the Atmega 328p microcontroller. The peak voltage after signal conditioning is 4.44 V. With a voltage of 4.44 V, the MAW is able to communicate with the Atmega 328p microcontroller. The frequency recorded is 50.20 Hz which also compares well with the frequency obtained from the low signal and the amplified signal with minimal tolerance.

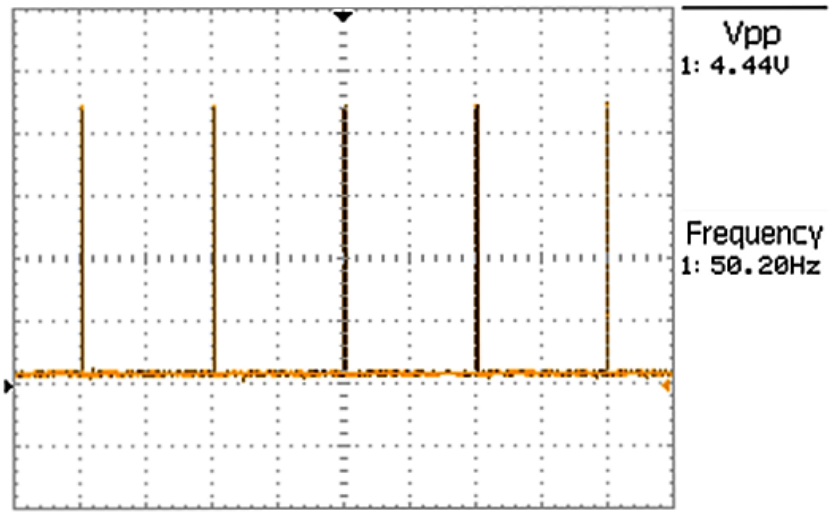

Figure 4.4: Output waveform from the signal conditioning circuit

4.2 BFA Initialisation Parameters

The initial values of the Dimension of the search space (p), Total number of bacteria in the population (S), Number of chemo-tactic steps (Nc), Swimming length (Ns), Number of reproduction steps (Nre), Number of elimination-dispersal events (Ned), Elimination-dispersal probability (Ped) and the size of the step taken in the random direction specified by the tumble $C(i)$ had to be determined. The results of the initialisation parameters used in this work are shown in tables 4.1 to 4.7.

Table 4.1: Selection of number of bacteria (S)

S	Cost Function (J)
10	0.9931
20	0.9917
30	0.9884
40	0.9870
50	0.9951
60	0.9817
80	0.9810
100	0.9935

Table 4.2: Selection of number of chemotactic steps (Nc)

Nc	Cost Function (J)
10	0.9806
15	0.9900
20	0.9956
25	0.9822
30	0.9956

Table 4.3: Selection of the number of swim length (Ns)

Ns	Cost Function (J)
1	0.9880
3	0.9849
5	0.9900
7	0.9878
9	0.9855

Table 4.4: Selection of the number of reproductive step (Nre)

Nre	Cost Function (J)
1	0.9900
3	0.9814
5	0.9906
7	0.9900
9	0.9910

Table 4.5: Selection of the number of elimination-dispersal events (Ned)

Ned	Cost Function (J)
1	0.9867
3	0.9813
5	0.9819
7	0.9900
9	0.9823

Table 4.6: Selection of the number of probability of elimination-dispersal (Ped)

Ped	Cost Function (J)
0.1	0.9900
0.15	0.9834
0.2	0.9932
0.25	0.9824
0.3	0.9900

Table 4.7: Selection of the number of step size C(i)

C(i)	Cost Function (J)
0.005	0.9900
0.01	0.9900
0.05	0.9900
0.1	0.9900

For each case, the parameter corresponding to the least cost function was selected as the best value for initialisation. Hence in the simulation, the BFA used the following initialisation parameters: P=2, S= 80, Nc=10, Ns=3, Nre=3, Ned=3, Ped=0.25, C(i)= 0.005 as bolded in tables 4.1 to 4.7 respectively. The dimension of search space (p) of 2 is the acceptable value for initialisation hence not determined.

The optimised membership function for both the fuzzy input and output variables using BFA are shown in Figure 4.5 and Figure 4.6, respectively.

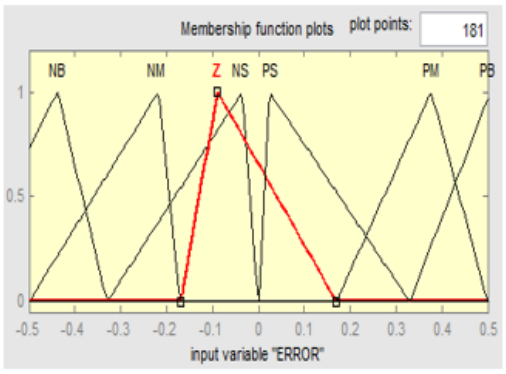

(a) Error

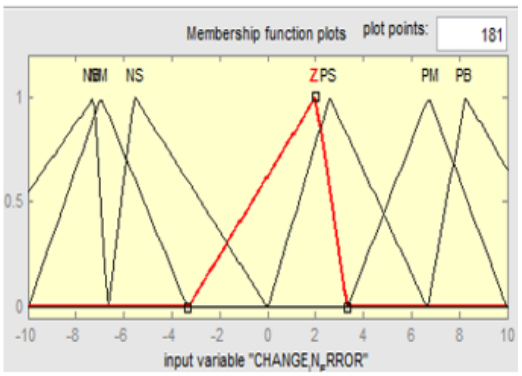

(b) Rate of change in error

Figure 4.5: BFA optimised inputs membership functions

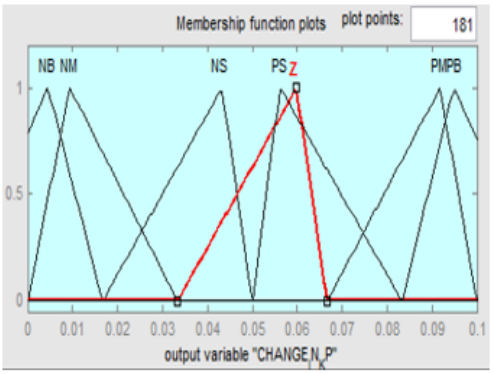

(a) Change in K_P

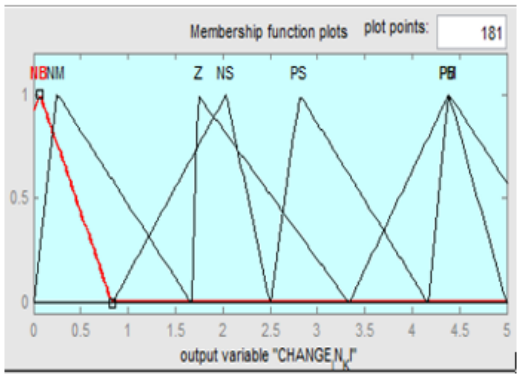

(b) Change in K_I

Figure 4.6: BFA optimised output membership functions

4.3 Simulation of the Various Controllers

In this work, a fuzzy-PI controller and BFA optimised Fuzzy-PI controller were designed and simulated. The final values for ΔK_p and ΔK_I obtained after simulation of the fuzzy-PI controller were 0.3906 and 2.4739, respectively. Also, the final values obtained after simulation of the BFA optimised Fuzzy-PI controller were 0.6968 and 2.0739 for ΔK_P and ΔK_I, respectively. The initial K_p and K_i gains used in this work for the conventional PI controller were 0.22 and 30.4 respectively. By using the adaptive gain updating equation, the new K_p and K_i values for the Fuzzy-PI controller and BFA optimised Fuzzy-PI controller were calculated as shown in Table 4.8.

Table 4.8: System response of the various controllers

Parameter	Proportional Gain(kp)	Integral Gain(Ki)	Rise Time(ms)	Settling Time(ms)	Percentage Overshoot(%)
Conventional PI	0.22	30.4	80.7	396.9	16.4914
Fuzzy-PI	0.6106	32.8739	81.1	265.8	10.1801
BFA Optimised Fuzzy-PI	0.9168	32.4739	84.2	260.3	5.7992

The response of the conventional PI controller showing the control parameters such as the rise time, settling time and the percentage overshoot is shown in Figure 4.7.

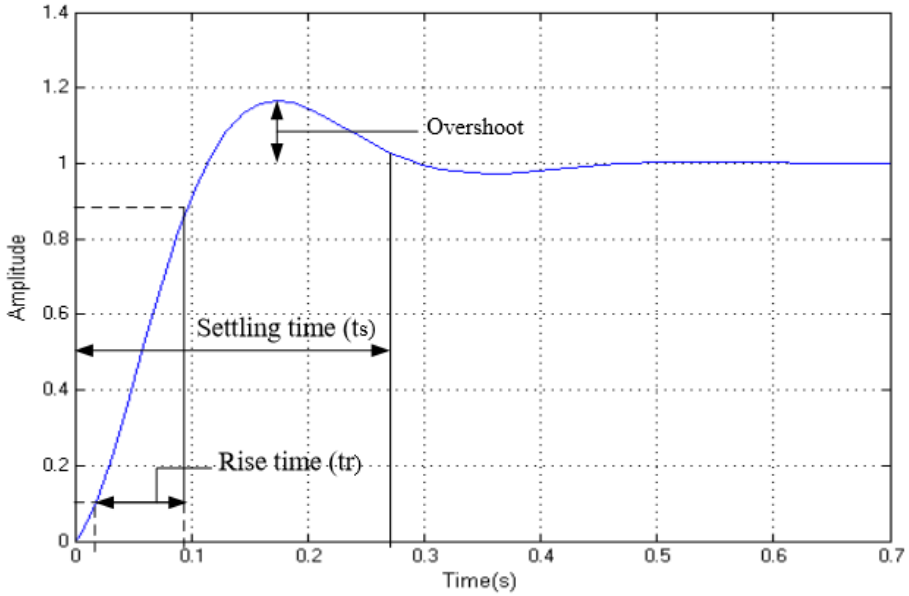

Figure 4.7: Control response of the conventional PI controller

The performance of the MHPP Synchronous generator using a unit step under conventional PI controller, Fuzzy-PI controller, BFA optimised Fuzzy-PI controller are shown in Table 4.8 and in Figure 4.8. These simulation results were obtained using MATLAB/SIMULINK.

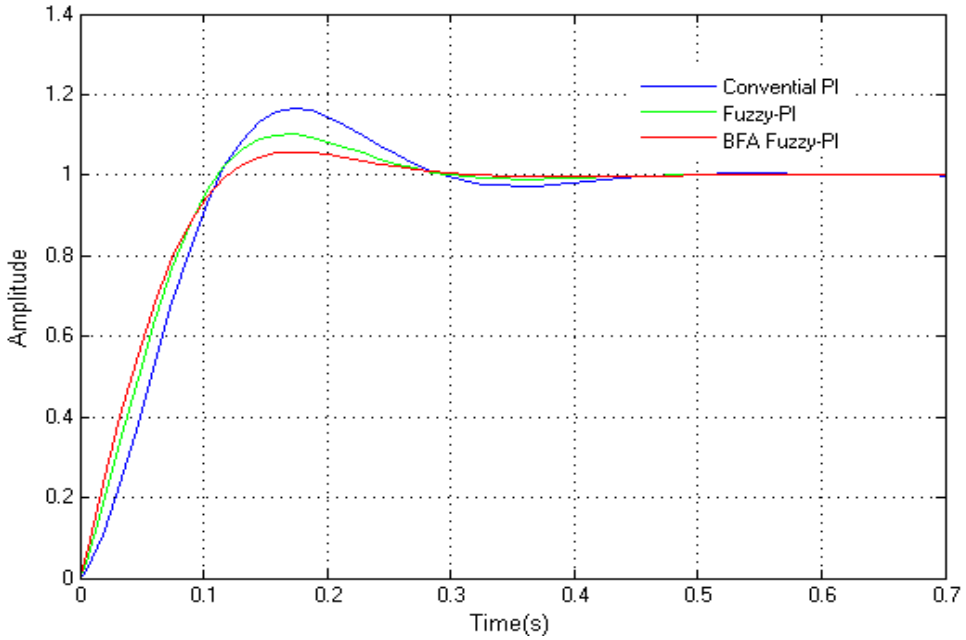

Figure 4.8: Combined control response of the various controllers

It can be observed from Table 4.8 and in Figure 4.8 that the BFA optimised Fuzzy-PI controller gives the best control response in terms of settling time and percentage overshoot as compared to the conventional PI controller and fuzzy-PI controller. The percentage improvement of the BFA optimised Fuzzy-PI controller in terms of settling time is 34.42% whereas that of the fuzzy-PI is 33.03%. Also the percentage improvement in terms of percentage overshoot for the BFA optimised Fuzzy-PI controller is 64.84% while in the Fuzzy-PI controller, the percentage improvement is 38.27%. However, there was a small percentage reduction in terms of rise time for the fuzzy-PI controller and the BFA optimised Fuzzy-PI controller with values of 0.49% and 4.3%, respectively which is quite insignificant.

This clearly depicts that using intelligent techniques such as fuzzy logic and optimising the membership functions using stochastic optimisation algorithms can greatly improve the control performance of conventional PI controllers in the frequency control of MHPP. Hence the problem encountered in the conventional PI controllers such as high overshoots and long settling times is minimised consequently ensuring a stable frequency control of the MHPP.

4.4 Frequency Control

4.4.1 Generator Load Variation without ELC

Table 4.9 depicts the frequency behaviour of the synchronous generator recorded under varying consumer load conditions without either ELC or frequency regulation mechanism. The graphical representation of Table 4.9 is also shown in Figure 4.9. It can be observed that as the consumer load decreases, there is a corresponding increase in frequency due to the decrease in load on the synchronous generator. It can be seen that when the consumer load is zero, the frequency increases to a high value of 63.87

Hz, which is not within the acceptable frequency tolerance, hence not acceptable in the frequency control of power system.

The effects of increase in frequency to such a very critical value can damage the generator due to the overheating of the windings, increase in vibration and wear of the mechanical bearings and consequently damaging any electrical appliance connected to the generator.

Table 4.9: Frequency variation with generator load without ELC

Voltage (V)	Consumer load (W)	Frequency (Hz)	Speed (RPM)	Ex. Current (mA)	Calculated Frequency using Speed (Hz)
220	160.31	50.00	3000	349	50.00
220	128.22	52.04	3122	286	52.03
220	97.02	54.10	3246	243	54.10
220	77.80	55.75	3345	226	55.75
220	54.04	56.98	3419	215	56.98
220	46.86	57.25	3435	211	57.25
220	41.56	58.22	3493	206	58.21
220	36.33	59.63	3578	203	59.62
220	33.68	60.46	3627	199	60.45
220	30.34	60.84	3650	196	60.83
220	25.73	61.58	3695	194	61.58
220	0.000	63.87	3832	190	63.86

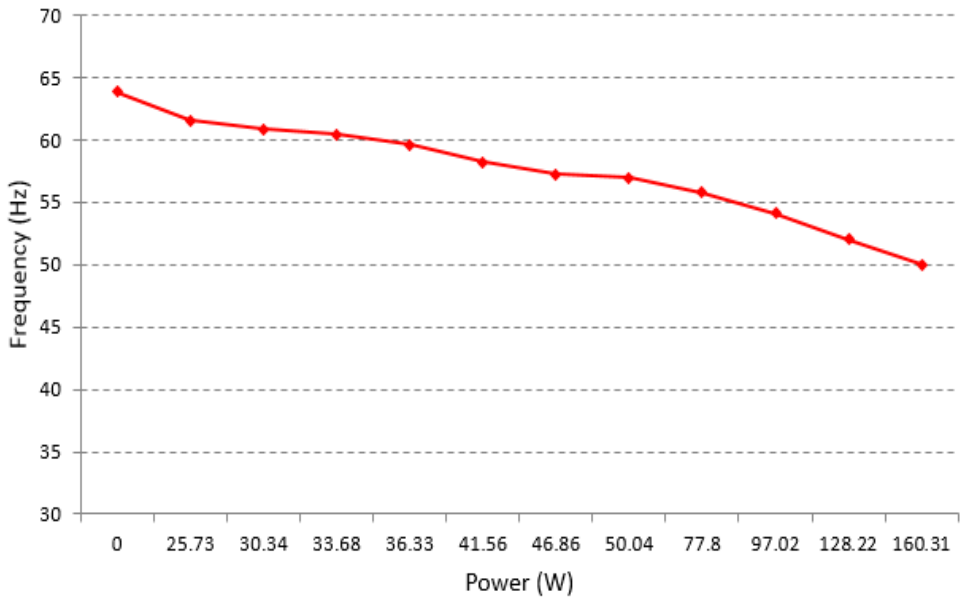

Figure 4.9: Frequency variation with consumer load without ELC

It is also observed from Table 4.9 and Figure 4.9 that as the consumer load decreases, the speed also increases to such a critical value as the frequency. This is because the speed of the synchronous generator is directly proportional to the frequency. Hence as expected, an increase in speed of the synchronous generator also resulted in an increase in frequency.

Also from Table 4.9, it can be observed that the frequency reading from the MAW sensor compares well with the calculated frequency obtained from the speed measurement using the tachometer. The percentage error for the MAW sensor was calculated to be 0.017% which is quite insignificant hence can be ignored. The results clearly depict the accuracy of the MAW sensor used as frequency sensor to the ELC.

4.4.2 Generator Load Variation with ELC

The variation of consumer load, damper load, main load and frequency under the control action of the ELC is shown in Table 4.10. The graphical representation of Table 4.10 is also shown in Figure 4.10. It is noted that, as the consumer load decreases from

full load to no load, the damper load also increases from no load to approximately full load maintaining the main load or the generator load approximately constant. It can also be noted that the load balancing by the ELC has maintained the frequency approximately constant at 50 Hz with the maximum frequency recorded being 50.46 Hz which is within the frequency tolerance limit of 49.5 Hz to 50.5 Hz of the Kenya power grid. These results show the effectiveness of the ELC to dump the excess power to the damper load hence maintaining the frequency constant since without the ELC the highest frequency recorded is 63.87 Hz.

Table 4.10: Frequency variation with generator load with ELC

Voltage (V)	Main load (W)	Consumer load (W)	Damper load (W)	Frequency (Hz)	Speed (RPM)
220	160.30	160.30	0.00	50.00	3000
220	160.45	129.42	31.03	50.10	3007
220	160.38	103.62	56.76	50.00	3000
220	160.45	80.55	79.89	50.10	3006
220	160.01	52.89	107.12	50.20	3013
220	159.27	43.62	115.66	50.35	3021
220	158.47	39.67	118.84	50.46	3028
220	160.23	34.95	125.28	50.10	3006
220	160.45	31.69	128.76	49.95	2997
220	160.38	28.38	132.00	50.00	3000
220	159.13	23.77	135.36	50.30	3019
220	158.91	0.00	158.91	50.40	3024

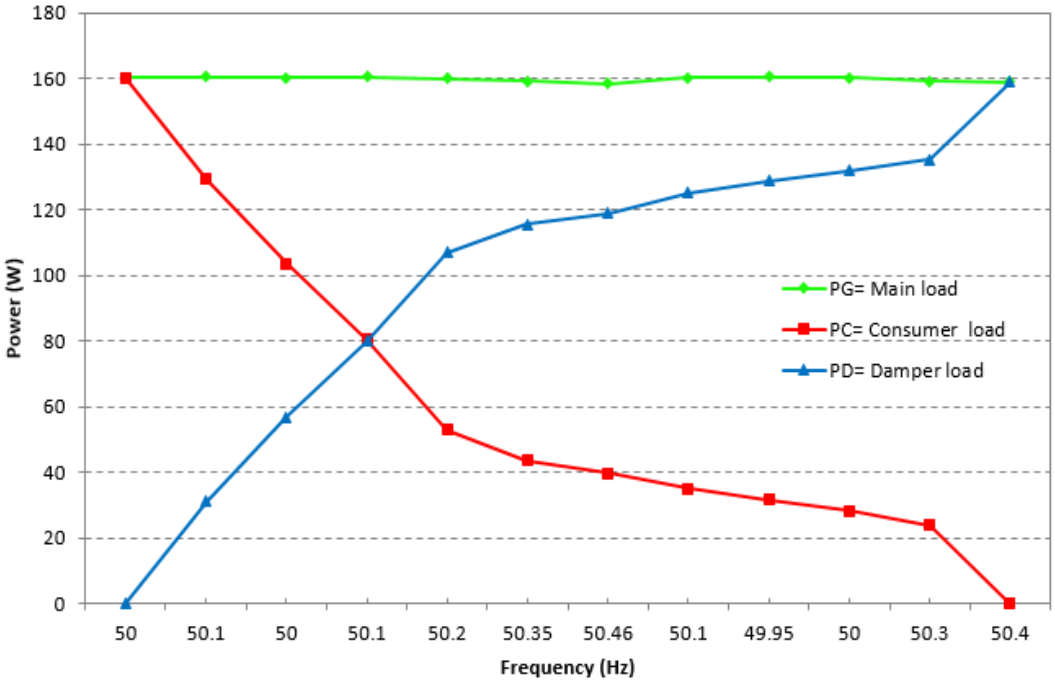

Figure 4.10: Main load, consumer load, damper load and frequency variation with ELC

The same results are also obtained for the main load, consumer load, damper load and speed under the control action of the ELC. This is because as stated earlier speed is directly proportional to frequency, hence the speed of the generator is also maintained constant as shown in Table 4.10. From the experiment, it was observed that the ELC takes 1.5 seconds to stabilise the frequency to 50 Hz with minimal tolerance when there is a change in consumer load.

It should however be emphasized that in all the results obtained the power factor is noted to be unity, since purely resistive balanced 3-phase loads are used as both consumer load and damper load respectively. Hence the challenge of operating at a low power factor arising from inductive and capacitive load and also the effects of unbalanced loading is therefore eliminated.

CHAPTER FIVE

5.0 CONCLUSIONS AND RECOMMENDATIONS

5.1 Conclusions

The design of an ELC to control the frequency of a MHPP has been achieved. Results obtained clearly show the effectiveness of the ELC to dump excess power to the damper load when the consumer load changes, and maintain the supply frequency at between 49.95 to 50.46 Hz. This helped maintain the total load on the generator constant and thus keeping the frequency of the synchronous generator constant. The BFA optimised Fuzzy-PI controller made it possible to design an ELC which controls the frequency of the generator within the required range of 50 Hz while responding to stabilise the frequency within 1.5 seconds when there is change in consumer load.

Again, from the results, it was observed that the MAW sensor was able to measure the frequency effectively with high accuracy when compared to the frequency measurement from the tachometer. This is a key finding of the MAW sensor used in ELC application since the MAW sensor has not been used as sensor to the ELC for MHPPs.

The designed controller cost $150 which is within reach of the rural communities as compared with other commercial controllers which cost between $10,000-$15,000.

Finally, the implementation of the designed ELC in a typical MHPP will be beneficial to remote communities in Kenya, Africa and the world at large. This is because they will be supplied with power at well regulated frequency and this will free the capacity of national grid for other industrial uses. The problem encountered as a result of frequency variation in MHPP such as damaging of the power generation equipment and household appliances will be averted. The ELC will also promote economic growth

especially in the remote communities due to the fact that small industries can operate effectively without any power interruption since the ELC will maintain the supply frequency within desired limits. Electrical equipment will be able to operate effectively for a long time without damage. This will thus improve the life of the people living in the rural communities in Kenya.

5.2 Recommendations

In this work, three-phase balanced, purely resistive loads were used as both consumer load and damper load resulting in the generator operating at unity power factor. In reality, the actual loads supplied by a MHPP have non-unity power factor. In addition, there may be imbalanced loading of the generator mainly due to the single phase loads connected in the system. Thus, there is a need for further investigation into the effect of system operation at non-unity power factor and imbalanced loading condition on the design and operation of the ELC.

In this work, the generator was designed to meet the load demand. However, as the consumer load grows and surpasses the generator capacity, the problem of system under-frequency may arise. Further research needs to be carried out to cater for situations where the demand is more than the supply and incorporate a load shedding algorithm in the ELC design so as to minimise the problems associated with under frequency.

REFERENCES

[1] M. R. Nouni, S. C. Mulick, and T. C. Kandpal, "Providing electricity to remote areas in india: an approach towards identifying potential areas for decentralized electricity supply," *Renewable and Sustainable Energy Reviews*, vol. 12, no. 5, pp. 1187–1220, 2008.

[2] UNDP, "Rural electrification and development in philipines: measuring the social and economic benefits," 2002.

[3] A. Chaurey, M. Ranganathan, and P. Mohanty, "Electricity access for geographically disadvantaged rural communities: technology and policy insights," *Energy Policy*, vol. 32, pp. 1693–1705, October 2004.

[4] O. Paish, "Small hydro power: technology and current status," *Renewable and Sustainable Energy Reviews*, vol. 6, pp. 537–556, February 2002.

[5] ESHA and IT Power, *Small hydropower for developing countries*. 26, Rue du Trône- B-1000 Brussels - Belgium, January 2006.

[6] International Energy Agency (IEA), "World energy outlook 2008." [Online].Available:2008http://www.worldenergyoutlook.com/database_ electricity/electricity_access_database.htm. [Accessed: February 24, 2015].

[7] A. Eberhard and K. Gratwick, "The Kenyan IPP experience. Program on Energy and Sustainable Development." No. 49. Stanford, USA: Center for Environmental Science and Policy, Stanford University, 2005.

[8] Kenya Power & Lighting Company (KPLC), "Annual report 2005-2006." Nairobi, Kenya: [Online]. Available:

2006http://www.kplc.co.ke/documents/annualrep2006.pdf. [Accessed: February 24, 2015].

[9] UNIDO, "UNIDO projects for the promotion of small hydro power for productive use." [Online]. Available:http://www.unido.org/fileadmin/user_media/About_UNIDO/ Evaluation/Project_reports/e-book_small-hydro.PDF. [Accessed: February 24, 2015].

[10] A. Harvey, *Micro-hydro Design Manual*. Rugby: Intermediate Technology Publications, 2006.

[11] H. Goyal, M. Hanmandlu, and D. P. Kothari, "An artificial intelligence based approach for control of small hydro power plants." Centre for Energy Studies, Indian Institute of Technology, HauzKhas, New Delhi-110016, 2014.

[12] S. Doolla and T. S. Bhatti, "Load frequency control of an isolated small-hydro power plant with reduced dump load," *IEEE Transactions on Power Systems*, vol. 21, pp. 1912 – 1919, December 2006.

[13] V. B. Singh, Y. R. Sood, N. Kushwaha, and Suryakant, "Review on electronic load controller," *International Journal of Scientific Engineering and Technology*, vol. 1, pp. 93–102, 2012.

[14] I. Tamrakar, "Development stages of ELC for micro hydro power plant," *E-novation*, vol. 2, p. 1, 2002.

[15] P. K. Kihato, J. N. Nderu, and G. M. Hinga, "Motor speed measurement using magnetostrictive amorphous wire," in *Proceedings of 2007 JKUAT Scientific, Technological and Industrialization Conference*, pp. 315–319, October 2007.

[16] C. K. Kitur, J. N. Nderu, and A. M. Muhia, "Frequency sensing of an isolated

pico-hydro power generation plant using magnetostrictive amorphous wire," *International Journal of Emerging Technology and Advanced Engineering*, vol. 2, pp. 1–5, August 2012.

[17] Y. K. Chauhan, S. K. Jain, and B. Singh, "A prospective on voltage regulation of self-excited induction generators for industry applications," *IEEE Transactions on Industry Applications*, vol. 46, pp. 720 – 730, January 2010.

[18] S. Khennas and A. Barnett, *Best practices for sustainable development of micro hydro power in developing countries*. Final synthesis report, Department for International Development, UK, 2000.

[19] M. Umar and A. Hussain, "Micro hydro power: A source of sustainable energy in rural communities: Economic and environmental perspectives," in *30th, AGM and Conference, PSDE*, pp. 1–34, 2015.

[20] Practical Action, "Micro-hydro power." [Online].Available:hppts//practicalaction.org/docs/technical_information_service/micro_hydro_power.pdf.[Accessed:March,2015].

[21] H. Luden, "Electronic load controller for micro-hydro systems." [Online]. Available: http://ludens.cl/Electron/picelc.html [Accessed: May 30, 2016], 2010.

[22] S. J. Chapman, *Electric machinery Fundamentals*. McGraw-Hill, Inc, New York, USA, 4th Edition, 2005.

[23] I. M. S. Hughes, *Electrical Technology*. McGraw-Hill Publishing Company Limited, New York, USA, 7th Edition, 1993.

[24] S. Mbabazi and J. Leary, "Analysis and design of electronic load controllers for microhydro systems in the developing world," Master's thesis, E-Futures, Uni-

versity of Sheffield, Sheffield, England, March 2010.

[25] H. Goyal and M. Hanmandlu, "An artificial intelligence based control for micro hydro power plants," *IJEIT*, vol. 1, October 2009.

[26] B. J. Kirby, D. C. Martinez, A. Rahmat, R. Guttromson, and J. Dagle, "Frequency control concerns in the north american electric power system." [Online]. Available: http://www.osti.gov/contact.html. [Accessed: May 30, 2016], 2002.

[27] B. S. Abdulraheem1 and C. K. Gan, "Power system frequency stability and control: Survey," *International Journal of Applied Engineering Research*, vol. 11, no. 8, pp. 5688–5695, 2016.

[28] G. Andersson, *Dynamics and Control of Electric Power Systems*. EEH-Power Systems Laboratory, Swiss Federal Institute of Technology, Zurich, 2012.

[29] Renewables Academy (RENAC), *Frequency and voltage regulation in electrical grids*. Federal Ministry for the Environmental, Nature Conservation and Nuclear Safety, Berlin, Germany, 2013.

[30] IEC60034-1, *Rotating Electrical Machine: Rating and Performance*, 2004.

[31] P. Kundur, *Power System Stability and Control*. McGraw-Hill, Inc, 1994.

[32] A. Nigussie, "Development of a dual mode frequency controller for standalone, micro and mini hydropower systems," Master's thesis, Electrical and Computer Engineering Department, AAiT, Addis Ababa, Ethiopia, July 2010.

[33] D. Henderson, *An Advanced Electronic Load Governor for Control of Micro Hydroelectric Generation*.

[34] J. Laghari, H. Mokhlis, A. Bakar, and H. Mohamad, "Application of computational intelligence techniques for load shedding in power systems: A review,"

Energy Conversion and Management, SciVerse Science Direct, vol. 75, pp. 130–140, 2013.

[35] I. Salhi, S. Doubabi, and N. Essounbouli, "Fuzzy control of micro hydro power plants," in *The 5th IET International Conference on Power Electronics, Machines and Drives (PEMD2010)*, Brighton, UK, April 2010.

[36] S. Doolla and T. S. Bhatti, "Automatic generation control of an isolated small hydro power plant," *Electric Power Systems Research*, vol. 76, no. 9-10, pp. 889–896, 2006.

[37] M. A. Wazed and A. Shamsuddin, "A feasibility study of micro hydroelectric power generation at sapchari waterfall, kharachari," *Journal of Applied science*, pp. 372–376, 2009.

[38] C. Penche, *Layman's Handbook on How to Develop a Small Hydro Site*. Brussels, June 1998.

[39] [Online].Available:www.british-hydro.org.uk.

[40] J. K. Authur, "Assessment of a typical small hydropower site for rural electrification in the western region of ghana," Master's thesis, Kwame Nkrumah University of Science And Technology, Ghana, May 2014.

[41] A. Gupta, "Modelling and simulation of an electronic load controller with synchronous generator using a three-phase controlled bridge rectifier," *International Journal of Advanced Electrical and Electronics Engineering*, vol. 2, no. 1, pp. 55–60, 2013.

[42] S. S. M. B. Singh and S. Gupta, "Analysis and design of electronic load controller for self-excited induction generators," *IEEE Transaction on Energy Conversion*,

vol. 21, pp. 5688–5695, 2006.

[43] "Automatic voltage control." [Online].Available:https://www.scribd.com/doc/294030927/Chapter-3-Voltage-Control[Accessed:June20,2016].

[44] N. Fischer, G. Benmouyal, and S. Samineni, "Tutorial on the impact of the synchronous generator model on protection studies," *SEL Journal of Reliable Power*, vol. 3, pp. 1–18, March 2012.

[45] Renerconsys, *Digital Load Controller for Synchronous Generator: Manual Instruction*, 2010.

[46] B. N. Mohan, T. M. Undeland, and W. P. Robbins, *Power Electronics*. John Wiley Sons Year, 3th Edition, 2003.

[47] K. Lending, Y. S. Koh, M. Low, and R. Bhadti, "An electronic load controller for micro-hydro power plants in the philippines," Master's thesis.

[48] C. Nagpal, R. Basheer, A. Thomas, R. Daniel, and I. Yusuf, "Analysis and design of electronic load controllers used in micro hydro power systems," *International Journal of Emerging Technology and Advanced Engineering*, vol. 4, pp. 26–31, February 2014.

[49] H. Salah, E. Nabulsi, and E. Dwikat, "Smart lighting control." [Online].Available:hppts//www.eng.najah.edu/sites/eng.najah.edu/files/project_presentation_5.pptx.[Accessed:June20,2016].

[50] S. A. AL-Mawsawi, N. Allaith, H. Qassim, and S. Dhiya, "An accurate formula for the firing angle of the phase angle control in terms of the duty cycle of the integral cycle control," *Journal of automation and systems engineering*, vol. 6, no. 1, pp. 30–35, 2012.

[51] Danaher Industrial Controls, *Encoder Application Handbook*. 2003.

[52] L. G. Scherer, C. M. Franchi1, and R. F. Camargo, "Advances in the modelling and control of micro hydro power stations applied on self-excited induction generators based on hydraulic turbine nonlinear model," *Materials and processes for energy: communicating current research and technological developments*, pp. 604–616, 2013.

[53] J. N. Nderu, P. K. Kihato, and G. M. Hinga, "Effect of motor-cage temperature on motor speed sensing characteristic of magnetostrictive amorphous wire," *IEEE Africon 2009 Nairobi*, pp. 1–5, September 2009.

[54] B. L. Theraja, *Fundamentals of Electrical Engineering and Electronics*. S. Chand Company LTD, New Delhi, 28th Edition, 1998.

[55] L. A. Zadeh, "Outline of a new approach to the analysis of complex systems and decision processes," *IEEE Transactions on Systems, Man, and Cybernetics*, vol. 3, pp. 28–44, January 1973.

[56] S. N. Sivanandam, S. Sumathi, and S. N. Deepa, *Introduction to fuzzy logic using MATLAB*. Springer-Verlag Berlin Heidelberg, 2007.

[57] C. C. Lee, "Fuzzy logic in control systems: fuzzy logic controller - parts 1 and 2," *IEEE Transactions on Systems, Man, and Cybernetics*, vol. 20, no. 2, pp. 404–435, 2010.

[58] J. H. Hwang, D. W. Kim, J. H. Lee, and Y. J. An, "Design of fuzzy power system stabilizers using adaptive evolutionary algorithm," *Engineering Applications of Artificial Intelligence*, vol. 21, pp. 86–96, February 2008.

[59] K. M. Passino, "Biomimicry of bacterial foraging for distributed optimization and control," *IEEE Control Systems Magazine*, vol. 22, pp. 52 – 67, June 2002.

[60] D. Swagatam, B. Arijit, D. Sambarta, and A. Ajith, "Bacterial foraging optimization algorithm: Theoretical, foundations, analysis, and applications," *Fundations of computational intelligence*, vol. 3, pp. 23–55, April 2009.

[61] E. S. Ali and S. M. Abd-Elazim, "BFOA based design of PID controller for two area load frequency control with nonlinearities," *International Journal of Electrical Power and Energy Systems*, vol. 51, pp. 224–231, october 2013.

[62] K. Mohammad, M. Seyed, M. Ali, and A. A. Gharaveisi, "A bacterial foraging optimization approach for tuning type-2 fuzzy logic controller," *Turkish Journal of Electrical Engineering and Computer Sciences*, vol. 21, pp. 263–273, December 2013.

[63] M. M. Ismail and M. A. M. Hassan, "Load frequency control adaptation using artificial intelligent techniques for one and two different areas power system," *International Journal of Control, Automation and Systems*, vol. 1, pp. 12–23, January 2012.

[64] I. Salhi and S. Doubabi, "Fuzzy controller for frequency regulation and water energy save on microhydro electrical power plants," *International Renewable Energy Congress*, pp. 106–112, November 2009.

[65] L. H. Hassan, H. A. F. Mohamed, M. Moghavvemi, and S. S. Yang, "Automatic generation control of power system with fuzzy gain scheduling integral and derivative controller," *International Journal of Power, Energy and Artificial Intelligence*, vol. 1, pp. 29–33, August 2008.

[66] I. Salhi, S. Doubabi, and N. Essounbouli, "Fuzzy control of micro hydro power plants," in *Proceedings of the 5th IET international conference on power electronics, machines and drives*, vol. 1, p. 497, Curran Associates, Inc, April 2010.

[67] E. Ozbay and M. T. Gencoglu, "Self-tuning fuzzy pi controlled system model for small hydro power plants," in *Proceedings of the 10th international conference on clean energy*, pp. 1–8, September 2010.

[68] P. Adhikary, S. Kundu, K. R. Pankaj, and A. Mazumdar, "Fuzzy logic based user friendly pico-hydro power generation for decentralized rural electrification," *International Journal of Engineering Trends and Technology*, vol. 4, pp. 507–511, 2013.

[69] V. Suhas, Kamble, and D. P. Kadam, "Design of fuzzy controller and supervisor for load frequency control of micro hydro power plant," *International Journal of Scientific and Research Publications*, vol. 4, January 2014.

[70] R. Dhanalakshmi and S. Palaniswami, "ANFIS based Neuro-Fuzzy controller in LFC of wind, micro hydro-diesel hybrid power system," *International Journal of Computer Applications*, vol. 42, march 2012.

[71] H. Goyal, M. Hanmandlu, and D. P. Kothari, "An artificial intelligence based approach for control of small hydro power plants," Master's thesis, Centre for Energy Studies, Indian Institute of Technology, HauzKhas, New Delhi-110016, 2014.

[72] O. Cordon, F. Herrera, F. Hoffmann, and L. Magdalena, *Genetic Fuzzy systems: Evolutionary Tuning and Learning of Fuzzy Knowledge Bases*. World Scientific Publishing, 2001.

[73] M. N. H. Siddique and M. O. Tokhi, "Ga-based neural fuzzy control of flexible-link manipulators," *Engineering Letters Advanced online publication*, vol. 13, pp. 1–10, August 2006.

[74] M. S. Boroujeni, R. Hemmati, and H. F. Boroujeni, "Load frequency control in multi area electric power system using genetic scaled fuzzy logic," *International Journal of the Physical Sciences*, vol. 6, no. 3, pp. 377–385, 2011.

[75] J. Hayato, "Design of self-tuning fuzzy controller for micro hydropower plants on irrigation dams,," Master's thesis, Addis Ababa Institute of Technology, Addis Ababa, Ethiopia, July 2011.

[76] A. Zargari, R. Hooshmand, and M. Ataei, "A new control system design for a small hydro-power plant based on particle swarm optimization fuzzy sliding mode controller with kalman estimator," *Transactions of the Institute of Measurement and Control*, vol. 34, no. 4, pp. 388–400, 2012.

[77] Y. Liu and K. M. Passino, "Biominicry of social foraging for distributed optimization: Models, principles and emergent behaviors," *JOTA*, vol. 115, pp. 603–623, December 2002.

[78] S. Mishra and C. N. Bhende, "Bacterial foraging technique-based optimized active power filter for load compensation," *IEEE Transactions on Power Delivery*, vol. 22, no. 1, pp. 457–465, 2007.

[79] A. Biswas, S. Dasgupta, S. Das, and A. Abraham, "A synergy of differential evolution and bacterial foraging optimization for faster global search," *International Journal on Neural and Mass-Parallel Computing and Information Systems*, vol. 6, pp. 607–626, December 2007.

[80] A. M. Muhia, “Speed control of single-phase induction motor using fuzzy logic technique with magnetostrictive amorphous wire speed sensor,” Master’s thesis, Jomo Kenyatta University of Agriculture and Technology, Nairobi, Kenya, 2013.

[81] C. Wang, “A study of membership functions on mamdani-type fuzzy inference system for industrial decision-making,” Master’s thesis, Lehigh University, Bethlehem, Pennsylvania, January 2015.

[82] M. K. Pandey, “Analysis of self tuning fuzzy PID internal model control,” Master’s thesis, Thapar University, Patiala, India, July 2011.

[83] K. Wang-Xiao, S. Zhong-Liang, Wnglei, and F. Dong-qing, “Design and research based on fuzzy self-tuning PID using matlab,” in *Proceedings of International Conference on Advanced Computing theory and Engineering*, 2008.

[84] Kenya Energy Regulatory Commission, *Kenya Electricity Grid Code*, March 2008 Edition, Nairobi, Kenya.

[85] S. K. Mallick and M. A. Khan, “Study of the design and tuning methods of PID controller based on fuzzy logic and genetic algorithm,” Master’s thesis, National Institute of Technology, Rourkela, India, May 2011.

[86] C. Hung-Cheng, *Bacterial Foraging Based Optimization Design of Fuzzy PID Controllers*. Springer Verlag Berlin Heidelberg, 2008.

[87] MathWorks, Inc, “Triangular membership function.” [Online].Available:hppts/ /mathworks.com/help/fuzzy/trimf.Html.[Accessed:February,2016].

APPENDICES

APPENDIX 1 Master and Slave Microcontroller Codes

Master Controller Codes

```
double kp=0.9168, ki=32.4739,input=0,output=0,setpoint=50,error=0,iTerm=0,monitor;
int mawInput = 8;
int pwmOutput=3;
int pwmSignal;
double lowtime,hightime, period,freq, pfreq;

void setup()
{
  Serial.begin(9600);
  pinMode(mawInput,INPUT);
  pinMode(pwmOutput,OUTPUT);
}

void loop()
{

   pwmSignal=(int)Control();
  analogWrite(pwmOutput,pwmSignal);
  delay(500);
  Serial.println(frequencyAcquisition());
  Serial.println(pwmSignal);
  Serial.println();

}

double frequencyAcquisition()
{
  hightime = pulseIn(mawInput, HIGH);
  lowtime=pulseIn(mawInput,LOW);

  period=hightime+lowtime;

  pfreq=(1000000/period);
```

```
  if(pfreq<=70)
  {
   freq=pfreq-0.7;
  }
  return freq;
}

double Control()
{
  input=frequencyAcquisition();

    error=input-setpoint;
    iTerm+=(ki*error);
    output=(kp*error)+iTerm;
    monitor=output;
    int upperLimit=255,lowerLimit=0;
    if(output>=upperLimit) output=upperLimit;
    if(output<=lowerLimit) output=lowerLimit;

  return output;

}
```

Slave Controller Codes

```
boolean zeroCross=false;
double pwmInput;
float firingDelay;
void setup()
{
  attachInterrupt(0,zeroCrossing,FALLING);
  pinMode(13,OUTPUT);
  Serial.begin(9600);
}
void loop()
{
```

```
  if(zeroCross==true)
  {
    Serial.println("Interrupt detected");
    pwmInput=analogRead(A0);
    Serial.println(pwmInput);

    firingDelay=map(pwmInput,0,1023,10,0);
    Serial.println(firingDelay);
    if(firingDelay<=9)
    {
      firingDelay=10-((pwmInput/910)*10);
          Serial.println(firingDelay);
      if(firingDelay<10)
      {
        delay(firingDelay);
        digitalWrite(13,HIGH);
        delay(20);
      }

    }

    zeroCross=false;
  }
  else digitalWrite(13,LOW);

  }

void zeroCrossing()
{
  zeroCross=true;
}
```